

Dottorato di Ricerca in
Biologia Cellulare e Molecolare
Ciclo XXVI

Settore Concorsuale di afferenza: 06/A2
Settore Scientifico disciplinare: MED/04

**High sensitivity analysis of
BRAF mutations in neoplastic and
non-neoplastic thyroid lesions**

Presentata da
Valentina Cesari

Coordinatore Dottorato
Prof. Vincenzo Scarlato

Correlatore
Prof. Giovanni Tallini

Relatore
Prof.ssa Annalisa Pession

ABSTRACT

The clonal distribution of $BRAF^{V600E}$ in papillary thyroid carcinoma (PTC) has been recently debated. No information is currently available about precursor lesions of PTCs.

My first aim was to establish whether the $BRAF^{V600E}$ mutation occurs as a subclonal event in PTCs. My second aim was to screen $BRAF$ mutations in histologically benign tissue of cases with $BRAF^{V600E}$ or $BRAF^{wt}$ PTCs in order to identify putative precursor lesions of PTCs. Highly sensitive semi-quantitative methods were used: Allele Specific LNA quantitative PCR (ASLNAqPCR) and 454 Next-Generation Sequencing (NGS).

For the first aim 155 consecutive formalin-fixed and paraffin-embedded (FFPE) specimens of PTCs were analyzed. The percentage of mutated cells obtained was normalized to the estimated number of neoplastic cells. Three groups of tumors were identified: a first had a percentage of $BRAF$ mutated neoplastic cells $> 80\%$; a second group showed a number of $BRAF$ mutated neoplastic cells $< 30\%$; a third group had a distribution of $BRAF^{V600E}$ between 30-80%. The large presence of $BRAF^{V600E}$ mutated neoplastic cell sub-populations suggests that $BRAF^{V600E}$ may be acquired early during tumorigenesis: therefore, $BRAF^{V600E}$ can be heterogeneously distributed in PTC.

For the second aim, two groups were studied: one consisted of 20 cases with $BRAF^{V600E}$ mutated PTC, the other of 9 $BRAF^{wt}$ PTCs. Seventy-five and 23 histologically benign FFPE thyroid specimens were analyzed from the $BRAF^{V600E}$ mutated and $BRAF^{wt}$ PTC groups, respectively.

The screening of $BRAF$ mutations identified $BRAF^{V600E}$ in “atypical” cell foci from both groups of patients. “Unusual” $BRAF$ substitutions were observed in histologically benign thyroid associated with $BRAF^{V600E}$ PTCs. These mutations were very uncommon in the group with $BRAF^{wt}$ PTCs and in $BRAF^{V600E}$ PTCs. Therefore, lesions carrying $BRAF$ mutations may represent “abortive” attempts at cancer development: only $BRAF^{V600E}$ boosts neoplastic transformation to PTC.

BRAF^{V600E} mutated “atypical foci” may represent precursor lesions of *BRAF*^{V600E} mutated PTCs.

TABLE OF CONTENTS

INTRODUCTION.....	1
1.1 The thyroid gland	1
1.1.1 Embryology and anatomy	1
1.1.2 Physiology.....	1
1.2 Human thyroid tumors	4
1.2.1 Benign and malignant thyroid tumors.....	4
1.2.2 Epidemiology	7
1.2.3 Risk factors	9
1.2.4 Staging and prognostic factors.....	11
1.2.5 Multi-step carcinogenesis of thyroid neoplasms.....	13
1.3 Papillary thyroid carcinoma (PTC).....	18
1.3.1 Histopathology	18
1.3.2 Histopathological variants and associated molecular alterations.....	20
1.3.3 Papillary thyroid microcarcinoma (mPTC).....	22
1.4 Oncogene <i>BRAF</i> and its role in papillary thyroid carcinoma.....	23
1.4.1 Gene and protein function.....	23
1.4.2 RAF protein structures.....	25
1.4.3 <i>BRAF</i> mutation prevalence	27
1.4.4 <i>BRAF</i> ^{V600E} mutation	30
1.4.5 Other <i>BRAF</i> mutations of V600 residue.....	31
1.4.6 Other <i>BRAF</i> mutations in exon 15.....	32
1.4.7 The role of <i>BRAF</i> mutation in the initiation and progression of PTC.....	35
1.4.8 <i>BRAF</i> in the diagnosis of PTC	36
1.4.9 The prognostic utility of <i>BRAF</i>	39
1.4.10 <i>BRAF</i> as a therapeutic target for PTC	41

1.4.1.1 Methods for detection of <i>BRAF</i> molecular alterations.....	49
1.5 Tumor heterogeneity	51
1.5.1 <i>BRAF</i> mutation and intratumoral genetic heterogeneity	51
1.5.2 Clinical implications of intratumoral heterogeneity	55
AIMS OF THE THESIS	59
MATERIALS AND METHODS	61
3.1 Ethic statement and selection of cases	61
3.2 Genomic DNA isolation and quantification	63
3.3 Mutational analysis: Allele Specific Locked Nucleic Acid quantitative PCR (ASLNAqPCR)	63
3.3.1 PCR design and conditions	65
3.3.2 Relative quantitation of <i>BRAF</i> ^{V600E} mutated allele.....	66
3.3.3 Analytical sensitivity.....	67
3.4 Mutational analysis: 454 Next-Generation Sequencing.....	68
3.4.1 Primers design.....	69
3.4.2 Amplicon library preparation.....	70
3.4.3 Emulsion PCR (emPCR).....	74
3.4.4 Recovery and enrichment processes	76
3.4.5 Parallel pyrosequencing	78
3.4.6 454 Sequencing System data handling.....	80
3.5 Analysis of <i>BRAF</i> clonality: evaluation of mutated neoplastic cells proportion	84
RESULTS	86
4.1 1 Aim 1 - Clonality of <i>BRAF</i>^{V600E} mutation in PTC	86
4.1.1 Analysis of PTCs for <i>BRAF</i> ^{V600E} by ASLNAqPCR	86
4.1.2 Distribution of <i>BRAF</i> ^{V600E} mutated neoplastic cells in PTCs and mPTCs by ASLNAqPCR.....	89
4.1.3 Analysis of PTCs for <i>BRAF</i> ^{V600E} by 454 NGS	91

4.1.4 Correlation of <i>BRAF</i> ^{V600E} mutated alleles and clinico-pathological features of PTCs.....	93
4.2 Aim 2 - Screening of <i>BRAF</i> mutations in exon 15 in histologically benign thyroid tissue	95
4.2.1 Exon 15 <i>BRAF</i> mutations in histologically benign thyroid of the <i>BRAF</i> ^{wt} PTC group	98
4.2.2 “Usual” exon 15 <i>BRAF</i> mutations in histologically benign thyroid lesions of the <i>BRAF</i> ^{V600E} mutated PTC group	99
4.2.3 Exon 15 <i>BRAF</i> mutations in psammoma bodies (PBs)	100
4.2.4 “Unusual” exon 15 <i>BRAF</i> mutations in histologically benign thyroid lesions of the <i>BRAF</i> ^{V600E} mutated PTC group	101
DISCUSSION	107
5.1 Aim 1 - Clonality of <i>BRAF</i>^{V600E} mutation in PTC	107
5.2 Aim 2 - Screening of <i>BRAF</i> mutations in exon 15 in histologically benign thyroid tissue	111
REFERENCES	115

CHAPTER 1

INTRODUCTION

1.1 The thyroid gland

1.1.1 Embryology and anatomy

The thyroid gland is a butterfly-shaped organ located on the anterior surface of the trachea at the base of the neck. It is the first endocrine gland to develop in the embryo: it begins to form from an outgrowth of the pharyngeal endoderm by the third week of gestation and ends by the eleventh. As the embryo grows it descends into the neck and for a short time the gland is connected to the developing tongue by a narrow tube, the thyroglossal duct. Thyroid remnants along this migration pathway, constitute in some individuals the pyramidal lobe whose incidence varies from 15% to 75%.

The thyroid gland consists of two lobes and weighs about 15-25 g in adults. Each lobe is about 4 cm in length, 15-20 mm in width and 20-39 mm thickness: the lobes are connected together by a thin band of connective tissue called the isthmus, which is reported to be about 20 mm in length and width and about 2-6 mm in thickness. The gland is covered by a thin fibrous capsule without true lobulations [1, 2].

1.1.2 Physiology

The functional unit of the thyroid gland is the follicle, a roughly spherical group of cells surrounding a central lumen filled with a protein-rich storage material called colloid. The follicles range in size 50-500 μm and are lined by cuboidal-to-flat follicular epithelial cells. The follicular cells are orientated with their bases near the capillary blood supply and the apices abutting the colloid. Follicular cells are responsible for iodine uptake and thyroid hormone synthesis.

The thyroid also contains the parafollicular cells, which are neuroendocrine cells also called C-cells because they produce calcitonin, a hormone involved in calcium homeostasis (Fig. 1.1).

The synthesis of thyroid hormones, L-triiodothyronine (T_3) and L-thyroxine (T_4), takes place in the follicular cells under the control of the hypothalamic-pituitary axis with negative feedback by the thyroid hormones. Thyrotropin releasing hormone (TRH), which is secreted from the hypothalamus, stimulates the release from the anterior pituitary gland of thyroid-stimulating hormone (TSH), which in turn stimulates the follicular cells to synthesize and secrete thyroid hormones. The hypothalamo-pituitary axis regulates the concentration of thyroid hormones in the circulation by a homeostatic feedback loop (Fig. 1.1).

Different follicles may be in different states of activity: in less active follicles, follicular cells have a more cuboidal appearance, whereas the active follicles contain columnar cells.

The process of thyroid hormone synthesis is complex: it demands the active uptake of iodide (I^-) in exchange for Na^+ by the follicular cells involving an ATPase-dependent transport mechanism. This enables the thyroid gland to concentrate iodide, which is oxidized to active iodine by hydrogen peroxide inside the follicular cell. This reaction is catalyzed by the heme-containing enzyme thyroid peroxidase (TPO). Then iodine is actively transported across the apical surface of the follicular cell by the same active process that occurs at the basal surface.

At the apical-colloid interface, iodine is immediately incorporated into the tyrosine residues of a large glycoprotein synthesized in the follicular cells, thyroglobulin. Once iodinated, thyroglobulin is taken up into the colloid of the follicle where TPO catalyzes a coupling reaction between pairs of iodinated tyrosine molecules still incorporated in the protein. The coupling of two tyrosine residues each iodinated at two positions (di-iodotyrosine, DIT) produces tetra-iodothyronine or thyroxine (T_4) whereas the combination of DIT with mono-iodotyrosine (MIT) produces tri-iodothyronine (T_3). Thyroid hormones are stored in this state and are released only after stimulation by TSH: then, thyroglobulin droplets are captured by the follicular cells by a process of pinocytosis. Fusion of

the droplets with lysosomes results in hydrolysis of the thyroglobulin molecules and release of T_4 and T_3 . Approximately 100 μg T_4 and about 10 μg T_3 are secreted from the gland each day, mostly in the form of T_4 with about 10% as T_3 . Eighty percent of the T_4 undergoes peripheral conversion in the liver and kidney to the ten times more active T_3 or to reverse T_3 (rT_3) that has no significant biological activity. Since very small quantities of other iodinated molecules, such as MIT and DIT as well as thyroglobulin, are also measurable in the circulation, thyroglobulin measurement in the serum is used, for example, to detect endogenous thyroid secretion when patients are taking oral T_4 replacement.

Once released from thyroglobulin, over 99% circulating iodothyronines are rapidly bound to the plasma proteins: 70% is bound to thyroxine-binding globulin (TBG), 10-15% to transthyretin (previously called thyroxine-binding prealbumin) and 20-15% to albumin. These bound forms are in equilibrium with a tiny fraction in the free form in the circulation: only the free thyroid hormones can act on target cells.

Thyroid hormones are lipid soluble and readily cross cell membranes: many of their actions are mediated by the binding to nuclear steroid hormone receptors that have higher affinity for T_3 . T_3 receptors are members of a family of nuclear transcription factors that regulate gene expression in target cells and may remain bound to DNA also in the absence of hormone binding. When T_3 binds to its receptor, it dimerizes with another T_3 receptor to form a homodimer or with a different receptor, especially the retinoic acid receptor, to form a heterodimer. Dimerization allows gene expression regulation. In most tissues (excluding brain, spleen and testis) thyroid hormones stimulate the metabolic rate by increasing the number and size of mitochondria, stimulating the synthesis of enzymes in the respiratory chain and increasing membrane $\text{Na}^+\text{-K}^+$ ATPase concentration and membrane Na^+ and K^+ permeability. There is also evidence of rapid, non-genomic effects that thyroid hormones can have on membrane receptors such as stimulation of sugar transport, Ca^{2+} ATPase activity and increased Na^+ transport in muscle [2].

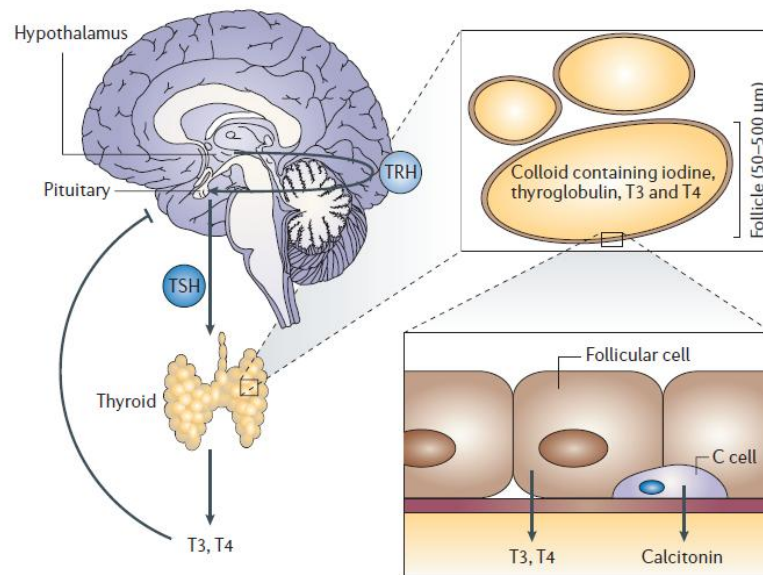


Figure 1.1. The thyroid gland and its control by the hypothalamic-pituitary axis [3].

1.2 Human thyroid tumors

1.2.1 Benign and malignant thyroid tumors

The follicular cell-derived cancers represent the vast majority of thyroid tumors and are subdivided into well-differentiated papillary and follicular carcinomas (DTC), and less-differentiated thyroid cancers, including poorly differentiated carcinoma and anaplastic (undifferentiated) carcinoma (Fig. 1.2). Papillary thyroid carcinoma (PTC), the focus of this thesis, will be discussed in section 1.3.

Follicular carcinoma (FTC) is a malignant epithelial tumor showing evidence of follicular cell differentiation and lacking the diagnostic nuclear features of papillary carcinoma (section 1.3.1). Follicular carcinomas are usually encapsulated solid tumors generally measuring more than 1 cm in diameter. Minimally invasive tumors are indistinguishable grossly from follicular adenomas except for thicker and more irregular capsule. Sometimes, widely invasive follicular carcinomas may lack any encapsulation. Neither architectural nor cytological atypical features, by themselves, are reliable criteria of malignancy since they may be found also in benign lesions, such as nodular (adenomatous)

goiter and adenoma. The diagnosis of malignancy depends on the demonstration of capsular or vascular invasion in histological preparations. Follicular carcinomas show variable morphology ranging from well formed colloid-containing follicles to solid or trabecular growth patterns with common coexistence of multiple architectural types. Follicular carcinomas are further subdivided into conventional, oncocytic and clear cell variants [4].

Oncocytes, also called Hürthle cells, oxyphilic cells or Askanazy cells, are characterized by abundant granular cytoplasm due to aberrant accumulation of mitochondria that may be a compensatory mechanism to intrinsic defects in the energy production machinery of the cell. Thyroid tumors are designated as oncocytic if at least 75% of their cells are represented by oncocytes [5]. Clear cells contain glycogen, mucin, lipid or dilated mitochondria, therefore, this cellular change may be prominent in oncocytic tumors [4].

Poorly-differentiated thyroid carcinoma (PDC) is a malignant follicular-cell neoplasm that shows loss of structural and functional differentiation. It occupies an intermediate position between differentiated and undifferentiated carcinomas both morphologically and behaviorally. There are three different histological patterns: insular, trabecular and solid. These lesions show characteristic widely infiltrative growth, necrosis, vascular invasion and numerous mitotic figures. The diagnosis relies on the identification of the patterns in the majority of the tumor together with infiltrative growth, necrosis and vascular invasion [4].

Anaplastic thyroid carcinoma (ATC) is a widely invasive malignant tumor that is histologically composed wholly or partially of undifferentiated cells without structural follicular-cell differentiation. There are three main morphological patterns: squamoid, pleomorphic giant cell and spindle cell. These tumors have a very poor prognosis [4]. Many poorly differentiated carcinoma and anaplastic carcinoma arise through the process of stepwise dedifferentiation of papillary and follicular carcinomas, even though some can develop *de novo* [6].

Follicular adenoma (FA) is a benign, encapsulated epithelial tumor in which the cells show evidence of follicular differentiation. The architectural pattern and cytological features differ from the surrounding thyroid tissue. The most common

architectural features are follicular or trabecular. The tumor cells can be cuboidal, columnar or polygonal with round, dark nuclei or occasionally enlarged and hyperchromatic. Occasionally, follicular adenomas can arise in a background of nodular hyperplasia from which is distinguishable by the encapsulation. By definition, capsular or vascular invasion are absent. Follicular adenomas are further subdivided into many histological variants such as the oncocytic type. Follicular adenoma may serve as a precursor for some follicular carcinomas [4].

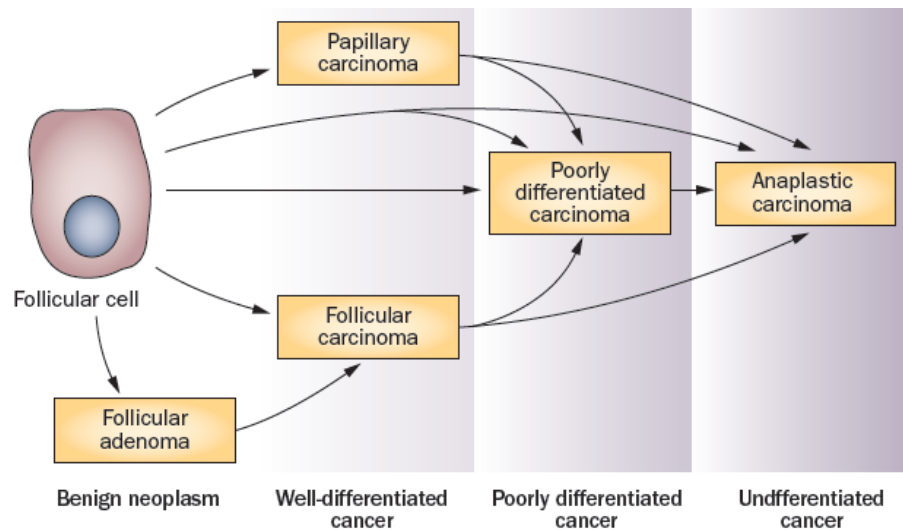


Figure 1.2. Scheme of step-wise dedifferentiation of follicular cell-derived thyroid cancer [6].

Medullary thyroid carcinoma (MTC) is a malignant tumor originating from C-cells. Approximately 25% of these neuroendocrine tumors are heritable: they are associated with multiple endocrine neoplasia (MEN) 2A and MEN2B or they arise as isolated heritable tumors in the familial medullary thyroid carcinomas (FMTC) syndrome.

Tumors in sporadic and heritable form are generally indistinguishable; however, the heritable forms are typically associated with C-cell hyperplasia. The tumors in patients with sporadic disease may vary considerably in size but are usually unilateral while the MEN2-associated tumors are frequently bilateral and multicentric. The tumoral cells frequently have a diffuse or nesting growth pattern and are composed of polygonal, round or spindle cells, which are positive for calcitonin [4].

1.2.2 Epidemiology

Thyroid tumors account for 1% of all malignancies and represent the most common malignancy of endocrine organs. The vast majority of thyroid tumors arise from thyroid follicular epithelial cells, whereas 3% of cancers, referred to as medullary thyroid carcinomas, originate from C-cells. Papillary carcinoma accounts for about 80% of all thyroid cancers, followed by follicular carcinoma (~15%), poorly differentiated carcinoma (<1%) and anaplastic carcinoma (<2%) [4, 7].

Thyroid cancer typically occurs in thyroid nodules, which are common and can be detected by palpation and imaging in a large proportion of adults, particularly in women, of increased age. Palpable thyroid nodules show an estimated prevalence in population-based studies of 3-4%. The prevalence of non-palpable thyroid nodules incidentally detected by imaging approaches is 40%-50% after the age of 60 years and is even higher on high-resolution ultrasound screening using sensitive high frequency (10-13 MHz) transducers [8-13].

However, the vast majority of thyroid nodules is benign and can be managed conservatively: approximately 5-15% of nodules examined by ultrasound and fine-needle aspiration (FNA) cytology are malignant [14-18].

Although thyroid tumors are uncommon in childhood, PTCs represent the most common pediatric thyroid malignancy. Most PTCs in adults occur in patients between 20 and 50 year of age with a female to male ratio of 4-5:1 [19].

In a 2004 survey, the average incidence in Europe has been reported to be 5.0 and 12.9 cases per 100,000 residents per year among men and women, respectively [20]. In 2006, the average incidence of thyroid cancer in Italy has been estimated at 5.2 and 15.5 cases per 100,000 residents per year among men and women, respectively [21].

Incidence of thyroid cancer has increased rapidly in the past 15 years (Fig. 1.3). Many countries, including Europe, have had a doubling of incidence since the late 1990s: the increase in incidence is almost exclusively attributable to papillary thyroid cancer [22].

The reasons why incidence of thyroid cancer is increasing are not completely understood, however, it has been proposed that it may be due to improved

diagnostic procedures that cause an increase in detection of small (<1 cm) and silent tumors incidentally noted on diagnostic imaging studies. Indeed, small papillary thyroid cancers account for most new diagnoses [23-25].

Contrary to the hypothesis that improved diagnosis is the main cause of increased incidence of thyroid cancer, the prevalence of larger tumors is also increasing. Furthermore, higher rates of aggressive papillary thyroid cancers are being detected, including those with extrathyroidal extension, the tall-cell variant of papillary thyroid cancer, and distant metastases [26-28].

Moreover, thyroid cancer mortality has remained unchanged or even increased in recent years [20, 24, 29-31]. These data suggest that other factors might be affecting the biology and incidence of thyroid cancer [22].

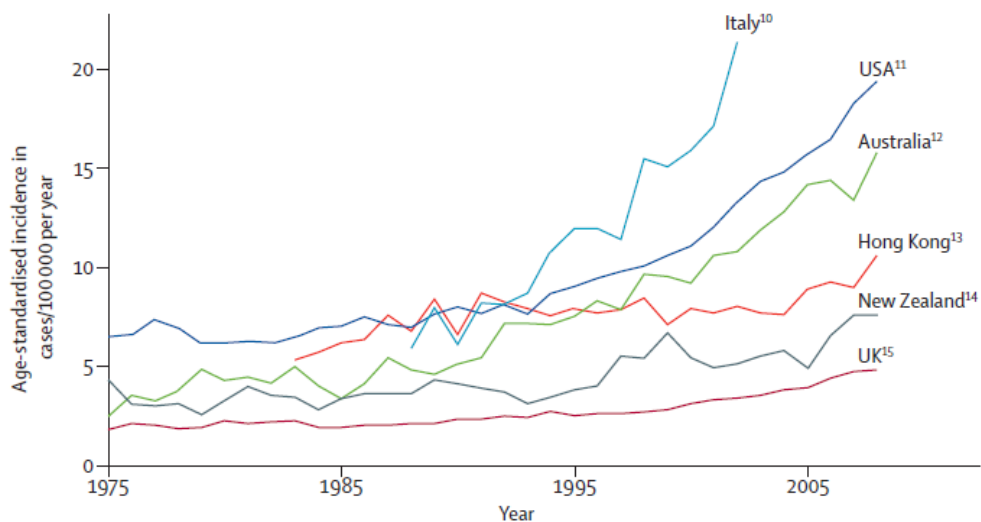


Figure 1.3. Incidence of thyroid cancer in women since 1975 [22].

1.2.3 Risk factors

Several risk factors have been linked to thyroid cancer including radiation exposure, reduced iodine intake, previous history of benign thyroid disease (such as nodules and autoimmune thyroid diseases), hormonal factors and family history (Table 1.4).

Radiation exposure as a consequence of radioactive fallout from nuclear weapons or power plant accidents is associated with papillary carcinoma, as evidenced by the effects on health of the atomic bombs of Hiroshima and Nagasaki (1945), nuclear testing in the Marshall Islands (1954) and Nevada (1951-1962), and the nuclear accident in Chernobyl (1986) [4, 32]. After the Chernobyl disaster, the effects of radiation exposure were most pronounced in children: the possible reasons were a higher susceptibility of thyroid to radiation damage since thyroid growth occurs primarily in childhood and the fact that children drank more contaminated milk, increasing their exposure to radioactive iodine [33]. In the more recent nuclear accident in Fukushima (2011), dairy radiation levels were closely monitored after the disaster. According to WHO report, among infants from the most heavily affected areas, radiation would add one percentage point to their lifetime chances of developing cancer. However, women would have a 70% higher chance of developing thyroid cancer in their lifetimes, 1.25 out of every 100 women [34].

Head or neck radiation treatments for benign condition in childhood is another risk factor for thyroid papillary carcinoma [35].

Radiations seems to be closer linked to aberrant gene activation through chromosomal rearrangement rather than intragenic point mutation probably because radiations cause double strand breaks in DNA [4, 33, 36].

Moreover, dietary iodine deficiency results in thyroid proliferation as a compensatory mechanism, known as goiter, and is linked to FTC. By contrast, PTC is the most frequent type of thyroid cancer in geographic regions of adequate or high iodine intake [4].

In PTC is frequent the presence of lymphocytic infiltration, indicating that immunological factors might be involved in tumor progression [3].

Epidemiological and morphological studies have suggested an increased risk of PTC in patients with Hashimoto's thyroiditis (HT), autoimmune thyroid destruction. Coexistent HT is found in 11% to 36% of thyroids resected for PTC [37, 38]. Several studies support the concept of increased risk of PTC in patients with HT, particularly in women, however the relationship between HT and PTC remains to be determined [38-41]. A possible link between PTC and HT may be provided by solid cell nests (SCN) of the thyroid, composed of cells that may actually represent a pool of stem cells of thyroid and found in normal thyroid but observed at higher frequency in association with PTC and HT [42-44]. It has been suggested that at least a subset of PTC may be derived from these nests of multipotent cells, which may give rise to follicular cells and C cells, and morphologically mimicking papillary thyroid carcinoma [42]. This view is supported by molecular analysis that indicate the presence of the same *BRAF*^{V600E} mutation, the most frequent *BRAF* mutation in PTC (section 1.4.4), both in the SCN and in the adjacent PTC [45]. Cells derived from SCN may also represent incompletely developed thyroid tissue predisposed to autoimmune reaction resulting in HT. Therefore, both HT and PTC may be initiated by the same population of stem cell remnants and may thus be etiologically related [37].

As previously discussed, well-differentiated thyroid carcinomas occurs primarily in young and middle aged adults and are more frequent in females than in males. These sex and age distributions of incidence indicate that female hormones might have a role in thyroid carcinogenesis. Indeed, the estrogen receptor is expressed by follicular cells and estrogen promotes their proliferation [46, 47].

There is also a genetic component in the risk of develop a thyroid follicular cell-derived carcinoma: it increases 3.2- and 6.2-fold when a parent and a sibling, respectively, have had thyroid cancer [48]. About 5% of patients with DTC have a familial disease. Patients with familial non-medullary thyroid cancer have more aggressive tumors and frequently show the phenomenon of "anticipation", earlier age at disease onset and increased severity in successive generations.

Some tumor syndromes have been linked to PTC. These inherited conditions, that are due to known germline mutations, include familial polyposis coli (FAP), Cowden disease, the syndromes referred to as familial site-specific papillary thyroid carcinoma, and perhaps Carney complex. However, the great majority of epithelial thyroid carcinomas seen in Cowden syndrome are follicular thyroid carcinomas: occasional PTCs observed typically belong to the follicular variant [4]. Other familial tumor syndromes that predispose to papillary carcinoma have been linked to several susceptibility gene loci, including syndromes associated with papillary renal cell carcinoma (1q21), clear-cell renal-cell carcinoma ((3;8)(p14.2;q24.1)), and multinodular goiter (19p13.2) [3, 49, 50]. However, the far more common sporadic tumors do not harbor mutations in these loci [3].

Etiological factors	Cancer type
High TSH	
Low iodine intake	Follicular, angiosarcoma
Dyshormonogenesis	Follicular
High iodine intake	Papillary
Radiation	Papillary, follicular, undifferentiated, medullary
Inheritance	
Cowden disease	Follicular
Familial adenomatous polyposis	Papillary
Familial papillary carcinoma	Papillary
Familial oxyphil cell carcinoma	Oxyphil cell papillary or follicular
Werner syndrome	Papillary, follicular
Carney complex	Papillary, follicular
Familial MTC, MEN2A, MEN2B	Medullary (preceded by C-cell hyperplasia)
Precursor tumor	
Follicular adenoma	Follicular
Papillary or follicular carcinoma	Undifferentiated
Hypercalcemia	Medullary (preceded by C-cell hyperplasia)
Thyroiditis	Lymphoma

Table 1.4. Etiological factors linked to the development of thyroid cancer [51].

1.2.4 Staging and prognostic factors

Since the extent of a cancer at time of diagnosis is essential to define treatment and its chance of success and also to allow comparison of groups of patients in clinical trials and who receive standard care, cancer staging systems are used.

The tumor-node-metastasis (TNM) cancer staging system is endorsed by the American Joint Committee on Cancer (AJCC) and the Union for International Cancer Control (UICC) and updated periodically. This system codes the extent of the primary tumor (T), regional lymph nodes (N), and distant metastases (M) and provides a “stage grouping” based on T, N, and M [52].

The seventh edition of the AJCC Cancer Staging Manual is most widely used (Table 1.5), although other classification systems exist and, for example, MACIS (metastasis, age, completeness of resection, invasiveness, and size) has some support as an alternative system [53, 54].

In TNM system, stage I disease includes patients less than 45 years of age with any T, any N, but without distant metastases (M0) and also most micropapillary cancers (TNM class T1a; Table 1.5). Patients older than 45 years of age are classified as stages I to IV [4].

	Definition
TX	Primary tumour cannot be assessed
T0	No evidence of primary tumour
T1	Tumour 2 cm or less in greatest dimension, limited to the thyroid
T1a	Tumour 1 cm or less, limited to the thyroid
T1b	Tumour more than 1 cm but not more than 2 cm in greatest dimension, limited to the thyroid
T2	Tumour more than 2 cm but not more than 4 cm in greatest dimension, limited to the thyroid
T3	Tumour more than 4 cm in greatest dimension limited to the thyroid or any tumour with minimal extrathyroidal extension (eg, extension to sternothyroid muscle or perithyroidal soft tissues)
T4a	Moderately advanced disease Tumour of any size extending beyond the thyroid capsule to invade subcutaneous soft tissues, larynx, trachea, oesophagus, or recurrent laryngeal nerve
T4b	Very advanced disease Tumour invades prevertebral fascia or encases carotid artery or mediastinal vessel
NX	Regional nodes cannot be assessed
N0	No regional lymph-node metastasis
N1a	Metastasis to level VI (pretracheal, paratracheal, and prelaryngeal/Delphian lymph nodes)
N1b	Metastasis to unilateral, bilateral, or contralateral cervical (levels I, II, III, IV, or V) or retropharyngeal or superior mediastinal lymph nodes (level VII)
M0	No distant metastases
M1	Distant metastases
Stage I	
Patient younger than 45 years	Any T, any N, M0
Patient older than 45 years	T1, N0, M0
Stage II	
Patient younger than 45 years	Any T, any N, M1
Patient older than 45 years	T2, N0, M0
Stage III	
Patient younger than 45 years	NA
Patient older than 45 years	T3, N0, M0; T1, N1a, M0; T2, N1a, M0; T3, N1a, M0
Stage IVA	
Patient younger than 45 years	NA
Patient older than 45 years	T4a, N0, M0; T4a, N1a, M0; T1, N1b, M0; T2, N1b, M0; T3, N1b, M0; T4a, N1b, M0
Stage IVB	
Patient younger than 45 years	NA
Patient older than 45 years	T4b, any N, M0
Stage IVC	
Patient younger than 45 years	NA
Patient older than 45 years	Any T, Any N, M1

Table 1.5. TNM classification system for differentiated thyroid carcinoma [22].

1.2.5 Multi-step carcinogenesis of thyroid neoplasms

According to the proposed model of thyroid carcinogenesis, risk factors, including exposure to radiation, induce genomic instability through direct and indirect mechanisms, resulting in early genetic alterations that involve the mitogen activated protein kinase (MAPK) signaling pathway. Oncogenic activation of MAPK signaling further increases genomic instability of thyroid carcinoma cells, possibly leading to later genetic alterations during cancer progression that involve other signaling pathways, cell-cycle regulators and adhesion molecules. This important role of genomic instability in thyroid cancer is highlighted in Figure 1.6 [3].

Follicular adenomas and carcinomas are frequently aneuploid with a high prevalence of loss of heterozygosity (LOH) involving multiple chromosomal regions. This chromosome instability is in contrast to the diploid or near-diploid content of most papillary carcinomas indicating discrete molecular pathways for these different types of thyroid tumors [55-57].

Transfection of mutant *BRAF*^{V600E} induces genomic instability in a rat thyroid cell line, manifesting as loss of chromosomal material, mitotic bridge formation and misaligned chromosomes [58-60].

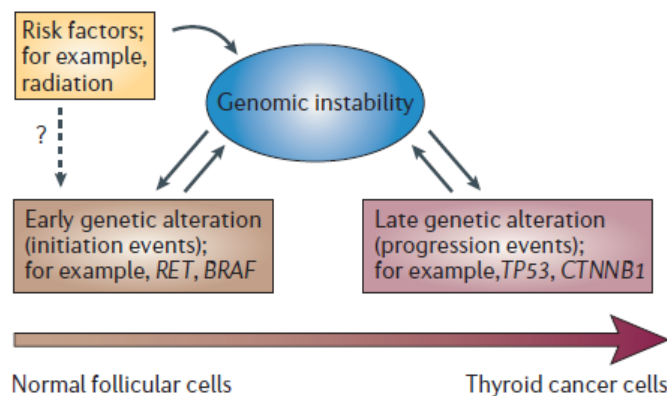


Figure 1.6. Genomic instability role in thyroid cancer.

Thyroid cancer initiation and progression occurs through gradual accumulation of various genetic and epigenetic alterations. In Figure 1.7 is depicted thyroid multi-step tumorigenesis model.

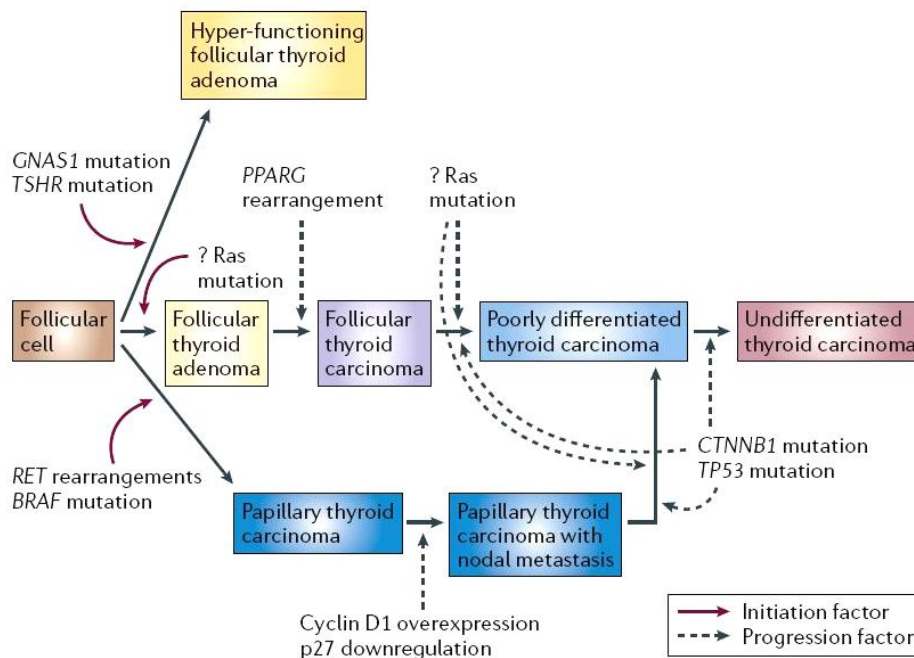


Figure 1.7. Thyroid multi-step tumorigenesis model [3].

Hyper-functioning follicular thyroid adenoma, tumors that are almost always benign lesions without a propensity for progression, follicular thyroid carcinoma and papillary thyroid carcinoma follow three distinct multi-step tumorigenesis pathways.

Gain-of-function mutations in the genes of TSH receptor (*TSHR*), a seven-transmembrane-domain G-protein-coupled receptor, and that encoding guanine nucleotide-binding α -subunit 1 (*GNAS1*), activate cAMP, thereby regulating thyroid hormone synthesis and the growth of follicular cells [61].

TSHR and *GNAS1* mutations occur in hyper-functioning thyroid adenomas but are rare in thyroid malignancies indicating that constitutive activation of the cAMP cascade alone is insufficient for the malignant transformation of thyroid follicular cells [3, 62].

In thyroid cancer critical genes are frequently mutated via two distinct molecular mechanisms: point mutation or chromosomal rearrangement. The main signaling pathways involved in thyroid carcinogenesis are MAPK and PI3K-AKT pathways (Fig. 1.8).

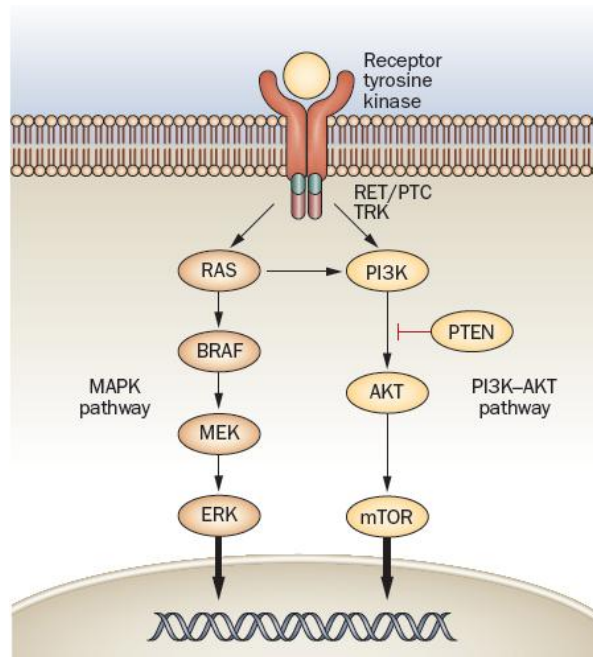


Figure 1.8. MAPK and PI3K-AKT signaling pathways [6].

Mutations and rearrangements described in thyroid cancer and their average prevalence are summarized in Table 1.9.

<i>Tumor type</i>	<i>Prevalence (%)</i>
Papillary carcinoma	
<i>BRAF</i>	45
<i>RET/PTC</i>	20
<i>RAS</i>	10
<i>TRK</i>	<5
Follicular carcinoma	
<i>RAS</i>	45
<i>PAX8-PPARγ</i>	35
<i>PIK3CA</i>	<10
<i>PTEN</i>	<10
Poorly differentiated carcinoma	
<i>RAS</i>	35
β -Catenin (<i>CTNNB1</i>)	20
<i>TP53</i>	20
<i>BRAF</i>	20
<i>AKT1</i>	15
Anaplastic carcinoma	
<i>TP53</i>	70
β -Catenin (<i>CTNNB1</i>)	60
<i>RAS</i>	50
<i>BRAF</i>	20
<i>PIK3CA</i>	20
<i>PTEN</i>	>10
Medullary carcinoma	
Familial forms <i>RET</i>	>95
Sporadic <i>RET</i>	50

Table 1.9. Molecular alterations and their average prevalence in thyroid cancer [17].

MAPK activation is crucial for tumor initiation: indeed, among known mutated genes in thyroid cancer can be found that encoding cell-membrane receptor tyrosine kinases *RET* and *NTRK1* and intracellular signal transducers *BRAF* and *RAS*. Papillary carcinomas may carry point mutations of the *BRAF* and *RAS* genes and *RET/PTC* and *TRK* rearrangements. These activating mutations are mutually exclusive and can be found in about 70% of papillary thyroid carcinomas [17, 63, 64].

Gain of function mutations of *RET* (REarranged during Transfection), located on chromosome 10q11.2, are involved in sporadic (~40%) and familial C-cell-derived medullary thyroid carcinoma (~80%), including multiple endocrine neoplasia 2A (MEN2A), MEN2B and familial medullary thyroid carcinoma [3, 65]. *RET* can be also altered by chromosomal rearrangements forming chimeric oncogenes, designated *RET/PTC*, that are involved in the development of papillary carcinoma. Somatic chromosomal rearrangement leads to fusion of the 3'-terminal sequence of *RET*, which encodes the tyrosine kinase domain, with the 5'-terminal sequences of heterologous genes. Wild-type *RET* is not normally expressed in follicular cells, whereas *RET/PTC* chimeric oncoproteins lack a signal peptide and transmembrane domain and are, therefore, expressed in the cytoplasm of follicular cells, under the control of the acquired promoters. Ligand-independent tyrosine phosphorylation is induced by constitutive dimerization of the fusion proteins and causes activation of signaling pathway [3, 66]. More than 17 *RET/PTC* rearrangements have been described [65]. In sporadic PTC the most common form is *RET* fusion with *CCDC6* (coiled-coil domain containing 6), also known as *RET/PTC1*, followed by *RET* fusion with *NCO4* (Nuclear coactivator 4), also known as *RET/PTC3*. These rearrangements represent more than 90% with *RET/PTC1* being detected in about two thirds and *RET/PTC3* in about one third of all positive cases [66]. *RET* rearrangements show high incidence (~80%) in PTC from patients exposed to radiations [67]. In PTC, they can be a subclonal event and can be also found in histologically benign thyroid nodules or in Hashimoto's thyroiditis [68-72].

The *RAS* gene family is composed by *KRAS*, *HRAS* and *NRAS*: these genes codify for G- proteins and their activation has been reported in all non-medullary thyroid tumors. Mutations of *KRAS* and *HRAS* have also been reported in sporadic medullary thyroid carcinomas. *RAS* mutations can frequently affect codon 61 of *HRAS* and *NRAS* in thyroid tumors and can be found in follicular adenomas (~35%), follicular carcinomas (~40%) and in the follicular variant of papillary carcinomas (~35%) [3, 6, 73]. Since *RAS* mutations can be also found in benign hyperplastic nodules, they are not specific for malignancy [74].

In follicular thyroid cancer, in addition to *RAS* mutations, another common event is *PAX8/PPAR γ* rearrangement [75]. The peroxisome proliferator-activated receptor- γ (*PPAR γ*), encoded by *PPARG* (located on chromosome 3p25), is a member of the steroid nuclear hormone receptor superfamily and is related to differentiating effects on adipocytes and insulin-mediated metabolic functions. Paired-box gene 8 (*PAX8*) encodes a transcription factor involved in the maintenance of the differentiated phenotype of thyroid follicular cells. *PAX8-PPARG* rearrangements were first identified in follicular thyroid neoplasms with the cytogenetically detectable translocation t(2;3)(q13;p25) that generates a chimeric gene encoding the DNA-binding domain of the thyroid-specific transcription factor *PAX8* and domains A-F of *PPAR γ* . The mechanisms of transforming activity remain to be fully understood [3]. *PAX8/PPAR γ* occurs in follicular thyroid carcinoma with a frequency of ~30%, and is also found in a small proportion of follicular adenomas (<13%) and of the follicular variant of papillary carcinomas (~10%) [73]. The activating mutations described in follicular carcinomas are also mutually exclusive and identified in approximately 80% of these cancers [17].

BRAF and *RAS* mutations are frequently found in both well-differentiated thyroid cancer and in poorly differentiated and anaplastic carcinomas, thus, probably representing an early event in thyroid cancer progression. However, thyroid cancer progression and dedifferentiation involve a number of additional mutations that affect other cell signaling pathways. Late events, not found in well-differentiated cancers but frequently found in anaplastic and poorly differentiated

carcinomas, include point mutations of the *TP53* and *CTNNB1* genes, encoding p53 and β -catenin respectively, as well as mutation in genes that encode effectors of the PI3K-AKT signaling pathway [6, 76-78].

1.3 Papillary thyroid carcinoma (PTC)

1.3.1 Histopathology

Papillary carcinoma (PTC) is a malignant epithelial tumor showing evidence of follicular cell differentiation, characterized by papillary growth and diagnosed on the basis of distinctive nuclear features. Papillary architecture is typically complex with branching in which the surfaces of the papillary cores are covered by neoplastic cells. In tumor lacking complex papillary structures, the diagnosis relies on the nuclear features. These diagnostic features include nuclear enlargement and irregularity, overlapping, clearing (ground glass or Orphan Annie appearance), grooves, and pseudoinclusions. Indeed, these nuclei are larger and more oval than normal follicular nuclei and contain hypodense chromatin. Moreover, they show the presence of grooves, often overlap one another and intranuclear inclusions of cytoplasm can be observed [4].

These nuclear features allow PTC to be distinguished from nodular goiter, follicular adenomas and diffuse hyperplasia sometimes showing papillary structures. Indeed, some of the histologic changes that can be observed in thyroid hyperplasia (HYP), an enlargement of the thyroid gland that does not result from inflammation or neoplasia and whose most common manifestation is the sporadic goiter, can sometimes lead to an incorrect diagnosis of malignancy [79].

In PTC a pure papillary growth is uncommon: this architectural pattern often coexist with other patterns such as varying sized follicles, solid and trabecular. Squamous metaplasia is common and, in cystic tumors, may be extensively present at the cyst lining. Intratumoral fibrosis, peritumoral lymphocytic infiltrates and psammoma bodies are also common features of these tumors [4, 80].

Psammoma bodies (PBs) are 50-70 μm in size rounded and concentrically lamellated calcifications observed in PTC and rarely in non-neoplastic lesions, including Hashimoto's thyroiditis, multinodular goiter or benign hyperplastic thyroid nodules [81-84]. They are present in paraffin sections of approximately 40-50% PTC cases. Psammoma bodies are usually present within the cores of papillae, in the tumor stroma, or in lymphatic vessels, but not within the colloid of neoplastic follicles [80]. As early as 1959, Klinck and Winship considered PBs in PTC as the remnants of dead papillae [85]. Residual neoplastic cells are sometimes observed intimately associated with PBs in PTC [86]. PBs are considered the result of focal areas of infarction of the tips of papillae, attracting calcium that is deposited on the dying cells [87, 88]. According to another theory, an intracellular accumulation of calcium by tumor cells leads to their death and release of the calcium. Progressive infarction of the papilla and following calcium deposition lead to lamellation. [86]. PBs may represent, also in benign lesions, the remnants of neoplastic papillae. The deposition of collagen and concentric calcification in the central vascular core may lead to compromise in nutrient supply to the tumor cells resulting in their degeneration or necrosis and disappearance. This may be one of the reasons behind finding of PBs in Hashimoto's thyroiditis and colloid goiters, in areas away from the PTC tumor mass. Moreover, the degeneration and necrosis of tumor cells following the formation of PBs may also explain partly the indolent course and excellent prognosis associated with PTC. Therefore, PBs may also act as a barrier against the spread of tumor cells [86]. However, in a recent study a significant correlation between the presence of PBs and tumor multifocality, extrathyroidal extension, and lymph node metastasis in PTCs was observed, suggesting that the presence of PBs may predict aggressive tumor behaviors in PTC patients [89].

1.3.2 Histopathological variants and associated molecular alterations

PTC can be further classified into numerous histologically distinct variants, including the most common classical PTC, follicular-variant PTC, and tall-cell PTC, and uncommon such as oncocytic, solid and cribriform subtypes, each with distinct growth patterns and behaviors [90].

Classical PTCs (PTC CI) are characterized by a complex branching architecture in which the surfaces of the papillary cores are covered by neoplastic cells [4].

Follicular variant PTCs (PTC FV) are composed almost exclusively of follicles having the characteristic nuclear features of PTC and may be encapsulated (approximately one third of the tumors) or non-encapsulated. The follicular variant is one of the most common and most diagnostically challenging: inter-observation variation in the diagnosis of these tumors, particularly the encapsulated type, is high since the nuclear features may be focal or poorly developed. Lymph node metastases and rarely hematogenous metastasis can occur despite complete encapsulation, however prognosis is similar to conventional PTC [4, 19, 91].

The tall cell variant of PTC (PTC TC) is a rare variant defined by cells that are at least three times as high as they are wide, an eosinophilic cytoplasm, and the nuclear features of PTC [4, 92].

Histopathological findings show the tumors to be a combination of papillary, trabecular or cord-like patterns while follicular structures are rare. This variant has been poorly defined because the height of the neoplastic cell is variable, depending also upon the plane of section, and because a significant proportion of tall cells is present in different types of papillary carcinoma leading to misdiagnosing. A diagnosis of the tall cell variant of PTC is made when $\geq 50\%$ of cells are tall cells [92].

In this variant necrosis, mitosis and extrathyroidal extension are common. Tall cell variant occur in older patients, often males, and shows a more aggressive clinical behavior than conventional PTCs [4].

As previously discussed in section 1.2.5, PTCs show typically mutually exclusive mutations occurring in approximately 70% of cases: these molecular alterations are associated with particular clinical, histopathological and biological tumor characteristics described in Figure 1.10 [6]. Indeed, *BRAF*^{V600E} mutation is typically found in papillary carcinomas with classic papillary and tall cell histology cell and is rare in the follicular variant of papillary carcinoma [93, 94]. By contrast, *BRAF*^{K601E} mutation is typically found in the follicular variant of papillary carcinoma. *BRAF* mutations will be further discussed in sections 1.4.4-1.4.6 [95, 96].

Moreover, virtually all PTCs that harbor a *RAS* mutation grow forming neoplastic follicles and no papillary structures and are, therefore, diagnosed as follicular variant of papillary carcinoma [93, 97]. Moreover, *BRAF* point mutation is most common in sporadic tumors, whereas *AKAP9-BRAF* rearrangement is more common in papillary carcinomas associated with radiation exposure. *AKAP9-BRAF* rearrangement results in a fusion protein containing the protein kinase domain and lacking the autoinhibitory N-terminal portion of *BRAF*. This mutant protein shows elevated kinase activity and transforms NIH3T3 cells. [36].

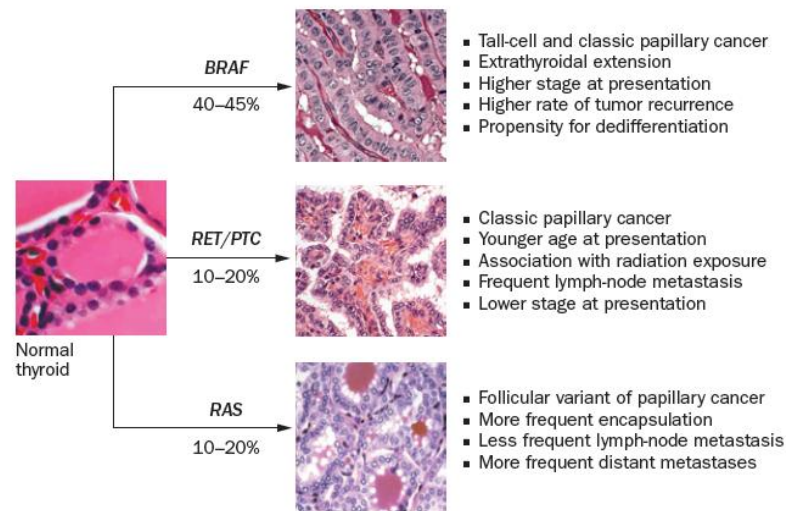


Figure 1.10. Average prevalence of molecular alterations in PTC and their association with clinical and histopathological features [6].

1.3.3 Papillary thyroid microcarcinoma (mPTC)

The term microcarcinoma includes different definitions used in the past, such as small carcinoma, minimal carcinoma, occult carcinoma, non-palpable carcinoma and incidentaloma. Since almost all the tumors are of papillary histotype, the preferred definition is now micro-Papillary Thyroid Carcinoma (mPTC). Papillary thyroid microcarcinoma is defined as papillary carcinoma of 1 cm or less in size commonly incidentally found in thyroids removed for other reasons, including benign clinical nodules or diffuse processes such as thyroiditis, and in autopsy series [4].

Indeed, mPTCs occur in up to 30% of autopsies and in up to 24% of surgical thyroidectomies performed for disorders unrelated to PTC [19, 98]. These tumors are commonly located near the thyroid capsule, are often non-encapsulated and sclerosing. In children mPTC can show a more aggressive behavior and rarely in adults may present with cervical nodal metastasis [4].

Indeed, papillary microcarcinoma is an extremely indolent tumor, however, up to 11% of thyroid microcarcinomas are the primary lesion to a lymph node metastasis presenting clinically as a neck mass and can exhibit local recurrences. In this situation, the tumor should be treated as a clinical cancer. Multifocality in mPTC is reported in 20% to 46% of cases and up to 40% of these patients can present with lymph node metastases [99]. Clinicopathological features, such as age more than 45 years, tumor size greater than 5 mm, male sex, multifocality, lymph nodes metastasis, and extrathyroidal extension have been reported to predict poor prognosis [100, 101]. The disease-specific mortality rate from mPTC is up to 2% in some series [102, 103].

Familial cases of papillary thyroid microcarcinoma with unfavorable behavior have also been reported [104]. Among risk factors, irradiation to the thyroid is considered predisposing for mPTC, however, this tumor does not show a strong sex predilection as compared with other thyroid diseases, which are more common in women [99].

Molecular analysis of mPTC showed the presence of *RET/PTC* rearrangements with a frequency of 42.3% and 52.0% in two different series and *BRAF* mutations in 17.6%-70% [105-111].

Therefore, both *RET/PTC* rearrangements and *BRAF* mutations may represent early genetic lesions in papillary thyroid cancer [112]. A high prevalence of this mutation was observed in certain histologic subtypes (classic, tall cell, subcapsular and occult sclerosing variants) in contrast to the follicular variant of papillary thyroid microcarcinoma [106, 108, 111].

1.4 Oncogene *BRAF* and its role in papillary thyroid carcinoma

1.4.1 Gene and protein function

The *BRAF* gene (v-raf murine sarcoma viral oncogene homolog B) is located on the long arm of chromosome 7 at position 34 (7q34) and covers about 190 kb. It contains 18 coding exons and 5 splice variants have been identified: the full-length transcript is made up of 2,480 bp and encodes a full-length protein of 766 amino acids (94 kDa) [113-115].

BRAF is a serine-threonine kinase belonging to the family of RAF proteins. There are three isoforms of RAF proteins originating from 3 independent genes in mammals: ARAF, *BRAF*, and CRAF (also called RAF-1) [116]. These serine-threonine protein kinases are intracellular effectors of the conserved RAS/RAF/MEK/MAPK signal transduction pathway (Fig. 1.11). This pathway is activated by growth factors, hormones, and cytokines and propagate signals from cell membrane receptor tyrosine kinases (RTKs) to the nucleus where transcription of genes involved in cell differentiation, proliferation, and survival is regulated [117].

The ligand-mediated activation of receptor tyrosine kinases triggers the release of guanosine diphosphate (GDP) and guanosine triphosphate (GTP) loading of the RAS GTPase: this active state of RAS G-proteins can cause activation of the MAPK and other signaling pathways, such as PI3K-AKT. Normally, the activated

members of the RAS family of proteins, including KRAS, HRAS, and NRAS, becomes quickly inactive due to their intrinsic guanosine triphosphatase (GTPase) activity and the action of cytoplasmic GTPase-activating proteins. RAS proteins are attached to the inner surface of the plasma membrane and their activation triggers recruiting of RAF kinases to the cell membrane for activation and result in phosphorylation and activation of downstream targets along the MAPK cascade. RAF triggers phosphorylation and thus activation of the mitogen-activated protein kinase (MAPK)-extracellular signal-regulated kinases 1 and 2 (MEK1 and MEK2), which in turn phosphorylate extracellular signal-regulated kinases 1 and 2 (ERK1 and ERK2) on threonine and tyrosine residues. ERK1 and ERK2 regulate cellular functions through phosphorylation of both cytosolic proteins and nuclear substrates such as transcription factors [118].

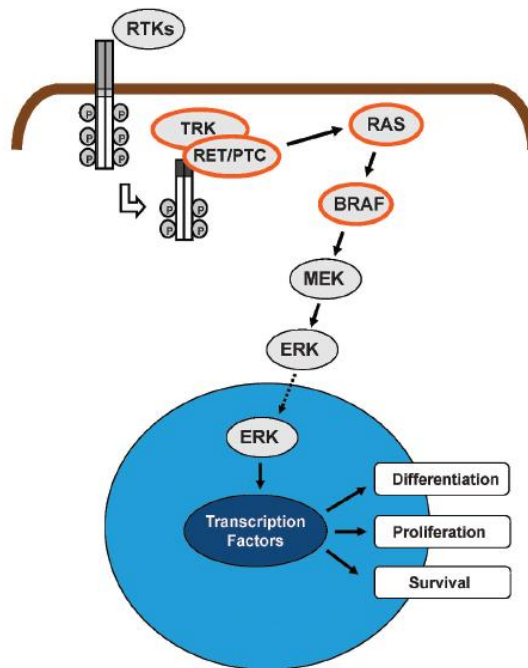


Figure 1.11. The mitogen-activated protein kinase (MAPK) signaling pathway [119].

1.4.2 RAF protein structures

All RAF proteins share three conserved regions (CR) with distinct functions: the regulatory domains CR1 and CR2 at the N terminus and the kinase domain CR3 at the C terminus (Fig. 1.12) [120].

CR1 encompasses a RAS binding domain (RBD) necessary for the interaction with GTP-bound activated RAS and with membrane phospholipids. CR1 contains also a secondary RAS-binding site, a cysteine rich domain (CRD), which is also required for the interaction of CR1 with the kinase domain for RAF autoinhibition [121, 122].

CR2 contains inhibitory phosphorylation sites involved in the negative regulation of RAS binding and RAF activation: their dephosphorylation is prerequisite for RAS binding and RAF activation [123].

CR3 includes the kinase domain with the activation segment, a region of 10-30 amino acids bounded by almost invariant DFG and APE motifs, in which the phosphorylation sites, threonine and serine residues necessary for kinase activation, are located.

There is also a negatively charged (N) region upstream of the CR3 whose phosphorylation is necessary for RAF activation and a glycine-rich loop (G-loop) which clamps ATP into the catalytic cleft forming a loop that anchors the β - and γ -phosphates of ATP [124].

Differences in the N region of ARAF, BRAF, and CRAF have an important role for the differential regulation of these isoforms: in CRAF, the phosphorylation of S338 and Y341 is necessary for activation by RAS (homologous to S299 and T302 respectively in ARAF). Unlike ARAF and CRAF, BRAF N-region carries a constitutive negative charge that primes it for activation. Indeed, in BRAF the constitutive phosphorylation of the serine 446 (homologous to CRAF S338) residue and the replacement of Y340 and Y341 by aspartic acids (D448 and D449) imply that dephosphorylation of negative regulatory sites and RAS binding are probably the only requirements for BRAF activation [118, 125-129].

In the inactive conformation RAF is believed to form a closed structure, with the regulatory domain (in particular the cysteine rich domain) interacting with the kinase domain. During activation, this closed conformation is destabilized

allowing for RAS binding and membrane recruitment, thus obtaining a stabilized ‘open’ active conformation [130, 131].

The recruitment to the plasma membrane is necessary for the activation of all RAF isoforms because the activation segment phosphorylation and, in the case of ARAF and CRAF, also N-region phosphorylation occur at the plasma membrane [130].

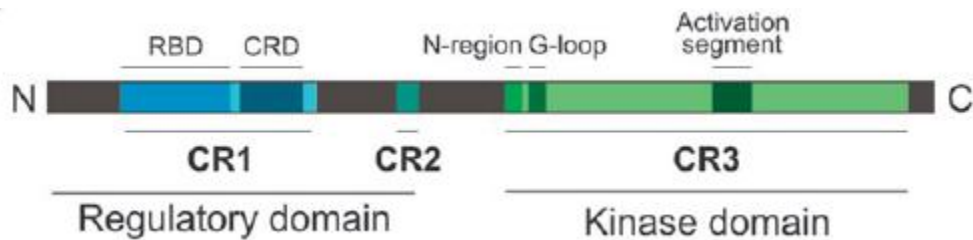


Figure 1.12. Common schematic structure of the RAF proteins [129]. CR 1-3, conserved regions; RBD, RAS-binding domain; CRD, cysteine-rich domain.

In BRAF the phosphorylation of threonine 599 and serine 602 (homologous to T491 and S494 in CRAF) in the activation loop of CR3 is essential for activation by RAS: T599 is the major activation segment phosphorylation site, whereas S602 is a relatively a minor one [125, 126, 132].

The crystal structure of BRAF has revealed intramolecular hydrophobic interactions between the glycine-rich loop (shown in green in Fig. 1.13) and the activation segment (shown in magenta in Fig.1.13) that establish a BRAF inactive conformation displacing the DFG motif in activation segment, which includes a catalytic aspartate residue, to a position that is incompatible with catalysis. Phosphorylations within the activation segment or amino acid substitutions in both regions of the kinase can break these intramolecular interactions and activate BRAF [129, 130].

T599 phosphorylation is essential for BRAF activation through the release of the activation segment and reorientation of critical residues into the correct position for catalysis: this residue is positioned at the interface of the glycine-rich loop and activation segment interaction domain and probably disrupts the interaction allowing the DFG motif to adopt the active conformation.

Moreover, D448 in the N region (shown in rust in Fig. 1.13) contacts R506 of the α C-helix (the interaction is shown by the red dashed line in Fig. 1.13) stabilizing the active conformation: this may be the reason why this aspartate is important for the basal and RAS-stimulated kinase activity of BRAF [130].

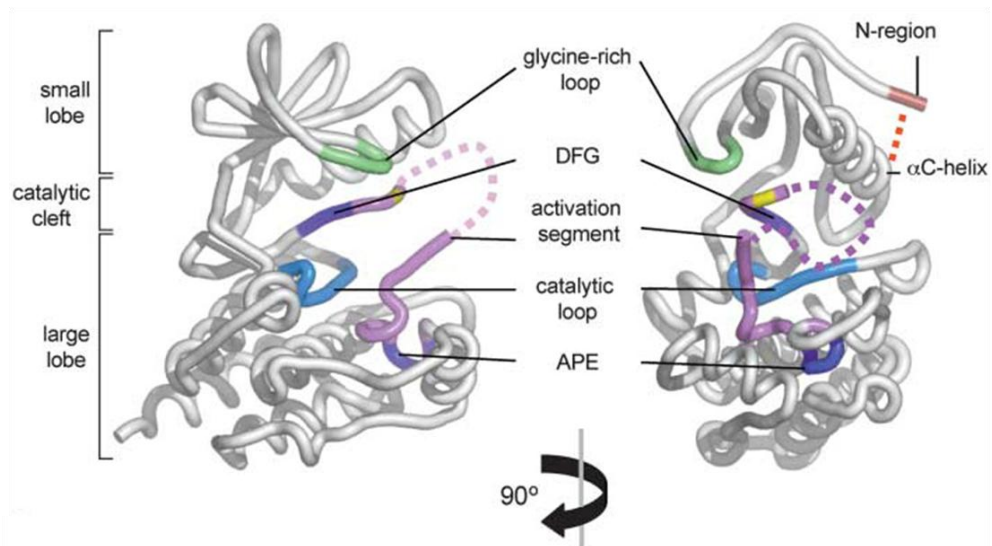


Figure 1.13. BRAF kinase domain structure. A portion of the activation segment is disordered and is indicated by the dashed magenta line. T599 phosphorylation site is colored yellow. In the structure of the BRAF kinase domain (residues 448-726), BAY43-9006, the inhibitor that BRAF was crystallized with, has been omitted [118].

Among the three RAF isoforms, BRAF is the most potent activator of the MAPK pathway and is by far the most frequently mutated RAF protein in human cancer: the explanation lies in these fundamental regulatory differences [126, 133].

1.4.3 *BRAF* mutation prevalence

BRAF-activating mutations were discovered in 2002 and enlarged the number of known genetic alterations that activate the MAP kinase pathway, further confirming the importance of this pathway in human cancer. BRAF is commonly activated by somatic point mutation in a range of human cancers. *BRAF* somatic missense mutations can be found malignant melanoma (27%-70%), colorectal cancer (5%-22%), serous ovarian cancer (~30%) and at lower frequency in a variety of other human cancers (1%-3%) [118, 134].

BRAF mutations in thyroid cancer show a prevalence second only to that in melanoma. Point mutations of the *BRAF* gene are the most common genetic alteration in thyroid papillary carcinomas: they can be found in 40%-45% of these tumors [135, 136].

Activating point mutations of the *BRAF* gene are clustered in the kinase domain in exons 11 (G-loop) and 15 (activation segment) of the gene: mutations in exon 11 of the *BRAF* gene were not found in thyroid cancer [63, 134-136].

Most of them are point mutations in exon 15 involving nucleotide 1799 that result in a valine to glutamate substitution at residue 600 (V600E): *BRAF*^{V600E} accounts for about 95% of *BRAF* mutation in thyroid papillary carcinomas. The association of PTCs with the *BRAF*^{V600E} mutation was demonstrated in numerous studies with patients from different geographical and ethnic backgrounds supporting the fundamental role of this mutation in the pathogenesis of thyroid papillary carcinoma [94, 119, 137].

In papillary thyroid carcinoma, *BRAF*^{V600E} is typically found in tumors with classic papillary (60%) and tall-cell histology (80%) and is rare in the follicular variant (10%) (Fig. 1.14) [93, 94].

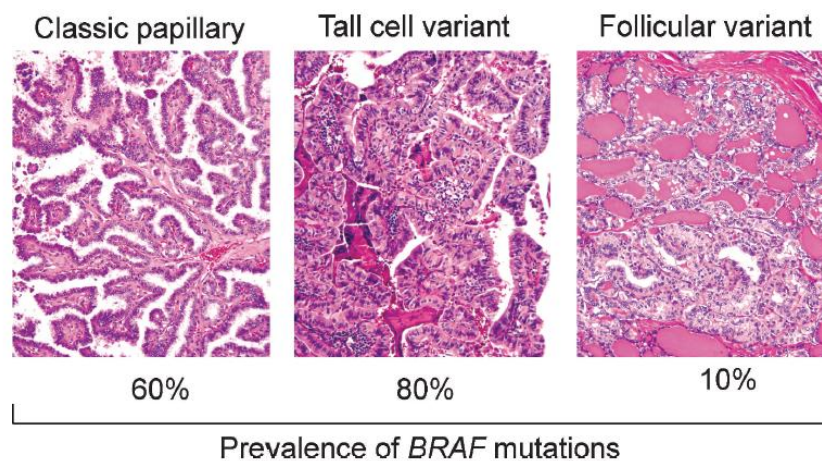


Figure 1.14. Prevalence of *BRAF* mutations in different histologic variants of thyroid papillary carcinoma (Hematoxylin-Eosin, original magnification $\times 100$) [119].

Therefore, *BRAF*^{V600E} mutation in papillary thyroid carcinoma shows a subtype-related prevalence that may explain the tendency of tall-cell and classic PTC subtypes to be more aggressive than follicular-variant PTC: this is consistent with

the idea that $BRAF^{V600E}$ mutation has a causal role in thyroid cancer's aggressivity [94, 138].

Since the other subtypes of PTC are uncommon, the prevalence of $BRAF^{V600E}$ mutation in these tumors has rarely been reported: in a study by Trovisco *et al.* $BRAF^{V600E}$ mutation was found in six out of 15 (40%) oncocytic-variant PTCs and six out of eight (75%) Warthin-like PTCs, but not in diffuse sclerosing PTCs, columnar cell variant PTC, hyalinizing trabecular thyroid tumors, or in mucoepidermoid thyroid tumors [96].

$BRAF^{V600E}$ mutation has also been found in poorly differentiated and anaplastic thyroid carcinomas (24%), especially in those tumors with the co-existence of areas of well differentiated papillary carcinoma. In these tumors both areas harbored $BRAF^{V600E}$ mutation suggesting that they were likely derived from $BRAF$ mutation-positive PTCs and that $BRAF^{V600E}$ is an early event in the tumorigenesis. $BRAF^{V600E}$ has not been identified either in follicular thyroid carcinomas, although in these tumors BRAF up-regulation may happen through increased gene copy number, or medullary thyroid carcinomas or benign thyroid neoplasms (adenoma or hyperplasia). Therefore, this mutation can be considered a quite specific marker of papillary thyroid carcinoma [94, 139, 140].

Other $BRAF$ mutations have been found in 1% to 2% of papillary thyroid carcinomas, including other point mutations, small in-frame insertions or deletions and rearrangements [119].

Among point mutations, $BRAF^{K601E}$ was detected in two follicular adenomas (one from a study in post-Chernobyl tumors), in the follicular variant of PTC (7-10% of PTC FV) and in one sample of a case of classical follicular thyroid carcinoma (the first case found of a classical FTC carrying a $BRAF$ mutation) whereas, as previously discussed, $BRAF^{V600E}$ mutation appears to be prevalent in PTC with a predominantly papillary architecture: these data support the hypothesis that the follicular variant of PTC shows genetic differences from conventional PTC [64, 96, 141-144].

1.4.4 *BRAF*^{V600E} mutation

BRAF^{V600E} mutation is a thymidine to adenosine transversion at nucleotide 1799 converting valine to glutamate at hot spot codon 600 (V600E) and resulting in constitutive activation of BRAF and the MAPK signaling pathway [130, 134].

This mutation had been previously called T1796A, based on the NCBI GenBank nucleotide sequence NM_004333, which missed a codon in exon 1 of the *BRAF* gene. The assessment of the NCBI GenBank nucleotide sequence NT_007914 version correctness caused a change in nucleotide numbering after nucleotide 94 (starting from ATG codon), therefore, this *BRAF* mutation is now designated T1799A [145].

BRAF^{V600E} activates BRAF kinase by mimicking phosphorylation of the activation segment through the insertion of a negatively charged residue beside the conserved regulatory phosphorylation sites T599 and S602: this substitution disrupts the association of the activation segment with the ATP-binding domain converting BRAF to a catalytically active conformation.

Since the substitution at the position of a regulatory phosphorylation site from a threonine or serine residue to an acidic amino acid cannot be generated by a single base change, such mutations are probably rare in human disease, therefore amino acids other than threonine and serine can be more frequently mutated to acidic residues to mimic phosphorylation and activate kinases. Thus, it's likely that a glutamate mutation at residue 600 occurs at high frequency because it only requires a single base substitution. This phospho-mimetic substitution is one of the most active mutants harboring an *in vitro* kinase activity about 500 fold greater than that of wild-type BRAF and enhancing ERK activation by about 4-fold in COS cells [94, 130, 134].

The transforming and oncogenic potential of the *BRAF*^{V600E} mutation has been widely shown: in NIH3T3 mouse embryonic fibroblast cells and murine melanocytes, this mutation stimulates constitutive ERK signaling, induces proliferation and transformation, and allows these cells to form tumors when assayed for tumorigenicity in nude mice [118, 130, 131, 134, 146].

$BRAF^{V600E}$ mutation represents a somatic genetic alteration in sporadic thyroid cancers and is not a germline mutation in familial non-medullary thyroid cancer [136, 147, 148].

Germline variations at the valine 600 residue were not found in a large case study of malignant melanomas too [149].

1.4.5 Other *BRAF* mutations of V600 residue

In addition to $BRAF^{V600E}$ mutation, numerous other *BRAF* substitutions have been rarely described in papillary thyroid carcinoma and other cancers and some of them have also been tested with respect to the activation or impairment of the kinase activity of BRAF.

In a functional study performed by Wan and colleagues, *BRAF* mutants were divided in three groups according to their *in vitro* basal BRAF kinase activity: in the high activity group were collected mutants approximately 130 ($BRAF^{E586K}$) to 700 ($BRAF^{V600D}$) fold more active than basal $BRAF^{wt}$, in the intermediate activity group those 1.3 ($BRAF^{G469E}$) to 64 ($BRAF^{L597V}$) fold higher than $BRAF^{wt}$ and in the impaired activity group those mutants whose basal kinase activities were reduced.

V600 residue can be mutated to other amino acids whose activities are similar to that of $BRAF^{V600E}$: these mutations can be found at a very low frequency in cancer (0.1% to 2%) probably because they are the result of tandem nucleotide changes, which are very rare. V600K is an example of such mutations [118, 130].

In a study by Brzezińska and colleagues, mutational screening of exon 15 of *BRAF* gene by direct sequencing in papillary thyroid carcinoma in the Polish population revealed the presence of two uncommon heterozygous missense mutations that had not been previously described in thyroid tumors. They observed in two cases the overlapping mutations V600K/V600E where the presence of V600E mutation was confirmed by real-time allele specific and in a different case a V600M mutation. V600K mutation is the result of a 2-bp change (GT1798-99AA), whereas V600M is a single nucleotide substitution in the first

nucleotide position (G1798A) in codon 600 of *BRAF* gene [150]. V600K mutation had not been previously described in thyroid tumors but it had been reported in human malignant melanomas as the second, regarding the frequency, after V600E mutation [149]. Authors suggested that G1798A and T1799A found by direct sequencing were most likely to occur on the same chromosome: thus, these in *cis* base substitution resulted in a V600K mutation in one allele [150]. This mutation seems to be characteristic for invasive and metastatic melanoma [151-153].

V600K is an activating mutation that causes a substitution of valine for a positively charged lysine in contrast to the *BRAF*^{V600E} negative charge substitution: this altered distribution of charged residues within the activation segment implies augmented *in vitro* kinase activity (~160 fold higher than *BRAF*^{wt}), although at a much lower level compared with *BRAF*^{V600E}, and ERK stimulation [130].

V600M and V600A (T1799C) mutations has been reported in other tumors such as melanoma and prostatic adenocarcinoma but, to the best of our knowledge, the result of substitutions of these uncharged nonpolar amino acid, methionine and alanine, for the uncharged nonpolar amino acid valine on *BRAF* kinase activity has not been tested [118, 152, 153].

1.4.6 Other *BRAF* mutations in exon 15

Many cancer-associated mutations described in *BRAF* cluster to the glycine-rich loop and the activation segment, the two regions of the kinase domain that are responsible for trapping *BRAF* in the inactive conformation (Fig. 1.15) [126].

Among *BRAF* exon 15 mutations that do not involve the “hot spot” codon 600, *BRAF*^{E586K} has been identified in ovarian cancer and melanoma [134, 154]. Glutamic acid 586 is highly conserved in *RAF* family of proteins being found at the corresponding position in all *RAF* orthologues and paralogues. This residue is located outside of the P loop and DFG motif on the opposite surface of the kinase domain from the DFG motif, thus is not involved in stabilizing the glycine-rich loop/activation segment interaction. E586 is part of a large surface responsible for the kinase autoinhibition through a potential intramolecular interaction with the

N-terminal domain probably disrupted by its mutation. The substitution of this negatively charged amino acid for the positively charged lysine, $BRAF^{E586K}$, produces an high activity mutant (~130 fold kinase activity higher than $BRAF^{wt}$) that stimulates strong constitutive ERK signaling in COS cells [118, 126, 130, 134].

Another mutation in exon 15, $BRAF^{G593D}$, has been described in colorectal cancer and, along with $BRAF^{V600E}$ mutation, in a follicular variant papillary microcarcinoma but the significance of this mutation remains uncertain and requires further studies [45, 155].

Mutations that occur at aspartic acid 594 ($D594$) cause in BRAF (as in other kinases) inactivation and thus these cancer mutants cannot phosphorylate MEK, activate CRAF, or stimulate cell signaling [130, 146]. Indeed, the carboxy oxygen of this highly conserved residue (the “D” of the DFG motif) plays a critical role in chelating Mg^{2+} and stabilizing ATP binding in the catalytic site [124]. These mutants therefore appear catalytically and biologically inactive: many mutants have been found in human cancer such as $BRAF^{D594N}$ in melanoma [154, 156, 157].

A mutation replacing alanine 598 with valine was identified in a follicular variant of papillary thyroid carcinoma (PTC FV). $BRAF^{A598V}$ induces local perturbation of the protein structure that may explain the up-regulation of the BRAF kinase activity and its MAPK downstream signaling factors such as ERK and MEK observed by functional analysis. Indeed, functional studies *in vitro* revealed that $BRAF^{A598V}$ leads to up-regulation of BRAF kinase activity with similar ERK activation in both $BRAF^{A598V}$ and $BRAF^{V600E}$ mutations [158].

As previously discussed, threonine 599 is the major activation segment phosphorylation site [132]. Replacement of threonine 599 with isoleucine strongly activates BRAF probably because the bulky side chain of isoleucine disrupts the inactive conformation of the activation segment similarly to what happens during threonine 599 phosphorylation. $BRAF^{T599I}$ heterozygous mutation has been described in melanocytic nevi and melanoma lesions where coexistence of $BRAF^{V600E}$ and $BRAF^{T599I}$ mutations was also observed in a specimen [153, 159]. According to the functional analysis by Wan and colleagues, it is an intermediate

activity kinase mutant (~30 fold higher than $BRAF^{wt}$) harboring much lower kinase activity compared with $BRAF^{V600E}$ that increases ERK signaling in COS cells and causes the transformation of NIH3T3 cells [130].

As previously discussed, another common $BRAF$ mutation reported in papillary thyroid carcinomas (PTC FV), in benign follicular adenomas and a case of classical follicular thyroid carcinoma is $BRAF^{K601E}$ [64, 96, 141, 143, 144]. It was also found in other tumors such as melanoma and colorectal carcinoma [160, 161]. It is a single nucleotide substitution in the first nucleotide position (A1801G) in codon 601 of $BRAF$ gene changing a lysine for a glutamate. $BRAF^{K601E}$ is a high activity kinase mutant (~140 fold higher than $BRAF^{wt}$) and greatly increase ERK and NF κ B signaling, and the transformation of NIH3T3 fibroblasts [130, 146]. Lys601 has an important role in ligand activity, selectivity and protein stabilization, proposing an explanation of the observed strong kinase activation for the $BRAF^{K601E}$ mutated form [162].

Heterodimerization may play a pathophysiological role in cancer: less frequent mutations that cause impaired BRAF kinase activity, such as $BRAF^{G596R}$, cannot stimulate efficient activation of MEK, but can stimulate CRAF activity, which then activates MEK. Therefore, the ability of low-activity $BRAF$ mutants to activate the ERK pathway is dependent on CRAF protein [130].

The transactivation is obtained by low-activity $BRAF$ mutants found in cancer merely as a result of the formation of a heterodimer between the mutant BRAF and CRAF.

While physiological heterodimerization is induced by RAS activation, oncogenic BRAF mutants constitutively dimerize with CRAF [128, 163, 164].

Among small in-frame insertions or deletions surrounding codon 600 can be mentioned V599Ins, VK600-1E, V600D + FGLAT601–605ins and T599I-VKSR(600-603)del and T599I+V600delinsAL [165-171].

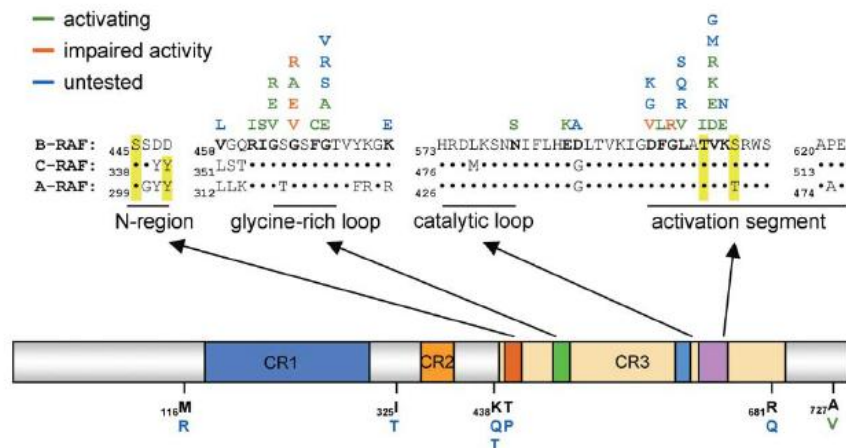


Figure 1.15. Some cancer-associated *BRAF* mutations. BRAF amino acids conserved in ARAF and CRAF are shown by a dot. The yellow bars indicate phosphorylation sites. DFG motif/activation segment is partly included in exon15 (codon 582 to 620). BRAF mutated residues in cancer are shown in bold, with the amino acid substitutions above the sequence. Activating substitutions are shown in green, those that impair BRAF kinase activity in red, and untested in blue. Mutated residues outside these core regions are shown below the schematic [118].

1.4.7 The role of *BRAF* mutation in the initiation and progression of PTC

The high frequency and specificity of *BRAF*^{V600E} mutation suggest that this mutation may play a fundamental role in the initiation of PTC tumorigenesis. This idea was supported by clinical findings such as high prevalence of *BRAF*^{V600E} in mPTC and by the results of experiments in thyroid follicular cells and in preclinical mouse models [96, 108, 111, 140, 172].

BRAF^{V600E} was shown to induce transforming features in thyroid follicular cells in culture, such as up-regulation of chemokines and their receptors which in turn stimulate proliferation and invasion [173]. Thyroid-induced expression of *BRAF*^{V600E} in transgenic mice, a model that better reflect non-hereditary human thyroid cancers, leads to the development of tumors with histological features that recapitulate the phenotype of *BRAF*-mutated PTC in humans [174, 175]. Therefore, *BRAF*^{V600E} mutation may represent the first hit or an early event in thyroid tumorigenesis.

However, sometimes *BRAF* mutation may be preceded by other genetic alterations occurring in already developed PTC as suggested by the observation that *BRAF*^{V600E} can be detected in lymph node metastasis but not in the corresponding primary tumors [176]. Moreover, papillary thyroid carcinoma with the *BRAF*^{V600E} mutation often presents with extrathyroidal invasion, lymph node metastasis, and advanced tumor stage [171, 177].

This finding are consistent with a role of *BRAF*^{V600E} mutation in facilitating the metastasis and progression of PTC in lymph nodes as evidenced by experiments in preclinical models: PTC induced in transgenic mice also undergo dedifferentiation and become more aggressive, suggesting a role in tumor progression and recapitulating the association of *BRAF* mutation in PTC with a poorer prognosis [175].

Some reports of the presence of *BRAF* mutation in both the differentiated PTC components and the poorly differentiated components in PDC and ATC of the thyroid suggest that *BRAF* mutation occurs early in the tumorigenesis and has also a role in disease progression [140, 178].

1.4.8 *BRAF* in the diagnosis of PTC

Thyroid nodules may be found by palpation in 4-7% of the general population, and this prevalence may approach 60% using high-resolution ultrasonography (USG), however, only a small proportion of these nodules is malignant [179].

The most reliable diagnostic test for thyroid nodules is Fine-needle aspiration (FNA) with cytological evaluation, which establishes the definitive diagnosis of a benign or malignant lesion in the majority of cases. However, a conclusive diagnosis can't be obtained by use of FNA in some cases that are diagnosed as indeterminate for malignancy. In 2011, a meta-review of 11 large studies from the USA published between 2002 and 2010, showed that a median of 72% (range 62-85%) of FNA were diagnosed as benign, 5% (1-8%) were malignant, 17% (10-26%) were indeterminate, and 6% (1-11%) were non-diagnostic. Among patients with FNA diagnosed as indeterminate by cytology who underwent surgery, a median of 34% (range 14-48%) had a malignant lesion. Since this occurrence is too high to recommend watchful waiting, the United States National Cancer

Institute (NCI) sponsored a State of the Science Conference in 2007 in Bethesda, to review diagnostic terminology and morphological criteria for cytological diagnosis of thyroid lesions. The Bethesda classification further divided the general category of indeterminate cytology into three subcategories: atypia of undetermined significance or follicular lesion of undetermined significance, with malignancy in 5-10% of cases; follicular neoplasm or suspicious for follicular neoplasm, with malignancy in 20-30% of cases; and suspicious for malignancy, with malignancy in 50-75% of cases [180, 181].

New preoperative diagnostic approaches for such nodules and for those cytologically inadequate are needed: a number of studies have shown that molecular testing of FNA samples to guide surgery or watchful waiting is helpful for the improvement of the accuracy of cytologic diagnosis of thyroid nodules [6, 182]. In Figure 1.16 is depicted the potential clinical management of patients with thyroid nodules on the basis of a combination of cytological examination and molecular analysis.

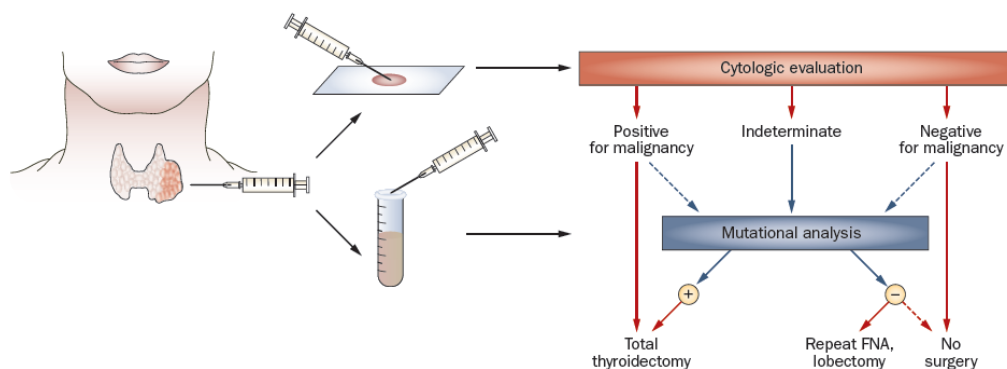


Figure 1.16. Diagnostic utility of molecular markers. FNA, fine-needle aspiration.

In this potential model of clinical management of patients with thyroid nodules combining cytological examination and molecular analysis, patients harboring nodules positive for mutations (high risk of cancer) are treated by total thyroidectomy. Patients harboring nodules with an indeterminate diagnosis on cytology and negative for mutations might require a repeated FNA and diagnostic lobectomy, although follow-up might be recommended for some of these patients, particularly those with the cytologic diagnosis of atypia of undetermined significance/follicular lesion of undetermined significance. Molecular testing of nodules found to be negative for malignancy by cytology may be useful to decrease the rate of false-negative cytologic results [6].

Most studies have explored the diagnostic role of *BRAF* mutation. Molecular testing of *BRAF*^{V600E}, complementary to cytology, significantly improves FNA diagnostic accuracy of thyroid nodules.

Molecular analysis of *BRAF*^{V600E} in 2766 FNA specimens has been performed in several prospective and retrospective studies, and also in studies of research (FNA performed on surgically removed thyroid glands) reviewed by Nikiforova and Nikiforov. In 580 out of the 581 *BRAF*^{V600E} nodules detected, the final histopathological finding was papillary carcinoma, with a false-positive rate of 0.2%. A significant proportion (15-39%) of *BRAF*^{V600E} FNA specimens in these studies were indeterminate or nondiagnostic by cytology and several FNA samples with benign cytology but positive for *BRAF*^{V600E} were found to be papillary carcinomas after surgery [7].

BRAF^{V600E} is highly specific to PTC and false-positive tests have been rarely reported: to the best of our knowledge, there are only 7 cases of false-positive *BRAF* testing documented in the literature. The first report, the case reported also in the meta-analysis mentioned above, was from Korea, where the *BRAF* mutation is highly prevalent, and describes a benign *BRAF* positive nodule histopathologically diagnosed as atypical nodular hyperplasia. The authors supposed that the atypical hyperplasia could have been a premalignant lesion [183].

Further cases of indeterminate *BRAF*-positive FNAs that were benign on final surgical pathology, were assayed using dual-priming oligonucleotide (DPO)-based multiplex polymerase chain reaction, which can detect *BRAF*^{V600E} in 2% of cells within a population of wild-type cells. The authors speculated that the false-positive results were a result of setting the positive cutoff as low as possible [179, 184, 185].

The biggest diagnostic improvement can be achieved by testing FNA samples for a panel of mutations rather than for a single mutation. The 2009 Revised American Thyroid Association (ATA) Management Guidelines for Patients with Thyroid Nodules and Differentiated Thyroid Cancer recommend the use of molecular markers, such as *BRAF*, *RAS*, *RET/PTC*, and *PAX8/PPAR γ* , to help the management of patients with indeterminate cytology [7, 186].

The current data on *BRAF* testing support its ancillary use to routine cytologic analysis: the development of cost-effective analyses may provide the driving force for widespread implementation of preoperative *BRAF* testing on thyroid FNA samples.

1.4.9 The prognostic utility of *BRAF*

Molecular testing of preoperative thyroid FNA samples and surgically removed thyroid tumors may play an important role in tumor prognostication. Molecular markers may improve the identification of tumor harboring a potential for more aggressive disease course and therefore requiring more extensive initial surgery, more aggressive treatment with adjuvant therapies and more frequent follow-up [186].

BRAF^{V600E} mutation is generally accepted as a reliable prognostic marker for papillary carcinoma. Patients with *BRAF*^{V600E} positive papillary thyroid cancers detected preoperatively may benefit from more extensive initial surgery. In fact, *BRAF*^{V600E} has been associated in many studies with aggressive histopathologic features of papillary carcinoma, including extrathyroidal extension, multicentricity, lymph-node or distant metastases and more advanced stage at presentation.

Moreover, *BRAF*^{V600E} in PTC has been associated with an increased risk of palpable nodal recurrence and the need for reoperative surgery [142, 187-189].

Patients with *BRAF*^{V600E} positive PTCs have also an increased chance of treatment failure of recurrent disease. These tumors show a decreased response to radioiodine treatment probably due to *BRAF* mutation-promoted loss of the expression of thyroid iodide-handling genes, including the gene for sodium iodide symporter (NIS), a thyroid-specific basolateral plasma membrane glycoprotein, involved in active transport of iodide into the thyroid follicular cells [59, 190].

The evidence for causality is supported by the fact that *in vitro* cessation of *BRAF*^{V600E} expression restored the expression of important genes involved in iodide metabolism that had previously been silenced by the inducible expression of *BRAF*^{V600E} [191]. The mechanism through which *BRAF*^{V600E} induces NIS

repression relies on the activation of an autocrine transforming growth factor β (TGF β) loop. *BRAF*-induced activation of TGF β and subsequent activation of the SMAD signaling pathway leads to NIS repression in thyroid cancer [192].

Therefore, *BRAF*^{V600E} also predisposes to tumor dedifferentiation. These less differentiated tumors with reduced ability to trap radioiodine are challenging to manage as anatomical localization of recurrences cannot be assessed and treatment with ablative doses of radioiodine is not effective. An increased dose of radioiodine for initial postoperative treatment, lower levels of suppression of TSH (achieved by administering a supraphysiologic dose of thyroxine to the patient) and closer postsurgical follow-up has been suggested for patients with *BRAF*-positive cancer [78, 171, 193].

These findings suggest that knowledge of *BRAF* mutation status can be used for more accurate risk stratification and management of PTC, from preoperative planning of initial surgical scale to postoperative decisions. However, *BRAF*^{V600E} mutation is found in ~45% of papillary carcinomas, whereas less than 10-15% of these tumors show an aggressive clinical behavior [6].

Therefore, it is probable that additional factors can modify the outcome of patients with *BRAF*^{V600E} positive tumors, such as age. In a study was observed that, even if *BRAF*^{V600E} mutation and aggressive histology characteristics are equally present in younger and older (≥ 65 years) patients, the association between *BRAF* mutation and increased risk of tumor recurrence is limited to older patients [194]. Moreover, not all *BRAF*^{V600E} positive papillary carcinomas are aggressive, but also not all aggressive papillary carcinomas carry this mutation [7].

Although the correlation between the *BRAF* mutation and more aggressive PTC prevail in most reports, many studies failed to confirm the association between the *BRAF* mutation and high-risk clinicopathological factors or poorer outcome [106, 195-197]. Discordant results concerning *BRAF*^{V600E} mutation prognostic significance may be due to heterogeneity in PTC at the molecular level or overlapping phenotypes from different genetic alterations [198].

Some studies suggested that *BRAF*^{V600E} is associated with aggressive features even in papillary thyroid microcarcinomas. This mutation in mPTC correlates

with either high rate of extrathyroidal tumor extension or lymph node metastasis or both of these features [111, 199-201].

Recently, Niemeier and colleagues suggested that a combination of histopathological features and the *BRAF* status was superior to pathology alone for clinical risk stratification of papillary thyroid microcarcinoma, allowing better prediction of extrathyroid tumor spread [112, 202].

Thus, *BRAF* mutational status may be helpful, in conjunction with conventional clinicopathological risk factors, in those cases where clinicopathological criteria alone would otherwise be unreliable in defining the risk stratification and management of PTC [6, 193].

1.4.10 BRAF as a therapeutic target for PTC

Differentiated thyroid carcinoma, specifically papillary and follicular thyroid carcinoma, account for more than 90% of all thyroid malignancies and have generally a favorable prognosis with 10 years survival in excess of 90%. Although mortality from differentiated thyroid cancer is low, disease recurrence is high in some subgroups of patients, 20-30% or even higher. An accurate assessment of the risk of individual patients is important in order not only to guarantee a treatment that minimizes chance of progression or recurrence, but also that has a good balance between benefits and harms [181, 203, 204].

Most of patients with differentiated thyroid carcinomas (85%) are cured with surgery (preferentially total thyroidectomy), radioactive iodine and TSH suppression. Disease recurrence usually occurs in the neck: the best treatment for these tumors is surgical with potential further radioactive iodine [205]. Metastatic thyroid cancer is treated with radioactive iodine if the metastases are radioiodine avid. However, about 5% of patients will develop more aggressive tumors: these patients harboring metastatic disease which fails to respond to radioactive iodine will eventually die of their disease [181]. Refractory disease is an advanced disease characterized either by the presence of at least one tumor focus without any uptake of radioiodine or by progression of the disease during the year after a

radioiodine treatment course. This aggressive behavior occurs more frequently in older patients, in those with large metastases or with poorly differentiated thyroid cancer. It shows a median survival after the discovery of distant metastases ranging from 3 to 6 years [206].

Cytotoxic chemotherapies for advanced or metastatic non-iodine avid thyroid cancers show no prolonged responses and in general have fallen out of favor. Indeed, traditional cytotoxic chemotherapies such as doxorubicin, taxol, and cisplatin are associated with a 25-37% partial response rate with rare complete remission, high toxicity and short duration of responses [205].

Given the generally poor outcomes associated with cytotoxic chemotherapy, patients with progressive or symptomatic metastatic thyroid cancer that is considered radioiodine refractory should be considered for treatment on a clinical trial with novel targeted therapies [186].

Discoveries about the pathophysiological basis of advanced thyroid cancer, such as the identification of specific oncogenic mutations that appear to be early genetic events in DTC and understanding the role of intercellular signaling between the tumor cell and the surrounding tumor microenvironment, led to development of novel antineoplastic therapies [207]. An important development was recognition of processes facilitating tumor growth, reflecting either normal (such as hypoxia-inducible angiogenesis) or abnormal (such as epigenetic modifications of chromosomal DNA and histones) adaptations. Angiogenesis is critical in supporting tumor cell growth and metastasis, supplying nutrients and oxygen, removing waste products, and facilitating distant metastasis [208]. A key proangiogenic factor is vascular endothelial growth factor (VEGF), that binds to two receptor tyrosine kinases, VEGFR-1 (Flt-1) and VEGFR-2 (Flk-1/KDR) involved also in MAPK signaling triggering [209]. In PTC, the intensity of VEGF expression correlates with a higher risk of metastasis and recurrence, a shorter disease-free survival, and *BRAF* mutation status. Indeed, *BRAF*^{V600E} positive PTCs tend to have higher expression of VEGF. Since the level of VEGF expression was shown to correlate with tumor size, extrathyroidal invasion, and stage, high levels of VEGF expression may be related to poorer clinical outcome and recurrence in *BRAF*^{V600E} PTC [198, 210].

The high prevalence and prognostic significance of the $BRAF^{V600E}$ mutation in PTC make it an interesting target for the development of molecular therapeutic options. As previously discussed, one reason for a poorer prognosis of patients with $BRAF^{V600E}$ mutated PTC is the resistance to the conventional radioiodine adjuvant therapy because this $BRAF$ mutation promotes the loss of the expression of thyroid iodide-handling genes, such as the gene for sodium iodide symporter (NIS) [190]. It was shown that inhibition of tyrosine kinase-activated pathways, using compounds that block receptor kinase activity directly or that inhibit the activity of downstream signaling kinases, induces thyroid cancer cell death *in vitro* and *in vivo* in preclinical mouse models [177, 211, 212].

The various small molecule inhibitors of activated BRAF serine/threonine kinase that have been developed are assigned to different categories, type I and type II, on the basis of their mechanism of action. In particular, they can selectively bind kinases with different conformation of the conserved DFG motif.

Type I tyrosine kinase inhibitors (TKIs) bind to a kinase in its active (“DFG-in”) conformation forming interactions with the hinge region and ATP binding site of the protein.

Type II inhibitors use the ATP binding site and an adjacent hydrophobic pocket created by the activation loop with the DFG motif being in an “out” conformation [130, 213, 214].

A number of drug candidates targeting $BRAF^{V600E}$ have entered clinical trials in recent years. Some of them, such as vemurafenib and dabrafenib, type I inhibitors, have shown clinical efficacy [214].

Type II inhibitors (such as sorafenib) were the first compounds introduced into the clinic for cancer therapy, however type I inhibitors may provide the necessary specificity to target successfully mutant BRAF kinases [215].

Sorafenib (BAY 43-9006, Nexavar) was the first ligand to be crystallized with BRAF and was designed as inhibitor active against both BRAF in its inactive conformation and CRAF (Fig. 1.17) [130]. Targeting BRAF in melanoma using Sorafenib has not been clinically effective [216-218].

Further studies suggested that its effects might not be mediated through BRAF inhibition, but through off-target effects. Using drug-resistant versions of

oncogenic BRAF generated by mutating the gatekeeper residue, sorafenib still inhibited the growth of tumors driven by the mutant protein [219]. Therefore, the failure of sorafenib to result in significant objective responses in *BRAF*-mutant melanoma in clinical trials has been interpreted as consistent with the non-BRAF mediated mechanism of action of the drug [220]. It was later shown that sorafenib mediates antitumor effects in renal cell cancer (RCC) independently of its ability to block BRAF^{V600E} signaling [219]. It was eventually approved for the treatment of RCC and unresectable hepatocellular carcinoma (HCC). The efficacy in these cancers is believed to be due to inhibition of other kinases such as VEGFR2, KIT, and Flt-3 [214]. Thus, while initially considered a selective RAF kinase inhibitor, sorafenib is a multikinase inhibitor that targets several receptor tyrosine kinases such as human VEGF receptors (VEGF-R) 1 to 3, PDGF receptor, and RET [221, 222]. The results of a recent meta-analysis suggest that sorafenib has only a modest effect in patients with radioiodine-refractory differentiated thyroid cancer and shows also a high incidence of adverse effects that may affect the quality of patients' life [223].

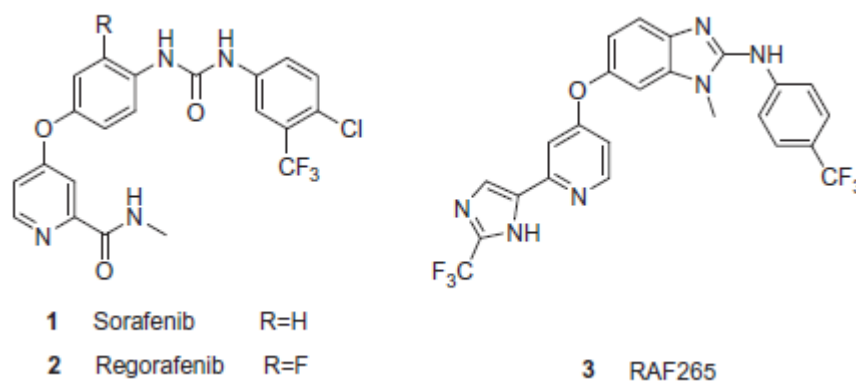


Figure 1.17. Type II inhibitors of BRAF [214].

Type I inhibitors with preferential binding to the kinase domain of BRAF in the active conformation demonstrated greater inhibitory potency against the BRAF^{V600E} mutant kinase than the wild-type [214].

Vemurafenib (PLX4032, RG7204, Zelboraf) is a potent kinase inhibitor of BRAF^{V600E}. Along with its sister compound PLX4720, vemurafenib was identified through a structure-guided discovery approach optimized for binding to the mutant kinase (Fig. 1.18) [224].

In preclinical models of melanoma, vemurafenib inhibited proliferation and ERK phosphorylation in cell lines bearing activating *BRAF* mutations in a dose-dependent manner, but no inhibition was noted in wild-type cell lines. Vemurafenib also potently inhibited proliferation of melanoma cell lines expressing other codon 600 *BRAF* mutations (V600D, V600K, and V600R) and showed potent activity in several human *BRAF*^{V600E} positive melanoma xenograft models [225].

However, MEK and ERK phosphorylation was unexpectedly increased in cell lines containing upstream mutations in *RET/PTC* or *RAS* with wild-type *BRAF*. This paradoxical signaling cascade activation by RAF inhibitors is likely due to paradoxical transactivation of dimerized RAF kinases. Drug binding to one member of RAF homodimers (CRAF/CRAF) or heterodimers (CRAF/BRAF) inhibits one protomer, but results in transactivation of the drug-free protomer. In *BRAF*^{V600E} tumors, RAS is not activated, thus transactivation is minimal and ERK signaling is inhibited in cells exposed to RAF inhibitors. Moreover, RAF inhibitors do not inhibit ERK signaling in cells that coexpress *BRAF*^{V600E} and mutant RAS [226].

In a first phase I study, treatment of metastatic melanoma with vemurafenib in patients with *BRAF*^{V600E} mutated tumors resulted in complete or partial tumor regression in the majority of patients. This clinical efficacy drastically contrasts with a complete absence of clinical response among those lacking the *BRAF*^{V600E} mutation underscoring the importance of the appropriate molecular target [227]. A randomized phase III trial demonstrated improved rates of overall and progression-free survival in patients with previously untreated metastatic melanoma with the *BRAF*^{V600E} mutation compared with dacarbazine, leading to the drug's approval in the USA (2011) and in Europe (2012) [228].

The recent approval of vemurafenib for patients with advanced melanoma harboring the *BRAF*^{V600E} represents the first FDA approval of a drug and a companion diagnostic mutation test to determine patient eligibility for treatment. The approved test only documents the presence of the V600E variant, however, assessing other *BRAF* mutations (such as V600K and V600D) and mutations in

other genes may have a more extensive impact on patient management and may be relevant to understand treatment resistance [229].

If a mutation is predictive of a drug response in one form of tumor then there may be some likelihood that the same drug could affect tumors from other origins with the same mutation. However, this hypothesis requires formal testing because the presence of a specific mutation may have different clinical implications depending on the origin of tumoral tissue. In fact, this intertumor variation is found in sensitivity to vemurafenib that is efficient both in *BRAF*^{V600E} mutated melanoma and ovarian cancer but not in *BRAF*^{V600E} mutated colorectal cancer [228-231].

This could be a result of feedback up-regulation of epidermal growth factor receptor (EGFR) after *BRAF*^{V600E} inhibition in epithelial colorectal cancer cells but not in melanoma cells, which are derived from the neural crest and have lower basal EGFR expression [230].

In preclinical studies in PTC, vemurafenib and PLX4720 were shown to block cellular proliferation of multiple *BRAF*^{V600E} mutant cell lines mimicking the experience with melanoma. Both compounds inhibited the proliferation of *BRAF*^{V600E} mutant cell lines, but not normal thyrocytes. MEK and ERK phosphorylation was also decreased upon vemurafenib and PLX4720 treatment in *BRAF* mutant thyroid carcinoma cells but not in normal thyroid cells or in cell lines harboring mutations of RAS or RET/PTC1 rearrangements. However, neither proliferation nor downstream kinase phosphorylation could be completely inhibited despite maximum drug concentrations, and feedback down-regulation of ERK phosphatases was suggested as a potential mechanism.

Vemurafenib and PLX4720 treatment induced a G1 block and altered expression of genes involved in the control of G1-S cell-cycle transition in a *BRAF* mutant cell line, without evidence of cytotoxicity of treatment. In a xenograft model in nude mice treated with vemurafenib, *BRAF* mutant tumor growth was slowed but not completely blocked and was associated with reduced MEK and ERK phosphorylation [232].

A tumor volume reduction was also observed in *BRAF* mutant xenografts treated with PLX4720. Furthermore, the tumors treated with PLX4720 were markedly

less invasive and contained increased nuclear localization of thyroid-specific transcription factors [233].

Vemurafenib was tested in a phase I trial in three patients with *BRAF* mutated metastatic DTC. The recently published results showed that among the three patients, one had a confirmed partial response with reduction of pulmonary target lesions by 31%, and the duration of response was 7.6 months before the disease progressed in the lungs and the bones. The time to progression was 11.7 months. The other two patients had stable disease, and the time to progression was 13.2 and 11.4 months, respectively. Two of the patients eventually died of their disease, one of whom had developed anaplastic transformation about one year after discontinuing vemurafenib. On the basis of these results, a phase II trial of vemurafenib has recently been initiated in patients with progressive metastases from *BRAF*^{V600E} mutant PTC [215, 234].

Dabrafenib (GSK2118436) is a potent ATP-competitive inhibitor of BRAF kinase and is selective for mutant BRAF (Fig. 1.18). It inhibits several of the codon 600 variants of BRAF, including V600E, V600K and V600D [215]. In a first-in-human dose escalation phase I trial, efficacy was studied in patients with *BRAF* mutated tumors, including those with other *BRAF* mutations in codon 600. Patients were divided in three cohorts: metastatic melanoma, melanoma with untreated brain metastases, and non-melanoma solid tumors. In patients with *BRAF* mutant non-melanoma solid tumors, apparent antitumor activity was observed in papillary thyroid cancer, gastrointestinal stromal tumor, non-small-cell lung cancer, ovarian cancer, and colorectal cancer. In patients with *BRAF* mutant melanoma treated with dabrafenib partial response was recorded in 69% of patients, including those with V600K and V600G mutations, and significant tumor reductions were seen in 90% of patients with intracerebral metastases. Of the 9 patients with *BRAF* mutated PTC included in the trial, 3 (33%) achieved partial response [235].

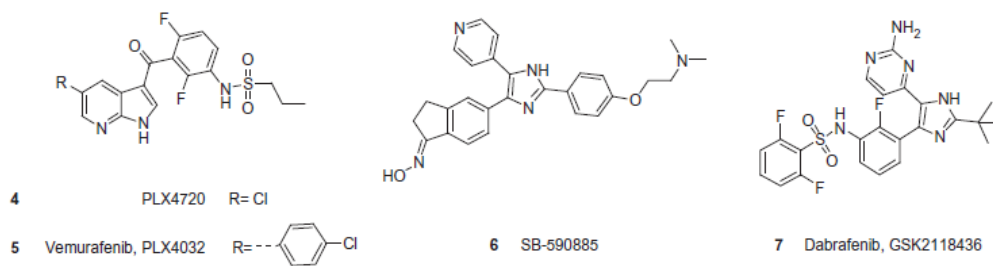


Figure 1.18. Type I inhibitors of BRAF [214].

Among melanoma patients, acquired resistance to vemurafenib therapy has been observed, associated with a variety of proposed mechanisms other than secondary *BRAF* mutations, such as RAS activation or enhanced signaling through CRAF [236-238].

As BRAF inhibitor therapy evolves also for DTC, it is likely that similar mechanisms of resistance will emerge, suggesting that monotherapies represent a first step in improving patient outcomes but can be insufficient to eradicate advanced and metastatic disease. Probably the identification of rational ways to combine individual therapies will be necessary for more effective outcomes. A strategy involves individual targeted therapies merged together or with selected traditional cytotoxic agents; another one suggest a sequential inhibition along the MAPK pathway, blocking both BRAF and MEK simultaneously in order to overcome acquired resistance to monotherapy with BRAF inhibitors observed in melanoma, mediated by reactivation of MAPK signaling [215].

Also in the field of thyroid cancer research individual therapies are being combined together in order to improve patient survival. Examples include the demonstration of synergistic effects of the *BRAF*^{V600E} inhibitor vemurafenib combined with the AKT inhibitor MK2206 in thyroid cancer cells harboring both the *BRAF*^{V600E} and PIK3CA mutations [239].

Another possible approach, based on observations in *BRAF*^{V600E} thyroid cancer cell lines, include combining BRAF with HER kinase inhibitors. A study suggests that thyroid cancer cells with mutant *BRAF* are resistant to vemurafenib compared with melanoma because this inhibitor induces the de-repression *HER3* transcription, diminishing the antitumor effects of RAF inhibitors. The

combination of vemurafenib with the HER kinase inhibitor lapatinib sensitizes *BRAF* mutant thyroid cancer cells to inhibitors [215, 240].

Novel molecular-targeted therapies seem to hold great promise for radioiodine-refractory and surgically inoperable thyroid cancers and are likely to become part of the standard treatment regimen for patients with thyroid cancer in the future.

1.4.11 Methods for detection of *BRAF* molecular alterations

The identification of specific mutations driving a cancer is important both for the development of targeted therapies and for screening of patients for personalized treatment.

The choice of techniques for clinical detection of molecular alterations in thyroid cancer specimens relies on the sample type available for analysis and the mutation types.

BRAF mutational analysis used in diagnostics to identify clinically relevant mutations can be performed using many different methods, however, the sensitivity and specificity of mutation detection varies for different methods used for testing [241].

Sanger sequencing is considered the “gold standard” technique for mutation detection. However, although it permits a screening of the entire nucleotide sequence of the target region, it is low throughput (mainly due to cost constraints), requires several distinct steps leading to higher contamination risk and lacks the sensitivity to detect small but significant subpopulations of tumoral cells [242, 243]. Indeed, it can only detect with sufficient accuracy mutations present in at least 10% of mutated DNA, corresponding to 20% of neoplastic cells with a heterozygous mutated allele [244, 245].

Analytic sensitivity of assays is a very important feature because tumoral cells may represent only a fraction of the available specimen. In fact, many routine samples contain large numbers of non-neoplastic reactive or inflammatory cells that can lead to false negative results. Therefore, microdissection of histologic specimens prior to DNA extraction is usually necessary to enrich for neoplastic cells in order to avoid false negative results. This tumor cell enrichment is not

feasible in the case of FNA specimens [245]. Furthermore, material available for molecular analysis from cytological specimens and FNAs may be restricted, especially when multiple tests are performed.

Moreover, tumors may show considerable heterogeneity in the presence of the mutation being targeted because of clonal evolution processes.

Efforts to enhance sensitivity have produced a variety of methods to detect the *BRAF* mutations based on different approaches but often designed to generate a qualitative (positive/negative) result rather than a quantitative result.

Qualitative assessment of single point mutations in thyroid disease, such as mutations at codons 600 and 601 of *BRAF*, can be achieved using different methods including allele-specific PCR, PCR-based single-strand conformation polymorphism (PCR-SSCP), PCR-restriction fragment length polymorphism (RFLP)-based analysis, PCR-melt curve analysis, PCR hybridization (including microarrays) and MALDI-TOF mass spectrometry [246].

MALDI-TOF (matrix-assisted laser desorption/ionization time-of-flight) mass spectrometry and oligonucleotide microarray are high-throughput and automated methods, however, can be time consuming and require the use of sophisticated platforms not always affordable by pathology laboratories [149, 247].

In addition, as previously discussed in section 1.4.8, a dual-priming oligonucleotide (DPO)-based multiplex PCR analysis was developed to detect the *BRAF*^{V600E}: this assay may detect the mutation in as few as 2% of cells in a FNA specimen of thyroid nodules [185].

Although allele-specific PCR assays are more sensitive than direct sequencing for detecting small numbers of mutant cells, they are limited by low specificity in discriminating single-base point mutations with natural DNA primers and by design to generate a qualitative result [246].

Among highly sensitive semi-quantitative molecular approaches to detect *BRAF*^{V600E}, an Allele Specific Locked Nucleic Acid quantitative PCR (ASLNAqPCR) was designed by our group and is described in section 3.3 [245].

Pyrosequencing is another highly sensitive semi-quantitative method that permits also to screen *BRAF* mutations in the entire target nucleotide sequence. In a study

by Guerra and colleagues it was used to detect the percentage of *BRAF*^{V600E} allele in genomic DNA of PTC specimens with a cutoff settled at 5% [248].

Recently, the development of next-generation sequencing (NGS) methods has enabled simultaneous detection of all known clinically relevant mutations in different genes as a single test and provides enormous amounts of novel information. Despite greater complexity compared with Sanger sequencing or alternative methods, next-generation sequencing offers high analytical sensitivity, screening of the entire target nucleotide sequence, semi-quantitative evaluation of the mutated allele and analysis of many samples in a single run (high throughput) thanks to the possibility of performing parallel analysis of a very large number of DNA molecules (massive parallel sequencing) [249].

454 Sequencing system allows confident calling of low-frequency variations: in a well designed and well executed experiment, rare variants with a prevalence of 1% or less can be analyzed [250].

This technological development has permitted the definition of the entire DNA sequence of common types of human cancers and is clarifying the extent of genetic heterogeneity in cancers, thus opening new possibilities but also practical challenges in the clinic (section 1.5.2) [251, 252].

1.5 Tumor heterogeneity

1.5.1 *BRAF* mutation and intratumoral genetic heterogeneity

Genetic and phenotypic variation can be identified in tumors affecting different tissue and cell types, in different metastatic tumors from a single patient or in individuals with the same tumor type (intertumor heterogeneity). Moreover, genetic and phenotypic variation can be also observed within a given tumor (intratumor heterogeneity) where populations of genetically distinct subclones can intermingle (as shown by subclones 1 and 2 in Fig. 1.19) or be spatially separated (as shown by subclone 3) as a result of physical barriers such as blood vessels or micro-environmental changes. This subclonal architecture varies dynamically throughout the disease course.

Genetic and epigenetic variation that results in phenotypic diversity can be found also within tumor subclones: intercellular genetic heterogeneity is generated by genetic instability, an ubiquitous characteristic of neoplasms fundamental to the processes of neoplastic progression [253].

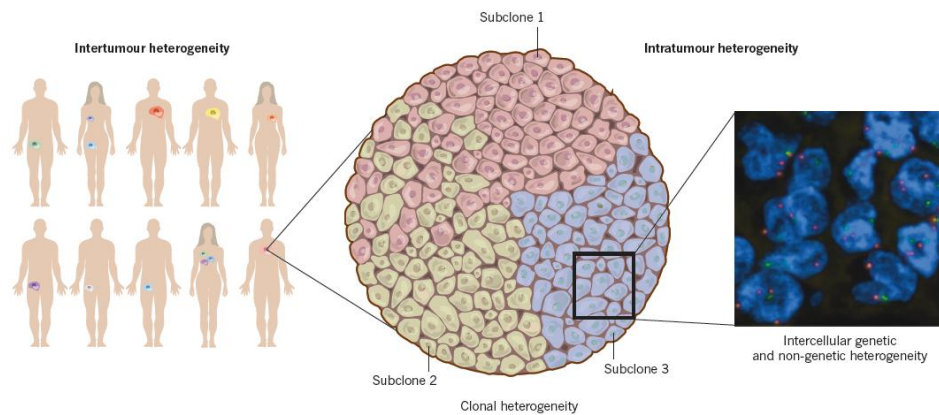


Figure 1.19. Intertumor and intratumor heterogeneity [253].

According to Nowell’s classical description of cancer as an evolutionary process, parallel to Darwinian natural selection, most neoplasms arise from a single mutated cell of origin, and tumor progression results from malignant clonal expansion secondary to additional stepwise acquired genetic and genomic alterations. Mutagenic processes are essentially non-purposeful and may reflect prior exposure to carcinogens, such as radiation exposure for *BRAF*. Many of the genetic and epigenetic alterations observed in neoplasms are selectively neutral (passenger or hitchhikers lesions), whereas other alterations confer a selective growth advantage (driver lesions).

Clonal evolution implies the interplay of selectively advantageous lesions, selectively neutral lesions, deleterious lesions and lesions that increase the rate of other genetic changes (mutator lesions) [254, 255]. Moreover, cancer clone genetic diversification and subclonal selection occurs within tissue microenvironments that provide both the venue and the determinants of fitness selection: changes to the microenvironment change also the fitness effects of these lesions [256].

The step wise acquisition of these alterations can result in the emergence of tumor subclones with phenotypic advantages such as invasion, proliferation, ability to colonize different organs.

The model of clonal evolution hypothesizes a series of clonal expansions: mutations that increase the ratio between rates of cell division of a clone and cell death will help the mutant clone to expand in the neoplasm. This subclonal dominance or “selective sweep” is the phenomenon of natural selection driving an allele to fixation. The spread of a lesion throughout the entire population is called “fixation” because, without competing alleles left, natural selection cannot change the frequency of the lesion in the population. Not all of the mutations that have gone to fixation are advantageous: also neutral mutations can spread to fixation. The fixation of neutral mutations can happen through genetic drift, a random and slow process or more likely through linkage to a selectively advantageous lesion. Since it is unlikely that the same neutral mutation would co-occur (hitchhike) with a selectively advantageous mutation across multiple independent neoplasms, the expansion of a mutation in many neoplasms is evidence for an advantageous mutation [254, 257]. However, if the time until the emergence of a next driver mutation in a competitor clone is shorter than the time required for a clone to sweep through the neoplasm, parallel clonal expansion is restrained by mutual competition (clonal interference). This situation may precede dominance of subclones early in cancer development [254].

Since 1976, clonal expansions as well as intertumor and intratumor genetic heterogeneity have been identified in several tumor types. Subclonal populations of mutated cells have been found in metastatic melanoma, esophageal adenocarcinoma, breast carcinoma, lung cancer, and colorectal carcinomas [258-265]. Moreover, the concept that not all tumors cells in primary tumors harbor the mutation implies that secondary metastases may or not, and in different amounts, retain the original set of mutations of the primary lesions.

In melanoma, Lin *et al.* observed by single-cell PCR and sequencing marked polyclonality of *BRAF* mutations in acquired melanocytic nevi: cells with rare *BRAF* mutations, such as *BRAF*^{T599I}, *BRAF*^{V600K} and *BRAF*^{V600A}, all of which

previously described in melanoma lesions, were found in nevi harboring also $BRAF^{V600E}$ mutation and $BRAF^{wt}$ cells [153].

They also found a similar heterogeneity of $BRAF$ mutations in primary melanomas in tumors that were wild-type by direct sequencing. They observed melanomas that contained tumor with $BRAF^{wt}$ cells, $BRAF^{V600E}$ and other activating $BRAF$ mutations (such as $BRAF^{K601R}$ and $BRAF^{V600M}$) in minor subpopulations that did not outgrow $BRAF^{wt}$ cells. However, $BRAF$ mutant alleles were positively selected during melanoma progression in recurrent primary tumor or metastases [152].

Yancovitz and colleagues have recently investigated intertumor and intratumor heterogeneity in melanoma using detection of the $BRAF^{V600E}$ mutation as a marker of clonality by semi-quantitative mutation-specific SNaPshot assay. Heterogeneity of the $BRAF^{V600E}$ mutation was observed both among multiple specimens from individual patients and within individual melanoma tumor specimens [265].

Clonality of the $BRAF^{V600E}$ mutation has been recently analyzed by Guerra and colleagues also in papillary thyroid cancer using a semi-quantitative pyrosequencing technique. This study has shown that clonal $BRAF^{V600E}$ is a rare occurrence in papillary thyroid cancer and is more frequently a subclonal event suggesting that usually it is not an early hit during PTC development.

Indeed, in this study most PTCs were found to have 5%-25% of $BRAF^{V600E}$ alleles, which corresponds to less than half of the cells within the tumor carrying heterozygous mutation [248].

The existence of intertumor and intratumor heterogeneity has important implications in clinical management. The current approach to molecular biomarker testing to inform cancer treatment focuses on interpatient tumor heterogeneity. However, intratumor heterogeneity is also clinically relevant because the presence of genetically distinct tumor subclones may account for resistance to targeted pharmacotherapy. Moreover, the status of predictive biomarkers may evolve during tumor progression not only under the selective pressure of microenvironment but also under the influence by exposure to cancer treatment that leads to the eradication of sensitive clones and emergence of often

pre-existing treatment-resistant subclones in metastatic disease that were present at minor frequency in the primary tumor [253].

As previously discussed, the impact of $BRAF^{V600E}$ on clinical outcome has been extensively investigated with conflicting results: the recent finding of subclonal $BRAF^{V600E}$ status in PTC may offer an explanation for these inconsistent results. In fact, Guerra and colleagues observed that a high percentage of $BRAF^{V600E}$ alleles is associated with high risk clinicopathological factors and predicts a poorer disease outcome. In particular, they found that higher frequency of multifocality, extrathyroidal extension, and lymph node metastasis in the tumors with percentages of the $BRAF^{V600E}$ allele of 30% or greater than in those harboring the $BRAF^{wt}$ allele, although without statistical significance in a reduced number of samples [248].

However, in a study by Gandolfi *et al.*, the occurrence and percentage of the $BRAF^{V600E}$ mutated allele was not preferentially associated with the development of either distant or lymph node metastases. Approximately 80% of lymph node metastases from mutated primary PTCs retained the $BRAF^{V600E}$ mutation and the average mutated allele percentage decreased as the tumor progresses from the primary site to the lymph node metastatic sites.

Therefore, the preoperative analysis of $BRAF$ mutational status by semi-quantitative methods might allow a molecular subtyping of PTCs, even if caution is required on the potential clinical application of $BRAF^{V600E}$ mutation as a negative prognostic factor [266].

1.5.2 Clinical implications of intratumoral heterogeneity

Recognition that intratumor heterogeneity has a role in resistance to targeted therapies suggests that an approach shift in therapy is required: it would be worth considering that each patient harboring a tumor may harbor genetically distinct cancer subclones with different genetic aberrations that may render them resistant to specific systemic therapies. Indeed, in metastatic disease, recent studies have shown the emergence of treatment-resistant subclones that were present at a minor frequency in the primary tumor [251].

As previously discussed in section 1.4.11, the possibility to include the concept of intratumor genetic heterogeneity in personalized medicine has been limited by the sensitivity of the methodology employed, especially automated Sanger sequencing, the principal method employed in clinical laboratories for many years [242].

However, the present stage of technological development in the future will probably improve the design of individualized treatment through the use of combinatorial therapeutic agents targeting also rare clones in order to reduce the chances of the emergence of resistant clones (Fig. 1.20) [267].

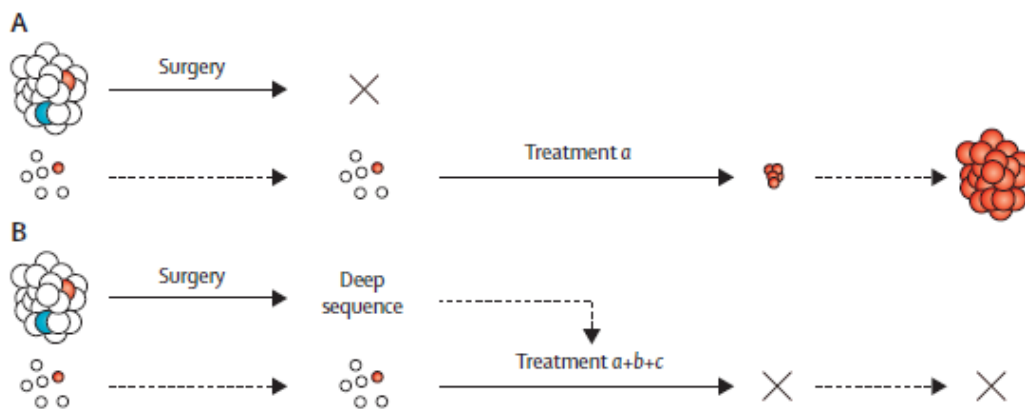


Figure 1.20. Adjuvant targeted therapy of primary tumors with clonal heterogeneity. The present situation is targeted therapy on the basis of the dominant clone after surgical resection (A). In the future, targeted therapy driven by deep sequencing after surgical resection of the primary tumor will be probably directed by the characteristics of both dominant and rare clones, with a combination of therapies (a, b, c) to eradicate all clones (B) [267].

Next generation sequencing was previously outside the purview of a clinical laboratory owing to the cost, high-performance computing capacity and the sophisticated bioinformatics expertise that was required for sequence alignment and mutation calling. The falling cost of NGS and the recent development of bench-top next-generation sequencing instruments, that offer high coverage of clinically relevant cancer genes with fast sequencing runs and manageable data size without the need for specialized computing, have made this method accessible for clinical laboratory.

Even if NGS offers large-scale nucleotide analysis including whole-genome sequencing, whole-exome sequencing and whole-transcriptome sequencing that

are essential for discovery projects, targeted sequencing of multiple specific genomic regions may offer advance in routine molecular diagnostics of cancer [251].

In the last few years, clinical laboratories have begun to investigate how to employ NGS for clinical testing, as this huge sequencing capacity opens up new possibilities for molecular diagnosis that Sanger sequencing technology could not offer but also implies challenges in clinical assessment [268, 269].

Clinical assessment of intratumor heterogeneity has some practical challenges. The Next Generation Sequencing Standardization of Clinical Testing (Nex-StoCT) workgroup recommends for all clinically actionable mutations an independent analysis using an alternative method to confirm the mutations found before reporting to the treating clinician [270].

However, mutation verification can delay the reporting of results to the oncologist. Moreover, when NGS identifies a low-frequency mutation, it cannot be confirmed by Sanger sequencing due to the limitations of sensitivity of this sequencing method. Lastly, when multiple mutations are detected, it's difficult to report clear results to clinicians who have to decide which mutation or mutations are clinically overriding. Therefore, the collaborative engagement of clinicians and scientists is essential to improve personalized cancer medicine [229, 251].

In a recent study by Marina N. Nikiforova and colleagues, targeted NGS was performed for simultaneous testing for multiple mutations in thyroid cancer using a custom mutational panel (ThyroSeq). This panel, proposed to improve the accuracy of cancer diagnosis and prognostication in thyroid nodules, provides quantitative assessment of mutant alleles. They observed that in PTCs, the vast majority of tumor samples (80%) had more than 25% of $BRAF^{V600E}$ mutant alleles, corresponding to more than 50% of cells carrying a $BRAF^{V600E}$ heterozygous mutation. Therefore, they considered $BRAF^{V600E}$ a clonal driver mutation in these tumors ascribing the lower abundance of $BRAF^{V600E}$ to a dilution of $BRAF$ mutant allele due to some degree of contamination by normal stromal, endothelial and inflammatory cells [271].

The ability of a single next-generation sequencer to perform simultaneous sequencing of short nucleic acid sequences in a massively parallel way allows a

laboratory the opportunity to detect multiple genetic alterations in a cost-effective manner. This opportunity is of great importance when there are many possible causative genes for a specific phenotype. NGS permits not only the analysis of many samples in a single run (high throughput), but also high sensitivity of mutation detection and semi-quantitative assessment of mutant alleles [268, 269]. Thus, NGS can provide new insights into the biology of thyroid cancer and is also expected to further improve the accuracy of routine molecular cancer diagnosis and prognostication in thyroid nodules.

CHAPTER 2

AIMS OF THE THESIS

At present, the intratumor heterogeneity is a key topic relevant to the field of cancer research. Intratumor heterogeneity consists in genetic variations within individual tumors. These genetic differences may affect responses to molecularly targeted treatments leading to drug resistance.

BRAF^{V600E} is the most frequent mutation detected in PTC and it is a promising target currently being evaluated for the treatment of advanced thyroid cancer.

Therefore, detecting clonality of *BRAF*^{V600E} mutation in PTCs is important in order to better understand the molecular basis of PTC development and evaluate the feasibility of using *BRAF*^{V600E} specific inhibitors.

Moreover, assessing the presence of other *BRAF* mutations in hot spot exon 15 using novel highly sensitive methods may be relevant to understand thyroid tumorigenesis and to inform treatment decisions.

Therefore, this project was undertaken to:

- **Aim 1**: establish whether the *BRAF*^{V600E} mutation is present in all tumor cells in a given tumor or if it occurs as a subclonal event in papillary carcinomas (PTCs), thus establishing how early an event is *BRAF*^{V600E} mutation.
- **Aim 2**: screen with high sensitivity *BRAF* mutations in exon 15 in histologically benign thyroid tissue of cases with *BRAF*^{V600E} or *BRAF*^{wt} PTCs in order to identify putative precursor lesions of papillary thyroid carcinoma.

In order to reach these goals, two high sensitive semi-quantitative methods were used: Allele Specific quantitative PCR (ASqPCR) with Locked Nucleic Acid (LNA) primers and 454 Next-Generation Sequencing (NGS).

CHAPTER 3

MATERIALS AND METHODS

3.1 Ethic statement and selection of cases

All information regarding the human material was managed using anonymous numerical codes and samples were handled in compliance with the Helsinki Declaration [272].

All cases were obtained from the Anatomic Pathology units of Bellaria and Maggiore Hospitals (Bologna, Italy) and diagnosed according to the histopathological typing of the World Health Organization (WHO) [4]. Stage was calculated according to tumor size, lymph node metastasis and distant metastasis at the moment of diagnosis (pTNM) designated by American Joint Committee on Cancer (AJCC) [53].

Aim 1. The case study for the first aim of the project was made up of 155 consecutive formalin fixed and paraffin embedded (FFPE) thyroid specimens of PTCs that were analyzed for $BRAF^{V600E}$ mutation by ASLNAqPCR (30 cases were also analyzed by 454 NGS).

Aim 2. For the second aim of the project, 75 histologically benign FFPE thyroid specimens from 20 cases with $BRAF^{V600E}$ and 23 from 9 cases with $BRAF^{wt}$ PTCs were analyzed by 454 NGS for the possible presence of $BRAF$ mutations in exon 15. Ten samples with histologically normal thyroid parenchyma were also analyzed by 454 NGS.

During the preanalytical phase of the specimens belonging to the first retrospective study, the Hematoxylin and Eosin (H&E) sections from each case were observed by a pathologist to select the blocks with the highest proportion of PTC neoplastic cells over non neoplastic thyroid cells, inflammation and necrosis. For the second project, the blocks carrying benign lesions not associated with histologically identifiable tumor cells were chosen for $BRAF$ exon 15 mutational screening. Type and number of histologically benign lesions analyzed from

$BRAF^{V600E}$ and $BRAF^{WT}$ PTC groups are summarized in Table 3.1. These types of histologically benign lesions are described in sections 1.2.1 and 1.3.1. “Atypical focus” is defined as a microscopic area with abnormal cells that show cytological atypia without the fully developed histologic hallmarks of malignancy.

Type of sample	$BRAF^{V600E}$ group	$BRAF^{WT}$ group
Atypical focus	32	5
Hyperplasia	13	3
Follicular adenoma	1	3
Oncocytic follicular adenoma	2	-
Psammoma body	3	3
Normal	24	9
Total	75	23

Table 3.1. Type and number of histologically benign lesions analyzed for possible presence of $BRAF$ mutations in exon 15.

Five 10 µm-thick serial sections for each case were cut from the blocks selected followed by one H&E control slide that was further reviewed by a pathologist in order to verify that the neoplastic or histologically benign areas previously chosen were still present and mark these enriched samples for genomic DNA isolation (Fig. 3.2).

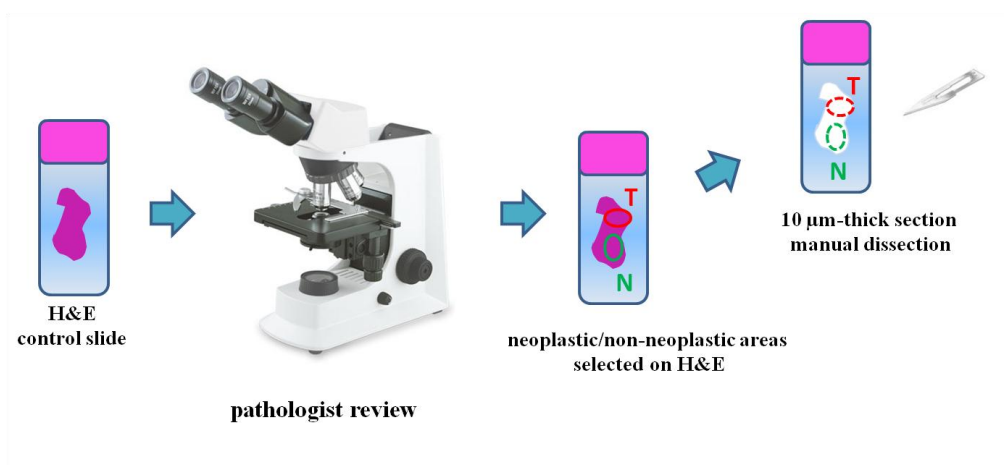


Figure 3.2. The pathologist review in preanalytical phase.

3.2 Genomic DNA isolation and quantification

The five 10 µm-thick slides were manually dissected with a sterile blade under microscopic guidance according to the area marked on H&E.

Tissues were then deparaffinised by incubation in xylene for 15 minutes at 60°C, then washed twice at room temperature with absolute ethanol and digested overnight with proteinase K at 56°C. Genomic DNA was then isolated using a column based commercial kit (High Pure PCR Template preparation kit, Roche) according to manufacturer's instructions and eluted in 65 µl of warmed up Elution Buffer.

The concentration of the genomic DNA extracted was assessed fluorometrically using the Quant-iT™ dsDNA HS Assay Kit on a Qubit™ Quantitation Platform (Invitrogen).

3.3 Mutational analysis: Allele Specific Locked Nucleic Acid quantitative PCR (ASLNAqPCR)

Allele-specific PCR is a hot spot mutation assay based on positioning the 3-prime base of a PCR primer to match a single point mutation allele in order to extend only the correctly matched primer under stringent conditions.

The assay used in this study, called Allele Specific Locked Nucleic Acid quantitative PCR (ASLNAqPCR), is based on molecular beacon probe as detection system. Molecular beacons (MBs) are single-stranded, fluorophore-labeled oligonucleotide hybridization probes that form a stem-and-loop (hairpin) structure. The loop is complementary to the target sequence, and the stem is formed by the annealing of complementary arm sequences that are located on both the ends of the probe sequence. A fluorophore, such as fluorescein (Fam), is covalently linked to the 5-prime end of the probe and a quencher dye, such as Black Hole Quencher®-1 (BHQ®-1) dye, is covalently attached to the 3-prime end. Molecular beacons do not fluoresce when they are free in solution because they are in closed loop shape and the proximity of the quencher prevents the

fluorophore from emitting light. When the probes encounter a target molecule, they form a probe-target hybrid that is longer and more stable than the stem hybrid. Hybridization with a target nucleic acid strand opens the hairpin and physically separates the reporter from quencher: this conformational change allows a fluorescence signal to be emitted upon excitation (Fig. 3.3) [273-275].

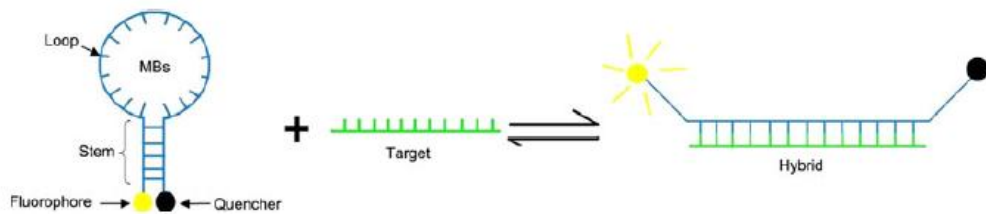


Figure 3.3. Molecular beacon (MB) probe structure and working principle [273].

The allele specific technique could lead to misprime when performed with natural DNA primers leading to inaccurate genotyping. Therefore, primers and beacon probes were modified with locked nucleic acids (LNA) to test the presence of the *BRAF*^{V600E} mutation [245].

LNA is a bicyclic nucleic acid analogue that contains a 2'-O, 4'-C methylene bridge which restricts the flexibility of the ribofuranose ring locking the structure into a rigid conformation with enhanced hybridization performance and biological stability (Fig. 3.4).

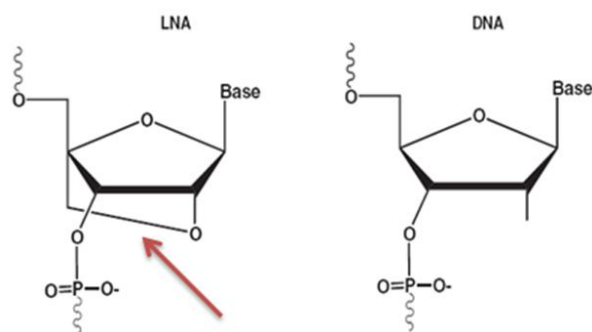


Figure 3.4. Locked nucleic acid (LNA) and DNA base structures.

ASLNAqPCR assay can be performed in any laboratory with real-time PCR equipment, doesn't require post-PCR manipulation (reducing the risk of contaminations and material loss), is cost-effective and rapid. The process is not

labor-intensive, in fact it requires about 3 hours after DNA extraction including about 30 minutes operator time to prepare the PCR reaction and load the plate, 1 hour and 30 minutes for the real-time run and 5 for data analysis. Moreover, this is a semi-quantitative method that gives information about the ratio of mutant and wild-type alleles. A limitation of ASLNAqPCR, inherent in all hot spot mutation assays, is that it identifies only the targeted mutations [245].

3.3.1 PCR design and conditions

Both primers and molecular beacon probe for ASLNAqPCR (Table 3.5) were designed using Primer3 software (<http://frodo.wi.mit.edu/primer3/>). Flanked molecular beacon arms were designed using the OLIGO 6.0 software reaching a temperature between 57°C and 61°C in the stem loop conformation.

Both primers and molecular beacon probe were modified with LNA as previously described by Latorra *et al.* using a tool on the Exiqon website (www.exiqon.com) that performs a melting temperature valuation [276].

In the forward primers recognizing wild-type or *BRAF*^{V600E} alleles, a single LNA nucleotide was placed at the 3' terminal position, where the mutation occurs, in order to avoid inaccurate genotyping. A universal reverse primer was designed for both alleles. The molecular beacon probe was internally LNA-modified allowing to maintain high sensitivity and specificity of signal and to avoid false positives and primer dimers. Both primers and probe were tested by MFOLD (<http://www.bioinfo.rpi.edu/applications/mfold/old/dna/>) to verify the absence of secondary structures that can hamper the annealing to the templates [245].

Gene	Forward Primer	Reverse Primer	Amplicon length
<i>BRAF</i> ASqPCR WT	TAGGTGATTTTGGTCTAGCTACAG+T	TTAATCAGTGGAAAAATAGCCTCA	117 bp
<i>BRAF</i> ASqPCR V600E	TAGGTGATTTTGGTCTAGCTACAG+A	TTAATCAGTGGAAAAATAGCCTCA	
<i>BRAF</i> ASqPCR BEACON	5'-FAM-CCGAAGGGGATC+CAGACAA+CTGTTCAAAGTGCCTTCGG-3BHQ-1 -3'		

Table 3.5. *BRAF* ASqPCR primers and molecular beacon probe. + precedes LNA nucleotides

ASLNAqPCR was performed with reagents from FastStart Taq DNA Polymerase kit (Roche) in a final 25 µl reaction volume containing: 0.2 mM dNTP mix, 1X PCR reaction buffer (with 2 mM MgCl₂), 2 mM MgCl₂ Solution, 1.25 U of FastStart Taq DNA Polymerase, 5 pmol of beacon probe, 1x ROX Reference Dye (Invitrogen), 10 pmol of both forward and reverse primers, 15-40 ng of genomic DNA from FFPE tissues and molecular biology grade water (UltraPure™ DNase/RNase-Free Distilled Water, Gibco) to final volume. Each reaction was covered with mineral oil (for molecular biology, light oil; Sigma-Aldrich).

Real-time PCR was performed using the ABI SDS 7000™ instrument (Applied Biosystems) with PCR conditions shown in Table 3.6: the use of a molecular beacon probe implies that the plate reading step is annealing.

Step	Temperature	Time	No. of cycles
Signal normalization	50°C	2'	1
Initial denaturation/ Enzyme activation	95°C	10'	1
Denaturation	95°C	30''	38
Annealing	60°C*	30''	38
Extension	72°C	30''	38

Table 3.6. PCR conditions for ASLNAqPCR. *Plate reading step.

A 2.5% agarose gel stained with GelStar™ Nucleic Acid Gel Stain (Lonza Bioscience) was performed to confirm the presence of specific PCR products.

3.3.2 Relative quantitation of *BRAF*^{V600E} mutated allele

The data analysis was performed using the threshold cycle (Ct) parameter: relative mutant allele copy number is determined during the exponential phase of realtime PCR using the ΔCt method [277]. If allele specific PCR finds a positive signal for the primer specific for the *BRAF*^{V600E} mutation, the ratio of *BRAF*^{V600E} mutated versus wild type alleles (R) can be calculated with the formula below:

$$\Delta Ct = Ct_{V600E} - Ct_{WT}$$

$$R = 2^{-\Delta Ct}$$

$$\% \text{ mutated cells} = R \times 100$$

Samples with a Ct above 36 for the wild type allele were considered failures because a mutant allele dropout caused by the low amount of genomic DNA cannot be excluded.

Examples of $BRAF^{wt}$ and $BRAF^{V600E}$ sample amplification plots analyzed by ASLNAqPCR are shown in Fig. 3.7.

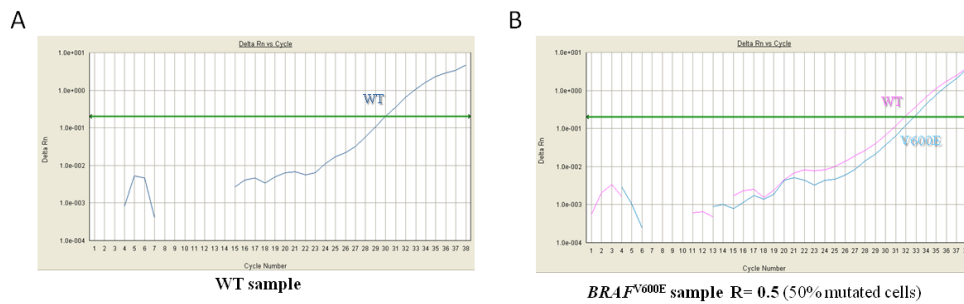


Figure 3.7. $BRAF^{wt}$ (A) and $BRAF^{V600E}$ (B) sample amplification plots by ASLNAqPCR.

3.3.3 Analytical sensitivity

The analytical sensitivity of ASLNAqPCR was assessed using serial dilution of DNA extracted from OCUT (an undifferentiated thyroid cancer cell line) and ARO (an anaplastic thyroid cancer cell line) that are $BRAF^{V600E}$ heterozygous. DNA isolated from the cell lines is spiked in a pool of healthy female donors DNA (DNA Female pool, Promega) and serially diluted as 50%, 20%, 10%, 5%, 1%, 0.1%, 0.01% mutant to wild type DNA ratios. The analytical sensitivity of ASLNAqPCR, that is the minimal amount of input DNA required to obtain reliable mutation detection with this method, is 0.1% (Fig.3.8). This very high analytical sensitivity allows quantification of mutated DNA in small neoplastic clones [245].

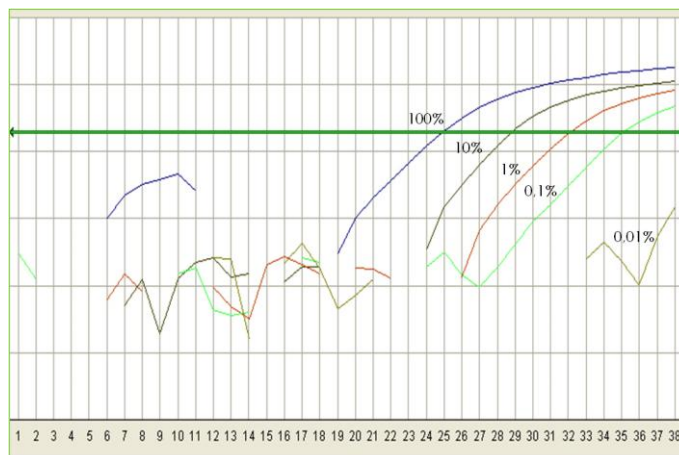


Figure 3.8. Amplification plots showing the analytical sensitivity of ASLNAqPCR. Serial dilution of the $BRAF^{V600E}$ mutated OCUT cell line DNA in wild type DNA.

3.4 Mutational analysis: 454 Next-Generation Sequencing

The screening of $BRAF$ mutations in exon 15 in histologically benign thyroid of cases with $BRAF^{V600E}$ or $BRAF^{wt}$ PTCs was performed by parallel pyrosequencing technology using the 454 GS-Junior[®] next-generation sequencer platform (Roche) according to the manufacturer's instructions [250].

The main Next-Generation Sequencing (NGS) technology advantages compared with the first generation Sanger sequencing technology are high throughput (linked with the possibility of parallel analysis of multiple samples) and reduced cost. NGS technologies also merge the possibility to screen for the presence of mutations the entire area of interest with the high analytical sensitivity of targeted mutation assays.

The founder company launched 454 Next-Generation Sequencing (454 NGS) in 2005 and was purchased by Roche in 2007. In late 2009, Roche commercialized the GS Junior System, a benchtop 454 sequencing system with simplified library preparation and data processing, able to perform 400 bp long sequencing reads in 10 hours. The distinguishing advantages of 454 Sequencing System are its speed and the read length compared with other NGS systems but the cost of reagents is higher [278].

454 NGS allows the parallel analysis of hundreds of amplicons of the same sequence (“reads”) and provides a quantitative estimation of the relative abundance of the mutated allele determining the number and percentage of mutated reads.

3.4.1 Primers design

In this study, primers designed for 454 NGS PCR reactions for the preparation of the amplicon library (Fig. 3.9) are bi-directional fusion primers made up of three parts: a universal sequencing tail, multiple identifiers nucleotide sequences (MIDs) and a template specific sequence (Integrated DNA Technologies Inc).

The 5'-portion is a 25-mer: the sequence is composed of an Adaptor and a “key” (shown in blue and red in Fig 3.9 respectively). The Adaptor sequences (A and B) are universal sequences involved in binding to the DNA Capture Beads (Lib-A), and annealing the emPCR Amplification Primers and the Sequencing Primers. The four nucleotide sequencing key “TCAG”, placed at the end of 5'-part of the fusion primer, allows the instrument to recognize where the amplicon sequence starts.

Multiplex IDentifiers (MIDs), shown in Fig.3.9 in orange, are “DNA barcodes” used to sort each amplicon after the sequencing Run by the data analysis software. In a given sequencing Run a specific target sequence is associated with a unique pair of MID and therefore is possible to determine which sample each read derives from: MIDs partly account for 454 NGS high throughput. These oligonucleotides (10-11 nucleotides long) were added between the sequencing key and the template specific primers of both forward and reverse primers.

The forward and reverse *BRAF* exon 15 specific primers are 21 nucleotides long and situated at the 3-prime end of the oligonucleotides previously described (Table 3.10).

Forward primer (Primer A-Key):
 5'-CGTATCGCCTCCCTCGCGCCATCAG-MID-template-specific-sequence-3'
 Reverse primer (Primer B-Key):
 5'-CTATGCGCCTTGCCAGCCCGTCAG-MID-template-specific-sequence-3'

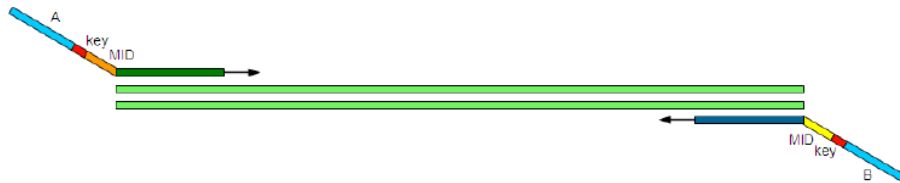


Figure 3.9. 454 Next-Generation Sequencing fusion primers.

Gene	Forward Primer	Reverse Primer
<i>BRAF</i> exon 15	CGTATCGCCTCCCTCGCGCCA	CTATGCGCCTTGCCAGCCCGC

Table 3.10. 454 Next-generation *BRAF* exon 15 specific primers.

3.4.2 Amplicon library preparation

PCR conditions

PCR was performed using a high fidelity hot-start protocol for amplicon generation in order to avoid amplification derived variations in the sequence and non-specific elongation at low temperatures (FastStart High Fidelity PCR System, Roche).

FastStart High Fidelity PCR System kit contains an Enzyme Blend (5 U/μl) consisting of a FastStart Taq DNA Polymerase with heat-labile blocking groups on amino acid residues and a chemically modified proofreading protein without polymerase activity both inactive below 75°C.

For a final 25 μl reaction volume, the following reaction mix was added to each well: 0.2 mM dNTP mix (Roche), 1X FastStart High Fidelity Reaction Buffer (with 1.8 mM MgCl₂), 1 mM MgCl₂ Solution, 1.25 U of FastStart High Fidelity Enzyme Blend, 6.25 pmol of both forward and reverse primers, 15-40 ng of genomic DNA from FFPE tissues and molecular biology grade water (UltraPure™ DNase/RNase-Free Distilled Water, Gibco) to final volume. Each

reaction was covered with mineral oil (for molecular biology, light oil; Sigma-Aldrich).

PCR was performed in a thermal cycler using the conditions summarized in Table 3.11:

Step	Temperature	Time	No. of cycles
Initial denaturation/ Enzyme activation	95°C	2'	1
Denaturation	95°C	30''	37
Annealing	60°C	30''	37
Extension	72°C	1'	37
Final extension	72°C	7'	1

Table 3.11. PCR steps for 454 next-generation sequencing amplicon library preparation

PCR products were run on a 2.5% agarose gel stained with GelStar stain (Lonza Bioscience) to screen them for the presence of the specific amplified DNA sequences (165 bp) and exclude a high presence of fusion primer dimers.

Library purification

The library preparation method of the 454 Sequencing System requires the PCR amplicon purification using a solid-phase paramagnetic bead purification system (Agencourt AMPure XP PCR Purification, Beckman Coulter).

This procedure delivers DNA without contaminant carryover such as salt, unincorporated dNTPs, enzymes and small molecular species such as free Adaptors and Adaptor dimers.

Briefly, in a well 20 µl of PCR products, 25 µl of molecular biology grade water (UltraPure™ DNase/RNase-Free Distilled Water, Gibco) and 65 µl of paramagnetic beads were mixed and incubated for 10 minutes at room temperature in order to allow the binding of PCR amplicons to the beads (Fig.3.12, step 1-2), then, after an incubation of the previous mixture on the magnet (Agencourt SPRIPlate 96 Super Magnet Plate) for 5 minutes at room temperature, the separation of PCR amplicons bound to magnetic beads from contaminants was obtained by supernatant discard (Fig.3.12, step 3). After washing twice PCR amplicons with 70% ethanol (Fig.3.12, step 4), elution of purified PCR amplicons from the magnetic particles (Fig.3.12, step 5) was

performed using 20 µl of 1x TE Buffer (10 mM Tris-HCl pH 8.0, 1 mM EDTA, Sigma-Aldrich). The purified PCR products were transferred away from the beads into a new plate (Fig.3.12, step 6) and were stable at 4° C until seven days.

It is important to remove any free and dimerized Adaptors from the library before performing an emPCR amplification because they can compete against amplicons for binding to the Capture Beads during the preparation of the emPCR amplification reaction, the short size of dimers makes them good templates for amplification in the emPCR amplification reaction, and they would also be included in the quantification of the amplicons causing them to represent a sizable fraction of the final reads.

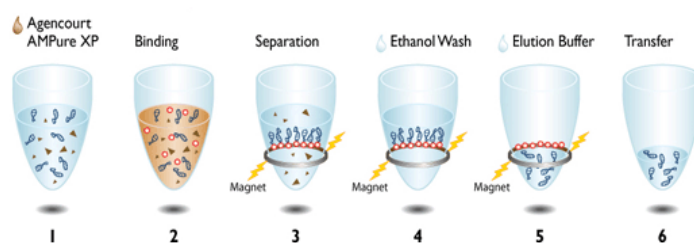


Figure 3.12. Library purification process overview.

The amplicons are quantitated separately and then pooled for emPCR amplification and sequencing, in equimolar representation.

Library quantitation

Post-cleanup of PCR products, the amplicons were fluorometrically quantitated using the Quant-iT PicoGreen[®] dsDNA quantitation Assay Kit (Invitrogen) and measured with the QuantiFluor[®]-ST Fluorometer.

Quantitation and pooling accuracy are very important in order to ensure that each amplicon is adequately represented in the sequencing Run.

An eight point standard curve was prepared according to the manufacturer's instructions performing serial dilution of the DNA standard provided in 1x TE Buffer with the amounts of DNA per standard well listed in Table 3.13. The coefficient of determination value of the standard curve accepted to obtain accurate quantitation of samples was $R^2 > 0.98$.

Standards	DNA concentration
1	100 ng/well
2	50 ng/well
3	25 ng/well
4	12.5 ng/well
5	8.25 ng/well
6	3.13 ng/well
7	1.56 ng/well
8	0 ng/well

Table 3.13. DNA concentrations of the standard curve points.

The PicoGreen[®] dye was diluted to 1:200 with 1x TE and 100 µl of the diluted dye were mixed with 100 µl of both standard dilutions and 1:100 diluted samples before the quantitation of the standard curve points and the samples.

Amplicon dilution and pooling

The concentration of unknown samples was calculated in ng/µl from fluorescence signals by interpolation from the standard curve in an Excel-file that contained also the amplicon lengths allowing the concentrations of amplicons to be converted from ng/µl to molecules/µl using the following formula:

$$\text{Molecules}/\mu\text{l} = \frac{\text{sample conc}[\text{ng}/\mu\text{l}] \times 6.022 \times 10^{23}}{656.6 \times 10^9 \times \text{amplicon length}[\text{bp}]}$$

Then, single amplicons were diluted with 1x TE Buffer to 1×10^9 molecules/µl and pooled by mixing an equal volume (for example, 10 µl) of each amplicon.

The amplicon pool was diluted to 1×10^7 molecules/µl by adding 10 µl of the amplicon pool to 990 µl molecular biology grade water. This is a stop step: the 1×10^9 molecules/µl single amplicon dilutions, the pool and the 1×10^7 molecules/µl dilution can be stored at -20°C.

3.4.3 Emulsion PCR (emPCR)

Emulsion PCR (emPCR) is a PCR amplification within aqueous droplets that function as amplification microreactors in an oil-aqueous emulsion allowing multiple simultaneous PCR reactions to be performed. Each droplet contains all reagents necessary for PCR reaction and can encapsulate an individual bead annealed to a single DNA fragment. This annealing occurs because sepharose beads carry immobilized primers complementary to the library A or B adaptors respectively: thus the amplification of the DNA fragment can be performed both in forward and in reverse (Lib-A method). During the amplification the immobilized primers are elongated by the DNA polymerase so the PCR products remain attached to the bead surface. After the emulsion PCR amplification, each droplet contains a bead carrying several thousand clones of the same template sequence captured by the bead (Fig. 3.14).

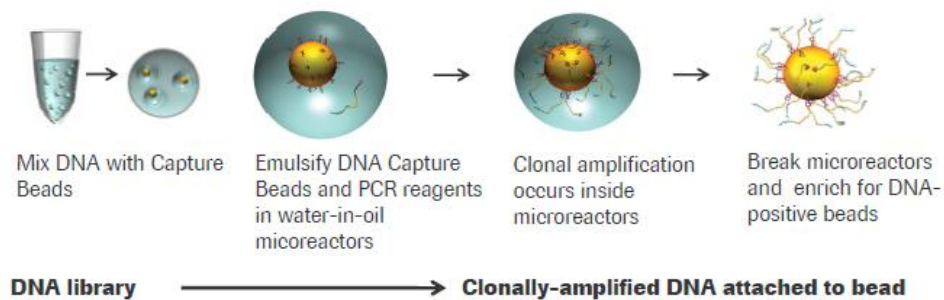


Figure 3.14. Emulsion PCR (emPCR) process.

First of all, the pool was further diluted in order to achieve 1.2 DNA molecules per DNA Capture Bead, whose total number is 5×10^6 , using the following equation:

$$\mu\text{l of DNA library per tube} = \frac{\text{desired molecules per bead} \times 5 \text{ million beads}}{\text{library concentration (in molecules}/\mu\text{l)}}$$

Considering the scarce volume calculated (0.6 μl), a 1:20 dilution of the pool was prepared in molecular biology grade water (UltraPure™ DNase/RNase-Free Distilled Water, Gibco) such that the volume to be added is higher (12 μl).

This 1:1 proportion of DNA fragments and beads guarantees a low number of both the beads carrying no DNA fragments (empty emPCR beads) and the ones with more than one DNA amplicon (mixed emPCR beads) due to stochastic variations during the emulsion PCR process. Thus, library quantitation is a critical step for 454 next-generation sequencing to avoid high presence of beads that can't produce readable sequences.

Two identical mixes, except for primers, were prepared in separated tubes as follows: 205 µl of molecular biology grade water (UltraPure™ DNase/RNase-Free Distilled Water, Gibco), 260 µl of Additive, 135 µl of Amp Mix, 35 µl of Enzyme Mix, 1 µl of PPiase and 40 µl of either primer A or B.

The volume of the Amplicon DNA library (12 µl) was added to both the tubes of washed Capture Beads A and Capture Beads B, then 600 µl of previously prepared mix containing either primer A or B were mixed with Capture Beads A or B respectively.

The emulsion was prepared pouring first the emulsion oil into the IKA Ultra Turrax stirring tube with 2 ml of 1x Mock Mix and shaking them at 4000 rpm for 5 minutes and then adding the entire volume contained both in the tube of captured library B and A mixing at 2000 rpm for 5 minutes after each addition.

The emulsion was dispensed in a 96-well plate aliquoting 100 µl in each well and PCR was performed in a thermocycler with the heated lid turned on using the amplification program summarized in Table 3.15. The emPCR preparation requires about two hours to be performed and the program takes about 6 hours to complete.

Step	Temperature	Time	No. of cycles
Initial denaturation	94°C	4'	1
Denaturation	94°C	30''	50
Annealing	56°C	4'30''	50
Extension	68°C	30''	50
Final hold	10°C	up to 16 h	1

Table 3.15. Emulsion PCR (emPCR) steps.

3.4.4 Recovery and enrichment processes

The emulsion was aspirated from the plate through a transpette into a 50 ml conical tube using a vacuum source: this Emulsion Breaking Apparatus is provided in the GS Junior Titanium Oil and Breaking Kit (Fig. 3.16)

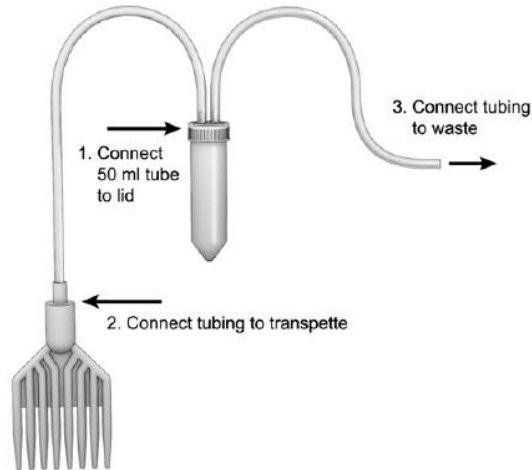


Figure 3.16. Vacuum-assisted Emulsion Breaking Apparatus.

The emulsion was broken and beads were washed using isopropanol and absolute ethanol followed by centrifugations.

The beads carrying amplified DNA are separated from empty beads by an enrichment process, whereas the ones with more than one DNA amplicon (mixed beads) are discarded after sequencing Run during data processing.

The enrichment was performed according to manufacturer's instructions.

Briefly, a Melt Solution containing NaOH was incubated with the washed beads: it removes the non-immobilized complementary strands from the beads thus PCR amplicons become single stranded. The Capture Beads carrying single stranded PCR amplicons were then incubated with biotinylated Enrich Primer A and Enrich Primer B: these primers anneal to DNA fragments on Capture beads. The Enrichment Beads, streptavidin-coated magnetic beads, capture all the beads carrying DNA fragments by the biotinylated Enrich Primers. A Magnetic Particle Concentrator (MPC) allows the DNA positive beads to be separated from empty beads that are discarded. Finally, the beads carrying DNA were recovered by Enrichment Primers denaturation using the Melt Solution, the Sequencing Primers were added and the beads were counted.

In this study, bidirectional sequencing was performed because it provides higher sequencing accuracy. Therefore, two kinds of primers, “Primer A” and “Primer B”, were used for target amplicon sequencing from either end. In order to consider a variant found as a valid mutation the independent confirmation of sequence by both forward and reverse reads was required because it reduces sequencing errors (see the section titled “*Assessment of variants*”).

The Seq Primer A e B (15 μ l each) anneal to the bead bound to hybridized to single-stranded PCR amplicons that serve as a template and their excess is removed through a series of washes.

The recovery and enrichment processes require about 2.5 hours to be carried out.

In order to evaluate the amount of enriched beads, the GS Junior Bead Counter was used: the recommended input bead number for a GS Junior sequencing Run is 500,000 enriched beads (5% enrichment) that corresponds to the top of the bead pellet at the level of the bottom edge of the window. The upper line corresponds to 2 million beads (20% enrichment) (Figure 3.17).

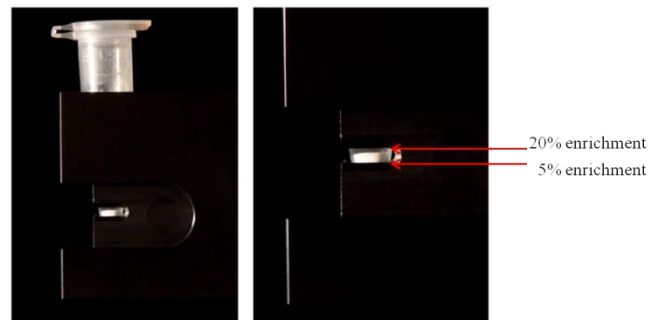


Figure 3.17. Bead counting and enrichment percentage.

3.4.5 Parallel pyrosequencing

The GS Junior Sequencing procedure consists of four steps: after the instrument's fluidics washing with Pre-wash Buffer, the PicoTiterPlate (PTP), a fiber-optic slide, was placed into a flow chamber, the Bead Deposition Device (BDD), for the following bead layers deposition (Fig 3.18), then the instrument was primed with reagents and buffers and the sequencing Run was performed.

Before the bead layers deposition, 350 μ l of BB2 Buffer, containing the Apyrase enzyme, were loaded onto the plate placed into the chamber.

The PicoTiterPlate (PTP) was then filled with DNA Beads, Packing Beads, Enzyme Beads and PPIase beads in separate layers by injection of bead suspensions followed by centrifugation in the order specified in Figure 3.18. These smaller beads surround the template beads and permit the NGS chemistry.

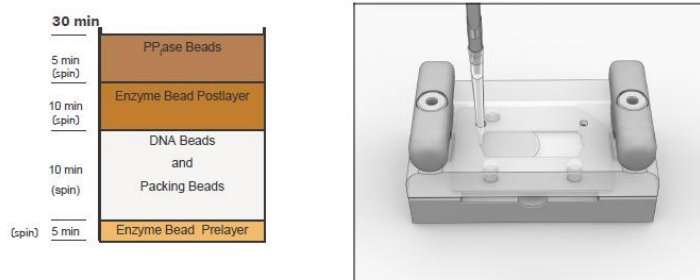


Figure 3.18. Bead Deposition Device (BDD) and procedure.

The DNA-carrying beads were deposited into the wells of the PicoTiterPlate (PTP), such that no more than a single bead carrying clonally amplified DNA is deposited into an individual well. In the Titanium version, the inner side of wells is titanium-coated in order to increase read length and reduce crosstalk between adjacent wells. Fundamental reagents for NGS chemistry are contained in the DNA Bead suspension (Polymerase, Polymerase Cofactor, BB2 Buffer and Packing Beads). The sequencing Run preparation requires about two hours to be performed.

The Roche 454 sequencing system implements pyrosequencing technology, method that relies on the detection of inorganic pyrophosphate release during

nucleotide incorporation converting it into proportional bioluminescence using enzymatic reactions [250, 269].

Instead of using dideoxynucleotides to terminate the chain amplification, in the pyrosequencing method the addition of dNTPs is performed sequentially in a fixed order and in limiting amounts: therefore DNA polymerase extends the primer and pauses until the addition of the next complementary dNTP. The incorporation of the complementary dNTPs onto the template causes a stoichiometrical release of pyrophosphate (PPi) that triggers the sequential reactions of sulfurylase and luciferase, the enzymes attached to the enzyme beads. ATP sulfurylase converts PPi to ATP in the presence of adenosine 5' phosphosulfate (APS). This ATP drives the luciferase-catalyzed conversion of luciferin to oxyluciferin that generates visible light in amounts that are proportional to ATP and, therefore, to the number of nucleotides incorporated (Fig. 3.19). Since ATP is also substrate for luciferase reaction, during nucleotide flow an ATP analogue, able to match thymine but not to be substrate for luciferase enzyme, is used. The unmatched nucleotides and ATP are converted to nucleoside monophosphate by the apyrase before the restart of the reaction with the next nucleotide. Another enzyme, pyrophosphatase (also referred to as PPIase) is flowed at the end of each nucleotide flow cycle to degrade any excess PPi. Hence, these enzymes avoid aspecific reactions. The sequential flow of the four dNTPs is performed 200 times during a Run which requires about ten hours to be performed.

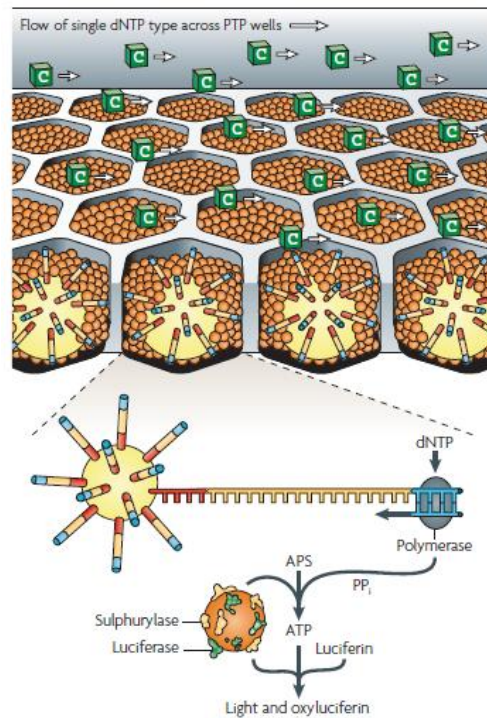


Figure 3.19. 454 Next-Generation Sequencing chemistry [269].

3.4.6 454 Sequencing System data handling

Data handling in the 454 Sequencing System consists of three phases: data acquisition, data processing and data analysis.

Data acquisition

During the data acquisition phase, carried out by the GS Junior Sequencer software, a set of raw digital images captured by the camera are recorded. Each image represents the surface of the PicoTiterPlate device during one nucleotide flow. If the DNA fragments immobilized on a bead located in a given well are extended during a nucleotide flow, light is emitted from the PTP well and detected by a high-resolution charge-coupled device (CCD) camera directly attached to the lower side of the PicoTiterPlate and captured on the image (Fig. 3.20).

Data processing

During the data processing phase, controlled by the GS Run Processor application, raw image data are converted into base-called results. Data processing requires two hours to be carried out and consists of two steps, image processing and signal processing (Fig. 3.20).

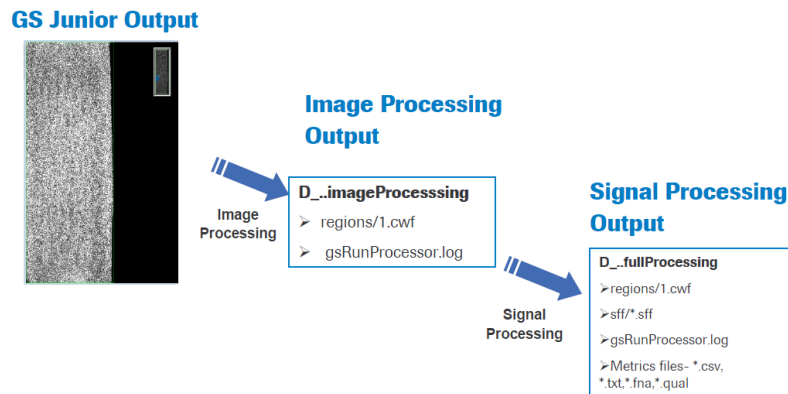


Figure 3.20. Data acquisition and processing.

The software first measures the amount of light emitted in each active well during each flow (image processing step) then it performs a series of automatic data correction steps that compensate for optical effects and chemical inefficiencies and segregates low quality reads and, finally converts signal intensities of high quality reads into a series of peaks called a flowgram (signal processing step). The height and the order of the peaks reveal the DNA sequence (Fig. 3.21). Therefore, GS RunProcessor produces a series of files including SFF (standard flowgram format) files containing the basecalled sequences and per-base quality scores.

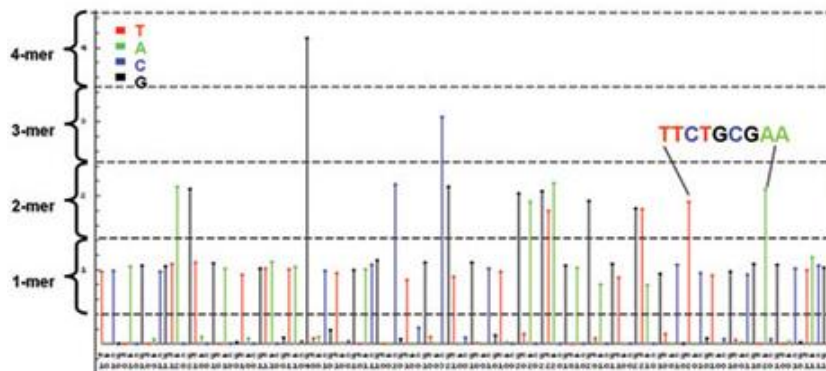


Figure 3.21. The flowgram.

Data analysis

During the data analysis phase, a software uses as input the reads and flowgrams output in SFF format obtained through data processing.

The GS Amplicon Variant Analyzer (AVA) software was used: it assigns each read to the proper amplicon using MID information, aligns amplicon reads to a reference sequence and thus identifies differences between the reads and the reference sequence providing also a quantitation of known or novel sequence variants. AVA trims the PCR primer sequences from the reads: the PCR specific primer part in the sequencing reads is by definition equal to the genomic reference sequence and thus independent of the individual sample that is sequenced. This software displays the variant positions and their frequency both with histograms and with a multiple alignment of forward and reverse reads to the reference (Fig. 3.22). 454 Sequencing system produces hundreds to thousands of clonal reads for each amplicon that results in unambiguous haplotyping intuitively displayed by AVA and in confident calling of low-frequency variations.

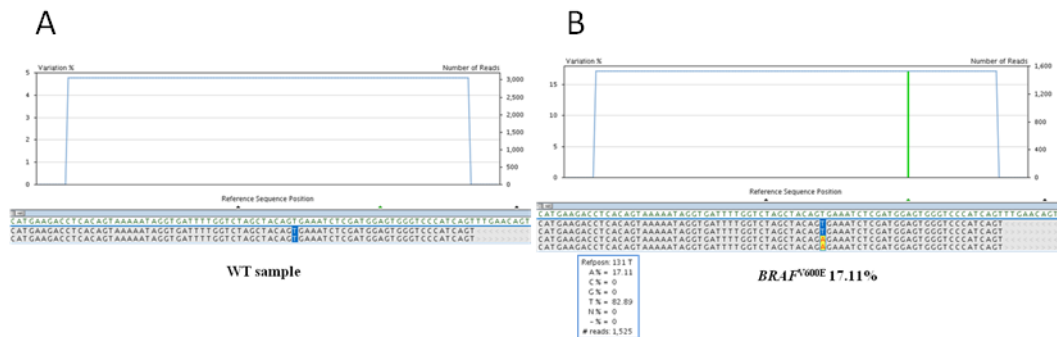


Figure 3.22. $BRAF^{wt}$ (A) and $BRAF^{V600E}$ (B) samples by 454 NGS.

Assessment of variants

The variations observed in the reads were carefully evaluated before considering them to be true variants in *BRAF* exon 15.

In this study a cutoff of 1% of total reads was set to consider *BRAF* exon 15 carrying the variant in a sample with a number of at least 10 mutated reads to believe that the variant is not an artifact.

Since C→T/G→A or A→G/T→C transitions can be artificially incorporated into DNA extracted from microdissected sections of samples fixed in formalin, 10 normal tissues from patients without neoplasms were also screened for the presence of *BRAF* exon 15 mutations in order to further validate uncommon mutations [279, 280].

Moreover, in order to reduce the risk of false positives, some features of the variants found in the reads were considered: the bidirectional support, the proximity of homopolymers, the noise level and the coverage.

Variants found in either forward or reverse reads, were excluded whereas the confidence in validity was strengthened if the frequency of a variant was similar in both directions. This corroborating evidence is particular important for variants found in close proximity of the trailing edge of a read that are considered less believable because sequencing quality can begin to drop off at the end of an amplicon read.

Pyrosequencing is quite imprecise in the sequencing of homopolymeric regions exceeding the length of a few nucleotides (longer than 6 bases): the presence of a homopolymer of the same nucleotide in close proximity upstream or downstream of the one impacted by the variant, could have caused an undercall or overcall due to known sequencing artifacts called carryforward and incomplete extension. Hence, also these variants were excluded.

Moreover, only the low frequency variants convincingly above the noise level, which is the presence of many low level frequency variations in the plot, and with high depth of coverage were considered. Synonymous variants were not reported.

After assessment of validity, an interrogation of the Catalogue of Somatic Mutations in Cancer database (COSMIC) and a literature search with PubMed

was performed in order to know if mutations observed were previously known in PTC, in other cancers or unknown [154].

Moreover, the tool PolyPhen-2 (Polymorphism Phenotyping v2) was used to predict possible impact of a given non-synonymous variant on the structure and function of the BRAF protein. This tool, through an *in silico* prediction algorithm considering sequence-based, structural and phylogenetic information, associates a score to each mutation and predicts that it will be benign (0-0.2), possibly damaging (0.2-0.85), or probably damaging (0.85-1) [281].

3.5 Analysis of *BRAF* clonality: evaluation of mutated neoplastic cells proportion

Since the analysis of genetic heterogeneity in tumors can be deeply biased by “contamination” with non-tumoral cells, two pathologists estimated the amount of neoplastic cells in each tumor sample and the percentage of mutated cells obtained by ASLNAqPCR or 454 NGS was normalized on this proportion thus obtaining a better appraisal of mutated neoplastic cells proportion.

Assuming *BRAF*^{V600E} heterozygous, the percentage of mutated cells obtained by ASLNAqPCR corresponds to the double of the mutated allele percentage.

The following formula (where R is the ratio of BRAF mutated versus wild type allele and X is the estimated percentage of neoplastic cells) was used for ASLNAqPCR method:

$$\% \text{ mutated neoplastic cells} = (R/X) * 100$$

Similarly, the percentage of mutated cells obtained by 454 NGS was normalized on the one of neoplastic cells using the following formula (where MR is the percentage of mutated reads by 454 NGS and X is the estimated percentage of neoplastic cells):

$$\% \text{ mutated neoplastic cells} = [(MR*2/X)] * 100$$

Statistical analysis was performed using GraphPad Prism 5.0 tool: results with a p-value < 0.05 were considered to be statistically significant.

CHAPTER 4

RESULTS

4.1 1 Aim 1 - Clonality of $BRAF^{V600E}$ mutation in PTC

4.1.1 Analysis of PTCs for $BRAF^{V600E}$ by ASLNAqPCR

For the first project, 155 consecutive FFPE thyroid specimens of PTCs were analyzed. These samples were genotyped for the presence of $BRAF^{V600E}$ mutation using the ASLNAqPCR semi-quantitative technique, which not only detects $BRAF^{V600E}$ but also permits to assess the percentage of $BRAF^{V600E}$ mutated allele. Eighty five out of 155 samples (54.8%), corresponding to 78 patients, aged from 25 to 79 years (mean 53 years) were mutated for $BRAF^{V600E}$. The frequency here observed is in line with that reported in literature for $BRAF^{V600E}$ mutation in PTCs [93].

$BRAF^{V600E}$ mutated PTCs were further subdivided according to size and histological diagnosis in: papillary microcarcinoma (mPTC), PTC-classic (PTC CI), PTC-follicular variant (PTC FV) and PTC-tall cell (PTC TC) (Fig. 4.1).

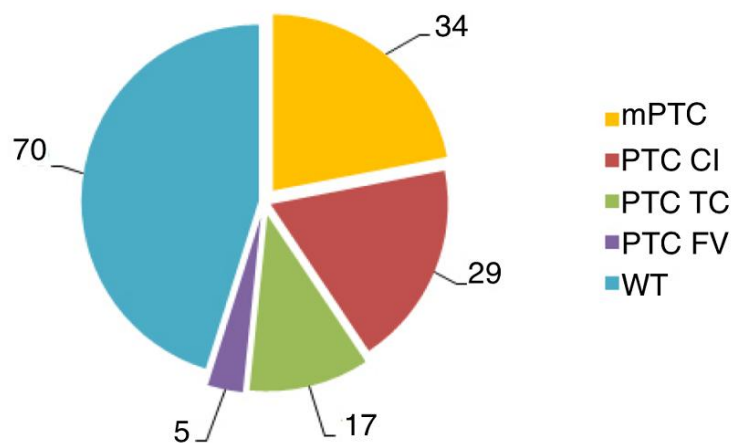


Figure 4.1. Distribution of analyzed PTC samples. PTC, papillary thyroid carcinoma; mPTC, papillary microcarcinoma; PTC CI, PTC-classic; PTC TC, PTC-tall cell; PTC FV, PTC-follicular variant; WT, wild-type PTC.

As discussed in section 3.5, the analysis of genetic tumoral heterogeneity can be deeply biased by “contamination” due to non-tumoral cell DNA (stromal, endothelial and inflammatory cells). For this reason, the analyzed areas were estimated by two pathologists evaluating the amount and the proportion of neoplastic cells within each sample. On the assumption that the $BRAF^{V600E}$ mutation is heterozygous in PTC cells, the percentage of mutated cells obtained by ASLNAqPCR corresponds to the double of the mutated allele percentage. In Figure 4.2 three representative $BRAF^{V600E}$ mutated tumors (PTC cases 67, 69 and 65) where the mutation is present in virtually all neoplastic cells (Fig. 4.2 A) and those of 3 representative $BRAF^{V600E}$ mutated tumors (PTC cases 24, 7 and 6) where the mutation is present in a minority of neoplastic cells (Fig. 4.2 B) are shown.

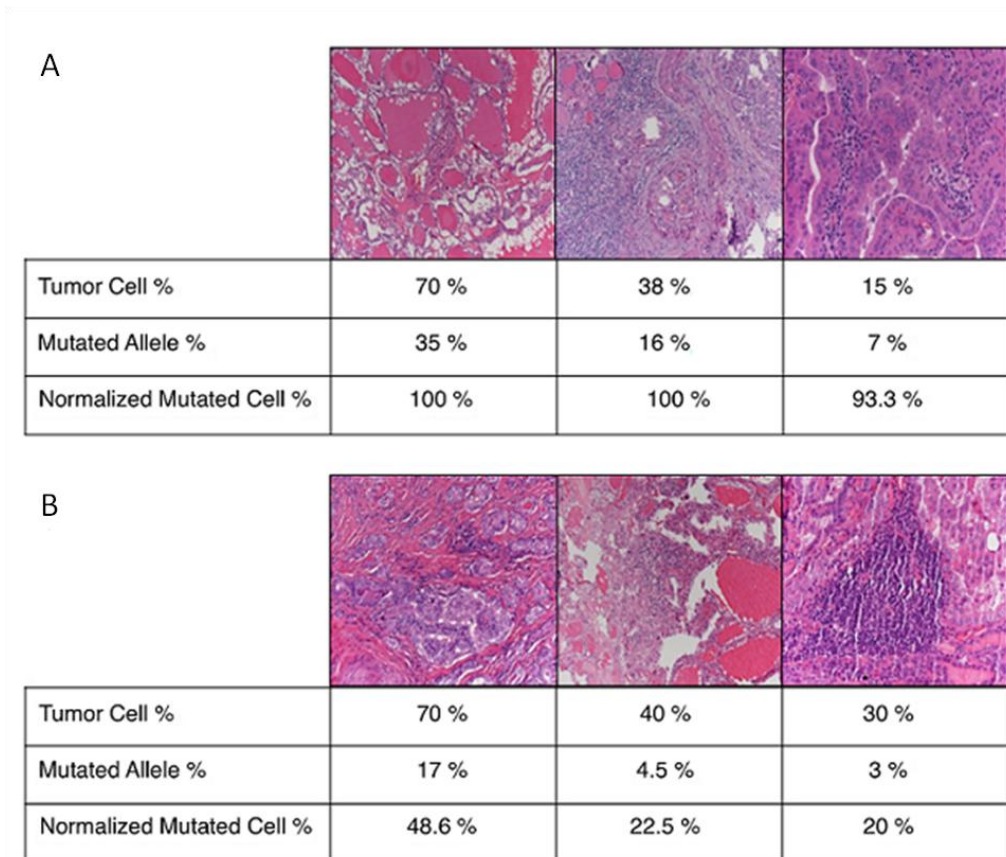


Figure 4.2. PTCs showing clonal (A) or subclonal (B) distribution of $BRAF^{V600E}$ mutation (H&E). The boxes show the percentage of neoplastic cells in the tumor, the percentage of $BRAF^{V600E}$ mutated allele obtained by ASLNAqPCR, and the percentage of $BRAF^{V600E}$ mutated cells after normalization to the estimated proportion of neoplastic cells within the tumor.

Of the 85 mutated PTCs, 51 were PTC (sized 11 to 55 mm) and 34 were diagnosed as papillary microcarcinoma (mPTC) (sized 3 to 10 mm) further subdivided in histological variants whose features are shown in Table 4.3 and Table 4.4 respectively. The calculated ratios ($R = 2^{-(Ct^{V600E}-Ct^{WT})}$) were between 0.01 and 0.82 (mean value 0.32, median value 0.29) and, after normalization to the proportion of neoplastic cells within the tumor, the percentage of neoplastic cells carrying the $BRAF^{V600E}$ mutation ranged from 4% to 107.1% (mean value 67.5% median value 65.0%).

PTC histology	Range of tumor size (mm)	$BRAF^{V600E}$ PTCs	Range of ratios (R)	Range of neoplastic cells (X)	Range of $BRAF^{V600E}$ neoplastic cells (R/X)*100
PTC CI	11-55	29	0.09-0.62	28%-80%	19.2%-104.8%
PTC TC	11-42	17	0.08-0.82	25%-80%	32%-107.1%
PTC FV	11-16	5	0.06-0.7	15%-70%	40%-100%
Total	11-55	51	0.06-0.82	15%-80%	19.2%-107.1%

Table 4.3. Features of histological variants of PTCs $BRAF^{V600E}$ mutated analyzed by ASLNAqPCR. PTC, papillary thyroid carcinoma; PTC CI, PTC-classic; PTC TC, PTC-tall cell; PTC FV, PTC-follicular variant.

In the 34 $BRAF^{V600E}$ mutated mPTC (equal to or less than 1 cm diameter) of the 85 $BRAF$ mutated samples the percentage of mutated neoplastic cells, after normalization to the proportion of neoplastic cells within the tumor, ranged from 4% to 106% (mean 63.8%, median 65.6%).

mPTC (≤ 1 cm) histology	Range of tumor size (mm)	$BRAF^{V600E}$ mPTCs	Range of ratios (R)	Range of neoplastic cells (X)	Range of $BRAF^{V600E}$ neoplastic cells (R/X)*100
PTC CI	3-10	16	0.03-0.8	3%- 80%	18.8%-100%
PTC TC	3- 10	8	0.06-0.55	6%-80%	62.5%- 106%
PTC FV	3-10	10	0.01-0.49	15%- 70%	4-100%
Total	3-10	34	0.01-0.8	3%- 80%	4-106%

Table 4.4. Features of histological variants of mPTCs $BRAF^{V600E}$ mutated analyzed by ASLNAqPCR. PTC, papillary thyroid carcinoma; mPTC, papillary thyroid microcarcinoma; PTC CI, PTC-classic; PTC TC, PTC-tall cell; PTC FV, PTC-follicular variant.

4.1.2 Distribution of $BRAF^{V600E}$ mutated neoplastic cells in PTCs and mPTCs by ASLNAqPCR

Three groups of tumors could be identified in $BRAF^{V600E}$ PTCs (Fig.4.5 A) and in $BRAF^{V600E}$ mPTCs (Fig.4.5 B): 1) tumors with less than 30% of $BRAF^{V600E}$ mutated neoplastic cells; 2) tumors with a percentage of mutated neoplastic cells between 30 and 80%; 3) tumors with more than 80% mutated neoplastic cells. In many PTC samples the mutation was detected in a large neoplastic cell sub-population: 37 of 85 tumors (43.5%) harbored the $BRAF^{V600E}$ in more than 80% mutated neoplastic cells. In 39 of 85 (45.9%) $BRAF^{V600E}$ mutated PTCs, the percentage of mutated neoplastic cells was between 30 and 80%. In 9 cases (10.6%) the percentage of $BRAF^{V600E}$ mutated neoplastic cells was below 30% and in a single case was less than 10%. The distribution of mutated neoplastic cells in mPTCs was virtually identical to that observed for PTC samples > 1cm (Fig. 4.5 B).

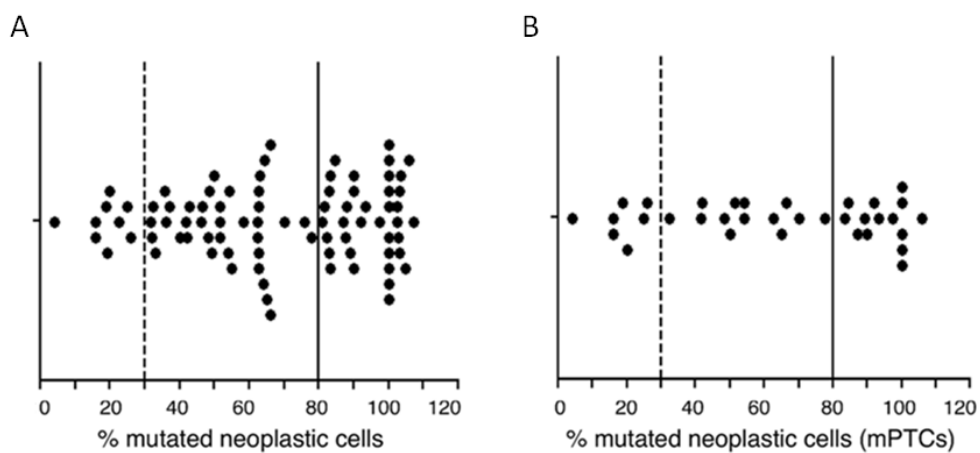


Figure 4.5. Percentage of mutated neoplastic cells in all PTCs (A) and in mPTCs (B). In x axe the percentage of mutated neoplastic cells is indicated. Dotted lines indicate 30% and solid lines indicate 80% of $BRAF^{V600E}$ mutated neoplastic cells, respectively.

Before normalization according to neoplastic cells, only one sample displayed a percentage of mutated neoplastic cells > of 80%, while the rest of the samples showed a lower percentage of neoplastic cells with $BRAF^{V600E}$ mutation (Fig. 4.6 A). The percentage of mutated neoplastic cells, before normalization to the

estimated proportion of neoplastic cells within the tumor, ranged from 1% to 82% (mean 32%, median 29%).

The non normalized results are similar to those previously reported in PTCs based on pyrosequencing analysis of the *BRAF*^{V600E} mutation [248, 266].

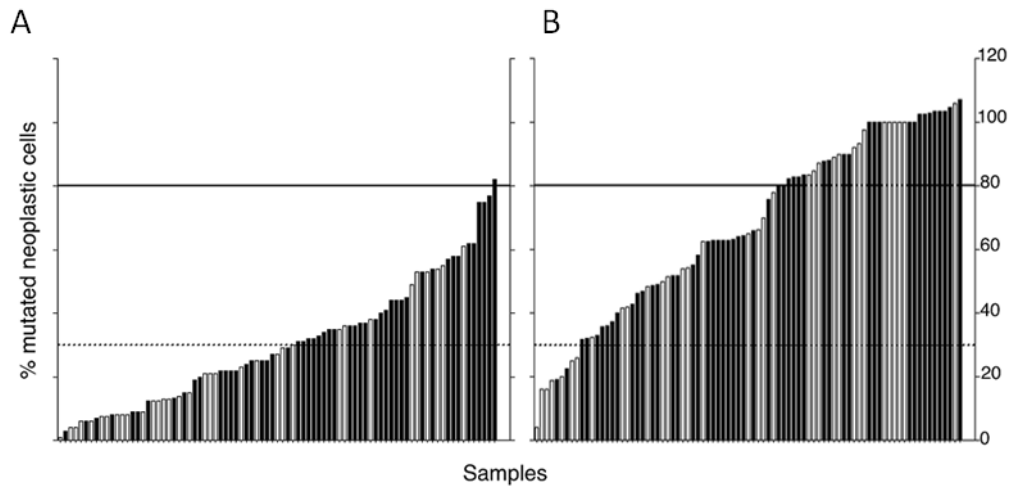


Figure 4.6. Percentage of mutated neoplastic cells in all PTCs before (A) and after normalization (B). In y axe the percentage of mutated neoplastic cells is indicated. Black bars, tumors > 1 cm; white bars tumors ≤ 1 cm (mPTC).

4.1.3 Analysis of PTCs for $BRAF^{V600E}$ by 454 NGS

To strengthen the validity of the analysis, 30 of the 85 $BRAF^{V600E}$ mutated PTCs were also analyzed using a second semi-quantitative technique, a 454 NGS targeted re-sequencing (Fig. 4.7). The presence of the mutation was confirmed in all 30 cases and no mutations other than the V600E were identified. The number of reads ranged from 160 to 1859 (average of 876 and a median of 882 reads).

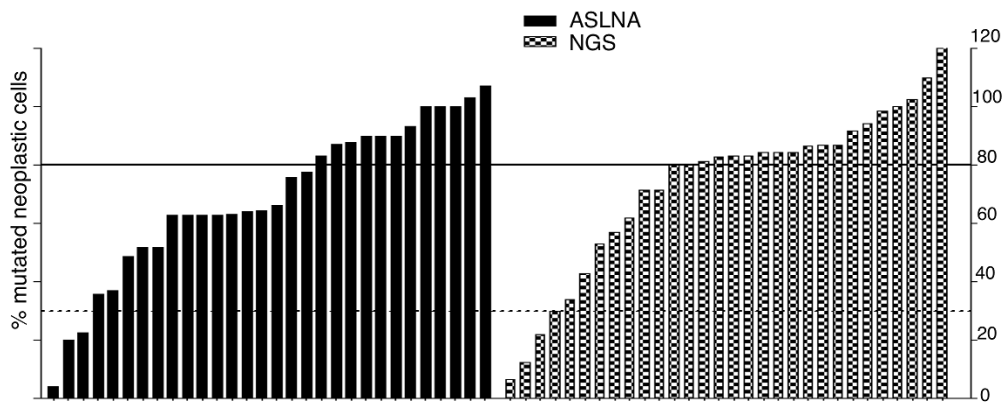


Figure 4.7. Percentage of mutated neoplastic cells in 30 $BRAF^{V600E}$ mutated samples using ASLNAqPCR (left) or 454 NGS (right).

The number of mutated neoplastic cells was similar with both ASLNAqPCR (mean 67.4% and median 65.0%) and 454 NGS (mean 72.3% and median 83.0%) corresponding to approximately 35-40% of $BRAF^{V600E}$ mutated alleles in each PTC sample. The paired t-test showed no statistical difference between the results of $BRAF$ mutational analysis performed by ASLNAqPCR and NGS ($p=0.1064$, Wilcoxon signed rank test) (Fig. 4.8).

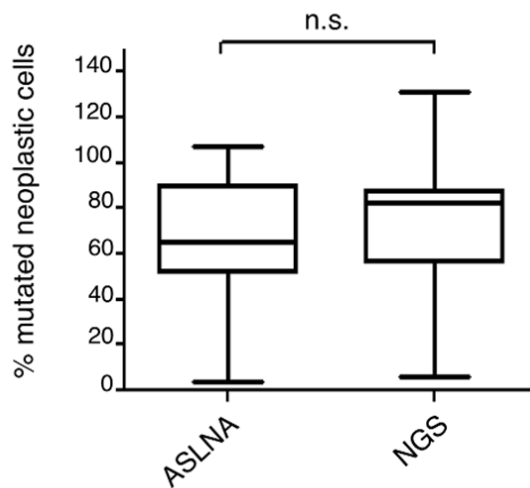


Figure 4.8. Box plots showing the percentage of mutated neoplastic cells in 30 samples using ASLNAqPCR and 454 NGS. ASLNA, Allele Specific Locked Nucleic Acid quantitative PCR; NGS, Next-Generation Sequencing.

Regression analysis showed a strong correlation between the percentage of mutated neoplastic cells detected by ASLNAqPCR and the value obtained by NGS ($r^2=0.6152$, $p=0.0002$, Spearman test) (Fig. 4.9).

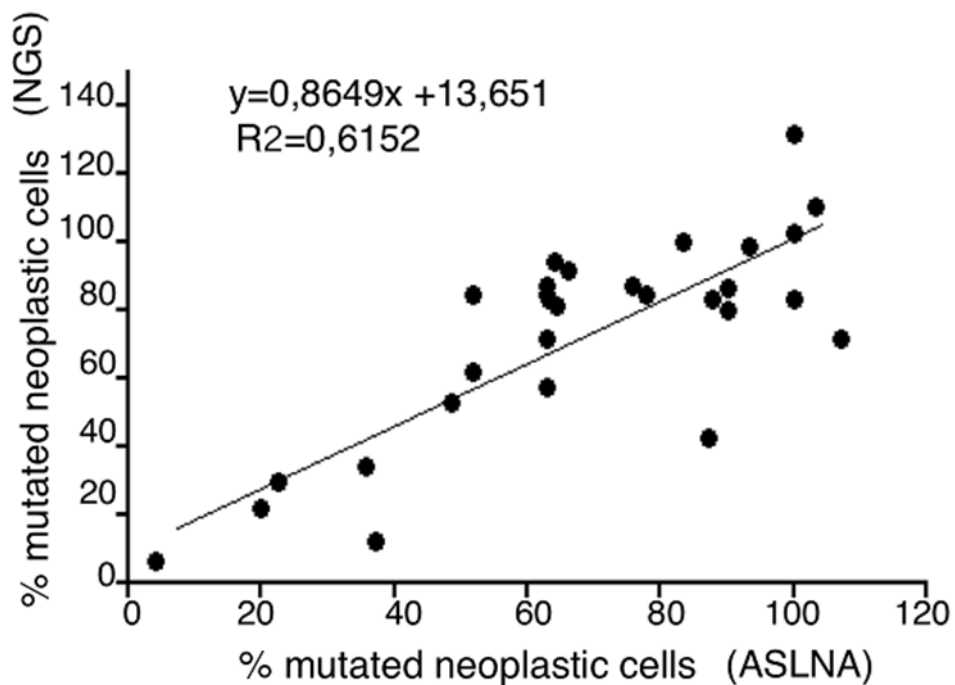


Figure 4.9. Correlation between the percentage of mutated neoplastic cells in 30 samples using ASLNAqPCR and 454 NGS.

4.1.4 Correlation of *BRAF*^{V600E} mutated alleles and clinicopathological features of PTCs

The distribution of PTC subtypes in the three *BRAF*^{V600E} groups observed was analyzed and is described in Table 4.10.

PTC histology	Mutated neoplastic cells within the tumor			Total
	<30%	30%-80%	>80%	
	PTC CI	2	17	
PTC TC	0	6	11	17
PTC FV	0	3	2	5
mPTC	7	13	14	34
Total	9	39	37	85

Table 4.10. Distribution of histological variants of PTCs in the three *BRAF*^{V600E} groups. PTC, papillary thyroid carcinoma; PTC CI, PTC-classic; PTC TC, PTC-tall cell; PTC FV, PTC-follicular variant; mPTC, papillary thyroid microcarcinoma.

The majority of classic PTCs (17/29 cases), belonged to the 30-80% *BRAF*^{V600E} group (Fisher's exact test $p=0.1107$). The majority of tall cell PTCs (11/17 cases) belonged to the >80% *BRAF*^{V600E} group (Fisher's exact test $p=0.0596$). The mPTCs were statistically associated with the tumor group featuring less than 30% *BRAF*^{V600E} mutated cells (chi-squared test $p=0.0440$; Fisher's exact test $p=0.0238$, <30% vs. 30-80% *BRAF*^{V600E} mutated cells; $p=0.0582$, <30% vs. >80% *BRAF*^{V600E} mutated cells; $p=1.000$, 30-80% vs. >80% *BRAF*^{V600E} mutated cells). The percentage of *BRAF*^{V600E} mutated cells was correlated with tumor size, patients' age, tumor stage and lymph node metastases (LNM): there wasn't any statistically significant correlation between the percentage of mutated neoplastic cells and the size of the tumor (Fig. 4.11 A), age of the patients (Fig. 4.11 B) and stage (Fig. 4.11 C).

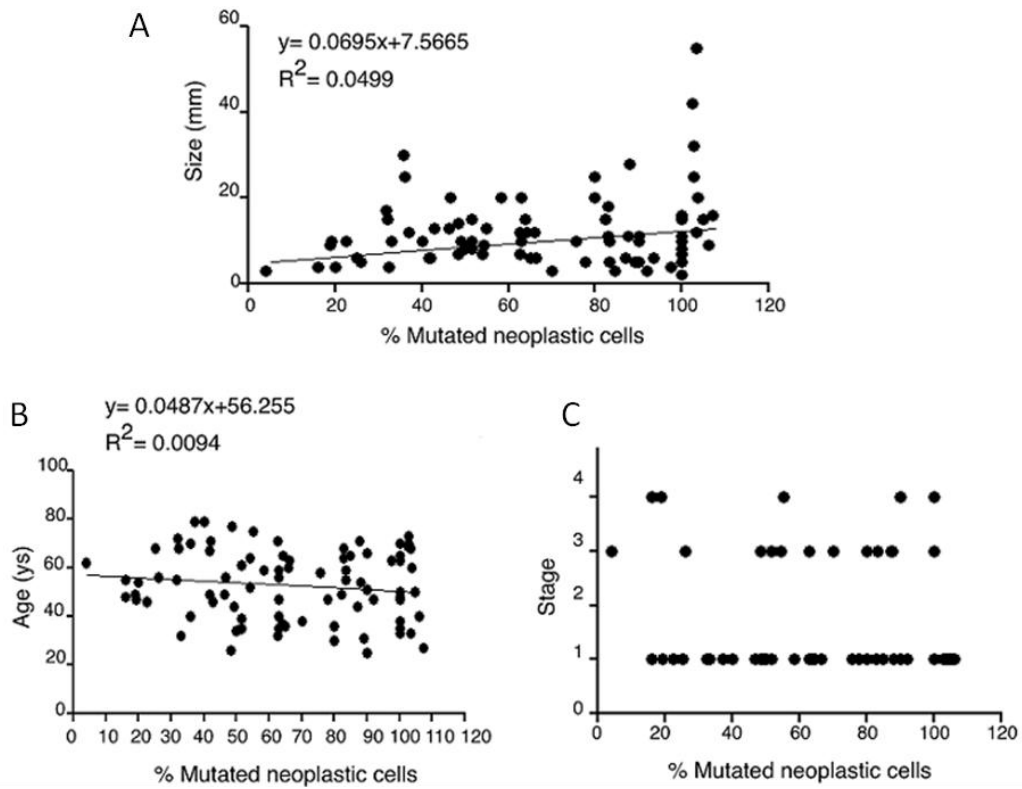


Figure 4.11. Correlation between the percentage of mutated neoplastic cells and the size of the tumor (A), age of the patients (B) and stage (C). Statistical correlation (Spearman test) between the percentage of $BRAF^{V600E}$ mutated cells within the tumor and size ($p=0.1121$), age ($p=0.4891$) and stage ($p=0.3089$).

Moreover, there was no statistical correlation between the percentage of mutated neoplastic cells and the presence of lymph nodal metastasis (Fig. 4.12 A, B).

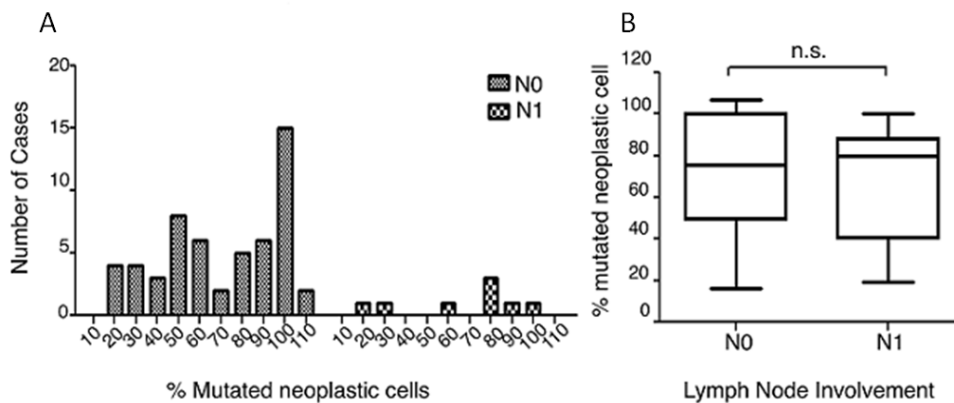


Figure 4.12. Histograms (A) and box plots (B) showing the distribution of mutated neoplastic cells in tumors without (N0) or with lymph nodal metastasis (N1). Statistical correlation (Mann-Whitney test) between the percentage of mutated neoplastic cells and the presence of lymph nodal metastasis ($p=0.7172$).

4.2 Aim 2 - Screening of *BRAF* mutations in exon 15 in histologically benign thyroid tissue

Seventy-five histologically benign FFPE thyroid specimens from 20 cases with *BRAF*^{V600E} mutated PTCs aged from 30 to 79 years (mean 47 years) and 23 from 9 cases with *BRAF*^{wt} PTCs aged from 29 to 70 years (mean 43 years) (unpaired t-test, p=0.2245) were analyzed by 454 Next-Generation Sequencing (NGS) semi-quantitative technique for investigating the possible presence of *BRAF*^{V600E} mutation and uncommon ones in exon 15. Ten samples with histologically normal thyroid parenchyma were analyzed by 454 NGS.

Each target sequence was analyzed from 123 to 4,345 reads per target (mean 1,358.8) with mutations ranging from 1% to 30%.

BRAF^{V600E} mutation was confirmed by 454 NGS in all 20 *BRAF*^{V600E} PTCs previously analyzed using other techniques (Sanger sequencing or ASLNAqPCR).

The histologically benign thyroid specimens are subdivided according to histological features in: “atypical focus”, hyperplasia (HYP), follicular adenoma (FA), oncocytic follicular adenoma, psammoma body (PB) and normal tissue.

Two out of 23 samples (8.7%) from the group with *BRAF*^{wt} PTCs showed the presence of 3 *BRAF* mutations. The proportion of *BRAF* mutations observed in histologically benign FFPE thyroid specimens from the group with *BRAF*^{wt} PTCs is shown in Table 4.13.

Histology	<i>BRAF</i> ^{mut}	<i>BRAF</i> ^{wt}	Total
	histologically benign samples	histologically benign samples	
Atypical focus	1 (20%)	4 (80%)	5
HYP	0	3 (100%)	3
FA	1 (33.3%)	2 (66.7%)	3
PB	0	3 (100%)	3
Normal	0	9 (100%)	9
Total	2 (8.7%)	21 (91.3%)	23

Table 4.13. Detection of *BRAF* mutations in histologically benign FFPE thyroid specimens from the group with *BRAF*^{wt} PTCs. HYP, hyperplasia; FA, follicular adenoma; PB, psammoma body.

Twenty one out of 75 samples (28%) from the group with $BRAF^{V600E}$ mutated PTCs showed the presence of 21 $BRAF$ mutations in 14 codons. Four out of 21 samples (19%) carried the $BRAF^{V600E}$ mutation. The proportion of $BRAF$ mutations observed in histologically benign areas of $BRAF^{V600E}$ mutated PTCs is shown in Table 4.14. Mutations were observed in 6 out of 32 atypical foci (18.8%), 4 out of 13 hyperplasias (30.8%), 1 out of 2 (50%) follicular adenomas, 3 psammoma bodies (100%) and 7 out of 24 (29.2%) normal areas.

Histology	$BRAF^{mut}$	$BRAF^{wt}$	Total
	histologically benign samples	histologically benign samples	
Atypical focus ^a	6 (18.8%)	25 (78.1%)	32
HYP	4 (30.8%)	9 (69.2%)	13
FA	0	1 (100%)	1
Oncocytic FA	1 (50%)	1 (50%)	2
PB	3 (100%)	0	3
Normal ^a	7 (29.2%)	16 (66.7%)	24
Total	21 (28%)	52 (69.3%)	75

Table 4.14. Detection of $BRAF$ mutations in histologically benign FFPE thyroid specimens from the group with $BRAF^{V600E}$ mutated PTCs. HYP, hyperplasia; FA, follicular adenoma; PB, psammoma body. ^a

In one out of 32 atypical foci (3.1%) and in one out of 24 (4.2%) normal areas DNA analysis was unsuccessful due to acid nucleic degradation (2/75 samples, 2.7%).

There was no statistically significant difference in the occurrence of $BRAF$ mutations between the group of histologically benign thyroid specimens with $BRAF^{V600E}$ and the group of specimens with $BRAF^{wt}$ PTCs ($p=0.0546$, Fisher's exact test). Also the differences in the occurrence of $BRAF$ mutations between the atypical foci ($p=1.0000$), hyperplasias ($p=0.5286$), follicular adenomas ($p=1.0000$), psammoma bodies ($p=0.1000$) and normal tissues ($p=0.1492$) from the group with $BRAF^{V600E}$ PTCs and the ones from the group of specimens with $BRAF^{wt}$ PTCs were not statistically significant (Fisher's exact test).

An interrogation of the Catalogue of Somatic Mutations in Cancer database (COSMIC) and a literature search with PubMed was performed in order to know if mutations observed were previously described in PTC, in other cancers or

unknown [154]. The mutations here found were all single nucleotide substitutions (no indels were observed) and had been all previously described. The mutations that met the criteria defined in section 3.4.6 for the assessment of mutational calls were all missense mutations except for one nonsense mutation. In the 10 histologically normal thyroid samples analyzed by 454 NGS no mutations were found. Moreover, no mutations other than the V600E were identified in *BRAF*^{V600E} PTCs samples except for one case where the same mutation, T599I, was found at low frequency both in PTC (2.6% of 971 reads) and normal tissue (3% of 923 reads) from the same thyroid lobe (case No. 9, Table 4.23).

The tool PolyPhen-2 (Polymorphism Phenotyping v2) was used to predict possible impact of a given non-synonymous variant on the structure and function of the BRAF protein. This tool, through an *in silico* prediction algorithm, associates a score to each mutation and predicts if it could be benign (B) if the score is in the range 0-0.2, possibly damaging if the score is in the range 0.2-0.85 or probably damaging if it is in the range 0.85-1 (PD) [281].

BRAF^{V600E} and *BRAF*^{K601E} are here defined “usual” mutations according to the percentages reported in literature. *BRAF*^{V600E} is the most frequent genetic alteration in papillary thyroid cancer: it accounts for about 95% of *BRAF* mutation in PTC (40-45% of all PTC genetic alterations) [7, 135, 136]. *BRAF*^{V600E} is typically found in tumors with classic papillary (60%) and tall-cell histology (80%), and is rare in the follicular variant (10%) [93, 94]. By contrast, *BRAF*^{K601E} is typically associated to the follicular variant of papillary carcinoma (7-10% of FV PTC) [96, 142, 144].

4.2.1 Exon 15 *BRAF* mutations in histologically benign thyroid of the *BRAF*^{wt} PTC group

The *BRAF*^{E586K} and *BRAF*^{V600E} mutations were identified in the same focus of “atypical” cells from a patient with a *BRAF*^{wt} PTC (case No. 24, Table 4.15). The evidence that the mutations are on different strands determined that they are on different alleles (Fig. 4.16).

The *BRAF*^{K601E} mutation was found in one FA: the same mutation had been previously described in only in 2 FA [64, 141, 144]. According to PolyPhen-2 score, all these mutations may affect protein function. In functional *in vitro* studies it was observed that *BRAF*^{E586K}, *BRAF*^{K601E}, as well as *BRAF*^{V600E} have all elevated kinase activity[126, 130, 134, 146].

Protein change	Histologic variant of related <i>BRAF</i> ^{wt} PTC	Type of sample	Median percentage of mutated allele (reads)	In-silico prediction of effect on protein function (PolyPhen-2)		References	Possible kinase activity
				score	Prediction		
E586K	PTC FV Case No. 24	Atypical focus	5.5% (659)	1	PD	COSMIC: - melanoma - ovarian carcinoma	High activity mutant (Wan P.T. <i>et al.</i> , 2004; Emuss <i>et al.</i> , 2005)
V600E			15.2% (798)	0.971	PD	COSMIC: - thyroid carcinoma - others	High activity mutant (Davies <i>et al.</i> , 2002; Ikenoue T. <i>et al.</i> , 2003; Wan P.T. <i>et al.</i> , 2004)
K601E	PTC Cl Case No. 28	FA	21.1% (123)	0.784	PD	COSMIC: - PTC - FA - melanoma - benign melanocytic nevus - others Lupi C. <i>et al.</i> , 2007; PTC FV Soares P. <i>et al.</i> , 2003; Lima J. <i>et al.</i> , 2003; Trovisco V. <i>et al.</i> , 2005: FA	High activity mutant (Ikenoue T. <i>et al.</i> , 2003; Wan P.T. <i>et al.</i> , 2004)

Table 4.15. Type of *BRAF* mutations in histologically benign FFPE thyroid specimens from the group with *BRAF*^{wt} PTCs and their possible effects on protein function. PTC, papillary thyroid carcinoma; PTC Cl, PTC-classic; PTC FV, PTC-follicular variant; FA, follicular adenoma; PD, possibly or probably damaging mutation.

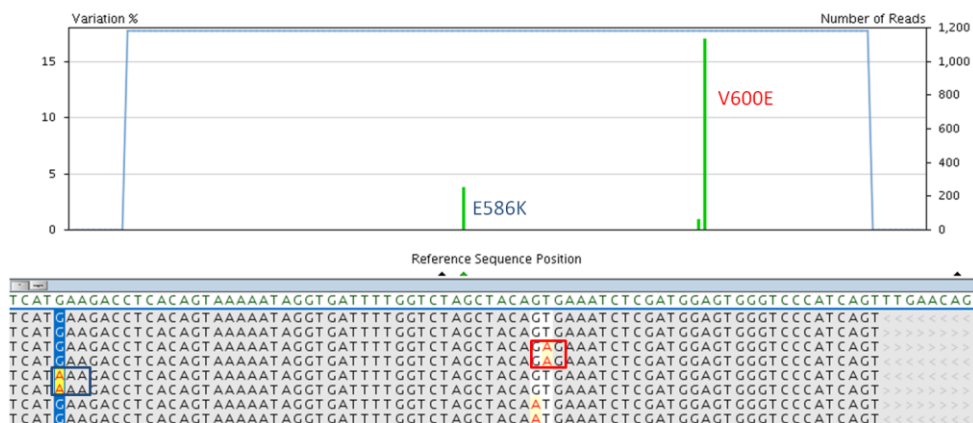


Figure 4.16. *BRAF*^{E586K} and *BRAF*^{V600E} mutations in an “atypical focus” from a patient with a *BRAF*^{wt} PTC (case No. 24). *BRAF*^{E586K} (blue box) and *BRAF*^{V600E} (red box) are on different strands.

4.2.2 “Usual” exon 15 *BRAF* mutations in histologically benign thyroid lesions of the *BRAF*^{V600E} mutated PTC group

The screening of exon 15 *BRAF* mutations by 454 NGS in histologically benign thyroid of cases with *BRAF*^{V600E} PTCs showed the presence of *BRAF*^{V600E} in one “atypical focus” of 32 (3.1%) and in all 3 psammoma bodies (PBs) found in this group of histologically benign specimens. Moreover, in a further case of “atypical focus” the presence of *BRAF*^{K601E} mutation was detected (Table 4.17).

Protein change	Histologic variant of related PTC	Type of sample	Median percentage of mutated allele (reads)
V600E	PTC FV Case No. 3	Atypical focus	4.9% (1091)
		PB	2.1% (949)
	PTC CI Case No. 6	PB	1.6% (1409)
		PB	2.3% (980)
K601E	PTC CI Case No. 6	Atypical focus	4.5% (947)

Table 4.17. “Usual” exon 15 *BRAF* mutations in histologically benign FFPE thyroid specimens from the group with *BRAF*^{V600E} PTCs. PTC, papillary thyroid carcinoma; PTC CI, PTC-classic; PTC FV, PTC-follicular variant; PB, psammoma body.

4.2.3 Exon 15 *BRAF* mutations in psammoma bodies (PBs)

A total of 6 PBs were here analyzed, 3 from histologically benign thyroid of patients with *BRAF*^{V600E} PTCs and 3 from patients with *BRAF*^{wt} PTCs. Only the 3 samples from *BRAF*^{V600E} PTC group were mutated using 454 NGS, in fact no mutations were found in PBs from the *BRAF*^{wt} PTC group. The PBs from *BRAF*^{V600E} PTC group harbored the following *BRAF* substitutions: V600E (all 3 cases), T599I (one case), K601R (one case) and V600A (one case) (Table 4.19). Functional studies showed that *BRAF*^{T599I} mutation leads to BRAF kinase with intermediate activity: lower kinase activity compared with *BRAF*^{V600E} but higher than *BRAF*^{wt} (Table 4.19) [130]. To the best of our knowledge, no information about *BRAF*^{K601R} kinase activity can be found in literature.

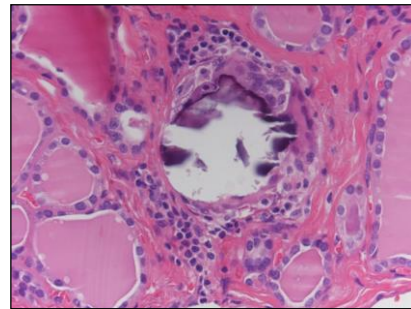


Figure 4.18. Psammoma body in case No.6 (H&E X 600).

Protein change	PB	PB	PB
	Case No. 3	Case No. 6	Case No. 8
T599I	X		
V600E	X	X	X
K601R		X	
V600A	X		

Table 4.19. Exon 15 *BRAF* mutations in PBs from the group with *BRAF*^{V600E} PTCs. Possibly and probably damaging mutations according to PolyPhen-2 score are shown in orange and benign mutation in blue. PB, psammoma body.

4.2.4 “Unusual” exon 15 *BRAF* mutations in histologically benign thyroid lesions of the *BRAF*^{V600E} mutated PTC group

Mutations previously described in PTC

Five “unusual” exon 15 *BRAF* mutations (G593D, A598V, T599I, V600K and V600M), previously reported in PTC and scored as possibly or probably damaging (PD) by PolyPhen-2 tool, were observed in 4 codons in 8 histologically benign thyroid samples of cases with *BRAF*^{V600E} PTC (Table 4.20). Previous functional studies *in vitro* revealed that *BRAF*^{A598V} leads to strong up- regulation of BRAF kinase activity whereas *BRAF*^{V600K} implies augmented *in vitro* kinase activity although at a much lower level compared with *BRAF*^{V600E} [130, 158].

Protein change	Histologic variant of related PTC	Type of sample	Median percentage of mutated allele (reads)	In-silico prediction of effect on protein function (PolyPhen-2)		References	Possible kinase activity
				Score	Prediction		
G593D	PTC TC Case No. 12	Atypical focus	17% (3180)	1	PD	COSMIC: - thyroid hyperplasia - large intestine carcinoma Cameselle-Teijeiro J. <i>et al.</i> , 2009: thyroid HYP Tie J. <i>et al.</i> , 2011: large intestine carcinoma	-
	PTC TC Case No. 13	Atypical focus	1.8% (683)				
A598V	PTC TC Case No. 13	Normal	7% (2116)	0.935	PD	COSMIC: - FV PTC - melanoma - glioma Santarpia L. <i>et al.</i> , 2009: FV PTC	Up-regulation comparable to BRAF^{V600E} (Santarpia L. <i>et al.</i> , 2009)
T599I	PTC FV Case No. 3	PB	2.3% (750)	0.652	PD	COSMIC: - large intestine carcinoma - melanoma - benign melanocytic nevus De Falco V. <i>et al.</i> , 2008; Chiose S. <i>et al.</i> , 2009: complex mutation in PTC Jingrong L. <i>et al.</i> , 2009: melanoma	Intermediate kinase activity: much lower kinase activity compared with BRAF^{V600E} (Wan P.T. <i>et al.</i> , 2004)
	PTC CI Case No. 9	Normal	3% (923)				
	PTC TC Case No. 13	Atypical focus	5% (2240)				
V600K	PTC CI Case No. 4	Oncocytic FA	5.8% (1554)	1	PD	COSMIC: - melanoma - benign melanocytic nevus - others Brzezińska E. <i>et al.</i> , 2007: PTC Lin J. <i>et al.</i> , 2011: melanoma	Intermediate kinase activity: much lower kinase activity compared with BRAF^{V600E} (Wan P.T. <i>et al.</i> , 2004)
V600M	PTC CI Case No. 7	Atypical focus	3.9% (889)	0.904	PD	COSMIC: - prostatic carcinoma - melanoma - others Brzezińska E. <i>et al.</i> , 2007: PTC Cho N.Y. <i>et al.</i> , 2006: prostatic carcinoma Lin J. <i>et al.</i> , 2011: melanoma	-

Table 4.20. “Unusual” exon 15 *BRAF* mutations previously described in PTC and scored as PD in histologically benign thyroid from the group with *BRAF*^{V600E} PTCs. PTC, papillary thyroid carcinoma; PTC CI, PTC-classic; PTC TC, PTC-tall cell; PTC FV, PTC-follicular variant; FA, follicular adenoma; PB, psammoma body; PD, possibly or probably damaging mutation.

Mutations reported in other tumors

Four “unusual” exon 15 *BRAF* mutations (V600A, S605N, S607P and Q609R), previously reported in other tumors (prostatic carcinoma, benign melanocytic nevus, melanoma and large intestine carcinoma) and scored as benign (B) by PolyPhen-2 tool, were observed in 5 histologically benign thyroid lesions of cases with *BRAF*^{V600E} PTC (Table 4.21). PolyPhen-2 score suggests that these amino acid changes are tolerated by the protein, however, to the best of our knowledge, no further functional studies have been performed.

Protein change	Histologic variant of related PTC	Type of sample	Median percentage of mutated allele (reads)	In-silico prediction of effect on protein function (PolyPhen-2)		References	Possible kinase activity
				Score	Prediction		
V600A	PTC FV Case No. 3	PB	2.4% (1148)	0.207	B	COSMIC: - prostatic carcinoma - benign melanocytic nevus Cho N.Y. <i>et al.</i> , 2006: prostatic carcinoma Lin J. <i>et al.</i> , 2009: melanocytic nevi	-
	PTC TC Case No. 12	HYP	1% (1534)				
S605N	PTC TC Case No. 12	HYP	1.4% (1534)	0.009	B	COSMIC: melanoma Deichmann M. <i>et al.</i> : melanoma	-
S607P	PTC CI Case No. 4	Oncocytic FA HYP	11.7% (1876) 30% (1119)	0.186	B	COSMIC: melanoma	-
Q609R	PTC CI Case No. 4	Normal	5.5% (1623)	0.017	B	COSMIC: - large intestine carcinoma - melanoma	-

Table 4.21. “Unusual” exon 15 *BRAF* mutations previously described in other tumors and scored as B in histologically benign thyroid from the group with *BRAF*^{V600E} PTCs. PTC, papillary thyroid carcinoma; PTC CI, PTC-classic; PTC TC, PTC-tall cell; PTC FV, PTC-follicular variant; HYP, hyperplasia; FA, follicular adenoma; PB, psammoma body; B, benign mutation.

Ten “unusual” exon 15 *BRAF* missense mutations (T589I, D594N, G596S, L597P, A598T, K601R, R603Q, G606E and S607F) and one nonsense mutation (R603*), previously known in other tumors (large intestine carcinoma, melanoma, benign melanocytic nevus, lung carcinoma and endometrial carcinoma) and scored as possibly or probably damaging (PD) by PolyPhen-2 tool, were observed in 9 histologically benign thyroid specimens of cases with *BRAF*^{V600E} PTC (Table 4.22).

Protein change	Histologic variant of related PTC	Type of sample	Median percentage of mutated allele (reads)	In-silico prediction of effect on protein function (PolyPhen-2)		References	Possible kinase activity
				Score	Prediction		
T589I	PTC CI Case No. 6	HYP	1.2% (1444)	0.886	PD	COSMIC: large intestine carcinoma Konishi K. <i>et al.</i> , 2006: colorectal adenoma	Up-regulated (Konishi K. <i>et al.</i> , 2006)
D594N	PTC CI Case No. 4	HYP	3% (507)	1	PD	COSMIC: - melanoma - benign melanocytic nevus - lung carcinoma Dahlman K.B. <i>et al.</i> , 2012: melanoma	Inactive (Heidorn S.J. <i>et al.</i> , 2010)
G596S	PTC CI Case No. 4	Normal	5.8% (328)	1	PD	COSMIC: melanoma Jovanovic B. <i>et al.</i> , 2008: melanoma	-
L597P	sclerosing PTC Case No. 2	Normal	3.7% (1234)	0.784	PD	COSMIC: large intestine carcinoma	-
A598T	PTC TC Case No. 12	HYP	13.8% (4345)	0.871	PD	COSMIC: melanoma Deichmann M. <i>et al.</i> , 2006: melanoma	-
K601R	PTC CI Case No. 6	PB	1.5% (691)	0.494	PD	COSMIC: melanoma Lin J. <i>et al.</i> , 2011: melanoma	-
	PTC TC Case No. 12	Atypical focus	7.5% (1122)				
R603Q	PTC CI Case No. 4	HYP	1.7% (1305)	0.786	PD	Tschandl P. <i>et al.</i> , 2013: benign melanocytic nevus	-
	PTC TC Case No. 12	HYP	2.4% (1771)				
R603*	PTC TC Case No. 12	HYP	2.1% (2572)	-	PD	COSMIC: - endometrial carcinoma - melanoma Feng Y.Z. <i>et al.</i> , 2005: endometrial carcinoma	-
G606E	PTC CI Case No. 6	Normal	2.3% (1564)	0.493	PD	COSMIC: melanoma Deichmann M. <i>et al.</i> , 2006: melanoma	-
S607F	PTC FV Case No. 8	Normal	3.5% (963)	0.998	PD	COSMIC: lung carcinoma Tschandl P. <i>et al.</i> , 2013: benign melanocytic nevus	-

Table 4.22. “Unusual” exon 15 *BRAF* mutations previously known in other tumors and scored as PD in histologically benign thyroid from the group with *BRAF*^{V600E} PTCs. PTC, papillary thyroid carcinoma; PTC CI, PTC-classic; PTC TC, PTC-tall cell; PTC FV, PTC-follicular variant; HYP, hyperplasia; PB, psammoma body; PD, possibly or probably damaging mutation; *, stop codon.

Three mutations other than $BRAF^{V600E}$ involved the Val600 residue: two mutations, $BRAF^{V600K}$ and $BRAF^{V600M}$, were scored as probably damaging (PD) by PolyPhen-2 tool, while $BRAF^{V600A}$ was scored as benign. Previous studies showed that $BRAF^{V600K}$, a mutation that causes a substitution of valine for a positively charged lysine (in contrast to the $BRAF^{V600E}$ negative charge substitution), is an activating mutation [130]. The result of substitutions of uncharged nonpolar amino acid (methionine and alanine) for the uncharged nonpolar amino acid (valine) on BRAF kinase activity has not been tested through functional studies. In Table 4.23 are summarized all exon 15 $BRAF$ mutations scored as possibly or probably damaging (PD) or benign (B) found in histologically benign samples from the group with $BRAF^{V600E}$ PTCs (A) and with $BRAF^{wt}$ PTCs (B).

A	$BRAF^{V600E}$ PTC	2		3		4				6		7		8		9		12		13		
		N	A1	PB	HYP1	HYP2	Onc FA	N1	N2	A1	HYP	PB	N2	A1	PB	N	N	A1	HYP	A2	A3	N
PD	E586K																					
	T589I										X											
	G593D																	X				X
	D594N					X																
	G596S									X												
	L597P	X																				
	A598T																			X		
	A598V																					X
	T599I			X														X			X	
	V600E		X	X								X			X							
	V600K						X															
	V600M													X								
	K601E									X												
	K601R										X								X			
	R603Q					X														X		
	R603*																			X		
	G606E											X										
	S607F															X						
V600A			X																X			
S605N																			X			
S607P				X		X																
Q609R							X															
B	$BRAF^{wt}$ PTC	24		28																		
		A1	FA																			
		E586K	X																			
		T589I																				
		G593D																				
		D594N																				
		G596S																				
		L597P																				
A598T																						
A598V																						
T599I																						
V600E	X																					
V600K																						
V600M																						
K601E		X																				
K601R																						
R603Q																						
R603*																						
G606E																						
S607F																						
V600A																						
S605N																						
S607P																						
Q609R																						

Table 4.23. Exon 15 $BRAF$ mutations scored PD or B in histologically benign thyroid from the group with $BRAF^{V600E}$ PTCs (A) and with $BRAF^{wt}$ PTCs (B). PTC, papillary thyroid carcinoma; N, normal; A, atypical focus; PB, psammoma body; HYP, hyperplasia; Onc FA, oncocytic follicular adenoma; FA, follicular adenoma; *, stop codon; PD, possibly or probably damaging mutation; B, benign mutation.

CHAPTER 5

DISCUSSION

5.1 Aim 1 - Clonality of *BRAF*^{V600E} mutation in PTC

The possibility to explore genetic heterogeneity and to include this concept in personalized medicine has been limited by the methodology employed, especially standard Sanger sequencing, the principal method used in laboratories for many years. Indeed, Sanger sequencing has low analytical sensitivity and does not allow semi-quantitative information on the proportion of mutated alleles [242]. However, the present technological developments, especially new deep sequencing methods, allow for understanding the extent of genetic heterogeneity in cancers.

Genetic and phenotypic variation can be intertumoral, when heterogeneity is identified in tumors affecting different tissue and cell types, in different metastatic tumors from a single patient or in individuals with the same tumor type. Moreover, it can be also intratumoral, when observed within a given tumor [253]. Subclonal populations of mutated cells have been found in metastatic melanoma, esophageal adenocarcinoma, breast carcinoma, lung cancer, and colorectal carcinomas [258-265]. The issue of tumoral heterogeneity in thyroid tumors is still debated [248, 266, 271, 282].

BRAF^{V600E} mutation is the most frequent genetic alteration in thyroid cancer and shows a high oncogenic potential in thyroid cancer murine models: these findings have supported the conviction that *BRAF*^{V600E} is the original transforming event for all *BRAF* mutated PTCs. However, two recent studies performed using pyrosequencing, a method that is both sensitive and semi-quantitative, showed that *BRAF*^{V600E} mutation is a rare occurrence in papillary thyroid cancer and is more frequently a subclonal event suggesting that usually it is not an early hit during PTC development [248, 266].

However, so far an important issue, the effect of non-neoplastic allele “contamination” (due to the presence of stromal, endothelial and inflammatory cells), has not been taken into consideration during the assessment of *BRAF*^{V600E} heterogeneity.

In this thesis, the *BRAF*^{V600E} allelic frequency in PTCs was evaluated by employing two different highly sensitive and semi-quantitative techniques, a mutation specific real-time PCR (ASLNAqPCR) and parallel next generation *BRAF* sequencing (454 NGS) targeted to exon 15 in order to validate the data. These techniques had both been previously used to quantify mutated allele percentages in tumor samples [245, 249].

To reduce the bias due to the presence of non-neoplastic cells within PTCs, two pathologists estimated the amount of neoplastic cells in each tumor sample and the percentage of mutated cells obtained by ASLNAqPCR or 454 NGS was normalized according to this proportion. Indeed, results highlight a notable change of data when the proportion of neoplastic cells within the samples was taken into consideration.

Three groups of tumors were identified: a first group (approximately 40-45% of the cases) had a percentage of mutated neoplastic cells greater than 80%; a second small group of tumors (approximately 10% of the cases) showed a number of *BRAF* mutated neoplastic cells below 30%; a third group (approximately 45-50% of the cases) had a distribution of *BRAF*^{V600E} between 30 and 80%.

In the first group of tumors, harboring a percentage of mutated neoplastic cells greater than 80%, *BRAF*^{V600E} occurred very early during tumorigenesis, probably representing the founding genetic alteration, and then propagated to all tumor cells reaching a clonal distribution.

In the second small group of tumors, carrying a percentage of *BRAF* mutated neoplastic cells below 30%, *BRAF*^{V600E} is likely to represent a late adaptive mutation during tumor progression. Noteworthy is that these PTCs would have been negative for *BRAF* mutation after Sanger sequencing.

In the third group, characterized by a heterogeneous distribution of $BRAF^{V600E}$, the majority of the PTCs showed more than 40% of the neoplastic cells carrying $BRAF^{V600E}$, therefore, even if not the founding event, the $BRAF^{V600E}$ mutation happened early during tumor development. However, the mutation had a subclonal origin since it was present within many but not all tumor cells.

Moreover, the same distribution of the $BRAF^{V600E}$ mutation and the same three groups of tumors were also found among the papillary microcarcinomas. To the best of our knowledge, this is the first study that has evaluated the distribution of $BRAF^{V600E}$ mutation in mPTCs. Since at least some mPTCs are papillary carcinomas diagnosed at a very early stage, it's possible to assume that cells harboring the mutation and wild type cells expand at a similar rate, so that the proportion between mutated and non-mutated cells is maintained during tumor growth. This hypothesis is also consistent with a model in which the $BRAF$ mutation can sometimes be acquired in already established tumors but early during tumorigenesis.

The highly sensitive semi-quantitative techniques used in this study, ASLNAqPCR and 454 NGS, and also pyrosequencing used in previous studies by Guerra *et al.* and Gandolfi *et al.*, revealed the existence of a subset of PTC harboring a subclonal distribution of the $BRAF^{V600E}$ mutation.

The mean number of mutated neoplastic cells within the tumor was about 67% using ASLNAqPCR and about 72% by 454 NGS, corresponding to approximately 35% of mutated alleles (considering the $BRAF^{V600E}$ mutation heterozygous). These numbers are higher than those reported by Guerra *et al.* and Gandolfi *et al.* and are in general agreement with the recent NGS data of Nikiforova *et al.* [248, 266, 271].

This discrepancy with the data reported by Guerra *et al.* and Gandolfi *et al.* is most likely due to the normalization on the estimated proportion of neoplastic cells within the tumor that we performed. Indeed, the proportion of mutated neoplastic cells in non normalized data is similar to that previously reported in PTCs based on pyrosequencing analysis of the $BRAF^{V600E}$ mutation.

No statistical association between the percentage of $BRAF^{V600E}$ mutated neoplastic cells and tumor size, stage, age at presentation, or presence of lymph node metastasis could be demonstrated.

In summary, this project demonstrated that in many PTCs the $BRAF^{V600E}$ has a homogeneous distribution in virtually all neoplastic cells and probably represents the founding genetic alteration. However, in a large percentage of PTCs, $BRAF^{V600E}$ has a heterogeneous distribution being present in many but not all neoplastic cells. Therefore, even if $BRAF^{V600E}$ is not always the initial event in the neoplastic thyrocyte transformation, it is acquired early during PTC tumorigenesis.

The presence of genetically distinct tumor subclones with different $BRAF$ status might influence the efficacy of and resistance to targeted pharmacotherapy and be useful to guide patient management. Indeed, in a situation of intratumor heterogeneity, cancer treatment may lead to the eradication of sensitive clones and emergence of often pre-existing treatment-resistant subclones.

Therefore, understanding the extent of genetic heterogeneity in cancer will probably improve the design of individualized treatment through the use of combinatorial therapeutic agents in order to reduce the emergence of resistant clones.

5.2 Aim 2 - Screening of *BRAF* mutations in exon 15 in histologically benign thyroid tissue

The present study revealed the occurrence of a total of 21 *BRAF* mutations at 14 sites in 21 histologically benign FFPE thyroid specimens out of 75 samples (28%) from the group with *BRAF*^{V600E} mutated PTCs and the presence of 3 *BRAF* mutations in 2 out of 23 samples (8.7%) from the group with *BRAF*^{wt} PTCs using the 454 Next-Generation Sequencing (NGS) semi-quantitative technique.

According to the World Health Organization Classification of Tumors of Endocrine Organs, published in 2004, there is no known precursor lesion of papillary thyroid carcinoma [4].

High sensitivity molecular analysis may be helpful in the assessment of early events in thyroid cancer development. In this study, high sensitivity semi-quantitative mutational analysis identified a *BRAF*^{K601E} mutation in one FA: the same mutation had been described in previous studies by conventional sequencing only in two follicular adenomas, one from a study in post-Chernobyl tumors [64, 141, 144]. This finding strengthens the hypothesis of an association between *BRAF*^{K601E} mutation and the follicular growth pattern also in benign thyroid tumors and suggests that high sensitivity mutational analysis will be helpful in the assessment of the frequency of this mutation also in benign thyroid tumors.

Moreover, high sensitivity mutational analysis identified the presence of *BRAF*^{V600E} mutation in psammoma bodies (PBs) here analyzed. PBs are rounded and concentrically lamellated calcifications observed in PTC and rarely in histologically benign lesions and considered the remnants of neoplastic papillae. Indeed, residual neoplastic cells are sometimes observed intimately associated with PBs in PTC during histological observation [86]. *BRAF*^{V600E} mutation was observed in all 3 psammoma bodies not associated with histologically identifiable tumor cells in the group of *BRAF*^{V600E} PTCs: this molecular analysis confirms the hypothesis long held by pathologists that PBs represent, also in benign lesions, the remnants of neoplastic papillae which once existed in these lesions.

In this study, $BRAF^{V600E}$ mutation was found also in “atypical foci”, areas of thyroid parenchyma with abnormal cells, but with morphologic alterations below the threshold that the pathologists consider to diagnose malignancy, i.e. papillary carcinoma. Two groups of cases were studied: one consisted of 20 cases with $BRAF^{V600E}$ mutated PTC, the other of 9 $BRAF^{wt}$ PTCs. Since $BRAF^{V600E}$ is a specific marker of papillary thyroid carcinoma, these lesions probably represent the precursors of $BRAF^{V600E}$ mutated PTCs. In the first group, the presence of the same $BRAF^{V600E}$ mutation in both atypical focus and PTC and the occurrence in the same thyroid lobe, suggest a histogenetic relationship between the histologically benign lesion and the PTC. In the second group, the presence of $BRAF^{V600E}$ mutation in the atypical focus and its absence in the tumor suggests a possible genetic heterogeneity of the tumor and the atypical focus.

In this case, also a $BRAF^{E586K}$ was identified in the same focus of “atypical” cells. $BRAF^{E586K}$ mutation, that may affect protein function according to physical and comparative considerations of PolyPhen-2 tool and with elevated *in vitro* kinase activity, may affect a different subclone in the atypical focus. Indeed, the different percentages of $BRAF^{E586K}$ and $BRAF^{V600E}$ mutated alleles lead to hypothesize that the two mutations occur into two different cellular clones.

454 Sequencing system allows not only targeted re-sequencing for each amplicon hundreds to thousands of times but also an unambiguous haplotyping. Brzeziańska *et al.*, performed mutational screening of exon 15 of $BRAF$ gene by direct sequencing in PTC and observed G1798A and T1799A mutations in the same PTC. They suggested that these substitutions were most likely to occur on the same chromosome resulting in a $BRAF^{V600K}$ mutation in one allele. $BRAF^{V600K}$ mutation is the result of a 2-bp change (GT1798-1799AA), whereas V600M is the result of a single nucleotide substitution in the first nucleotide position (G1798A) in codon 600 of $BRAF$ gene: these mutations had not been previously described in thyroid tumors. [150]. The study by Brzeziańska *et al.*, highlights the limits of Sanger sequencing in the assessment of genetic heterogeneity. These mutations were unambiguously observed also in this study. Indeed, three mutations other than $BRAF^{V600E}$ involved Val600 residue: $BRAF^{V600K}$ and $BRAF^{V600M}$ were scored as probably damaging by PolyPhen-2 tool, whereas $BRAF^{V600A}$ was scored as

benign. $BRAF^{V600K}$ and $BRAF^{V600M}$ were found in an oncocytic follicular adenoma and in an atypical focus respectively.

Previous studies showed that $BRAF^{V600K}$, which causes a substitution of valine for a positively charged lysine (in contrast to the $BRAF^{V600E}$ negative charge substitution), is an activating mutation. However, this variant was shown to have much lower kinase activity compared with $BRAF^{V600E}$ [130].

The result of substitutions of uncharged nonpolar amino acid such as methionine and alanine for the uncharged nonpolar amino acid valine on BRAF kinase activity has not been tested through functional studies [118, 152, 153].

No mutations (other than $BRAF^{V600E}$) were identified in nearly every $BRAF^{V600E}$ PTC sample. In only one case the same mutation, $BRAF^{T599I}$, was found at low frequency both in $BRAF^{V600E}$ PTC and normal tissue from the same thyroid lobe. In BRAF threonine 599 is the major activation segment phosphorylation site and its replacement with isoleucine activates *in vitro* BRAF similarly to what happens during threonine 599 phosphorylation. However, Wan *et al.* showed that also the protein product of this variant has much lower kinase activity *in vitro* compared with $BRAF^{V600E}$ [130]. The presence of the same $BRAF^{T599I}$ mutation at low frequency in both normal tissue and classic PTC indicates a weak action of this activating variant on thyrocytes.

Therefore, cell clones harboring $BRAF^{T599I}$ and $BRAF^{V600K}$ variants may have weaker growth advantage than those carrying the $BRAF^{V600E}$ mutation and may be undergo negative selection in the tumor or remain a minor subpopulation.

Similarly, marked polyclonality of $BRAF$ mutations was observed by Lin *et al.* in acquired melanocytic nevi: in their study, cells with rare $BRAF$ mutations, such as $BRAF^{T599I}$, $BRAF^{V600K}$ and $BRAF^{V600A}$, all of which previously described in melanoma lesions, were found in nevi harboring also $BRAF^{V600E}$ mutation and cells with wild-type $BRAF$ [153, 154]. However, they found frequent heterogeneity of $BRAF$ mutations also in primary melanomas that were wild type by direct sequencing. They found melanomas containing tumor cells with wild-type $BRAF$, $BRAF^{V600E}$ and other activating $BRAF$ mutations in minor subpopulations that did not outgrow $BRAF^{wt}$ cells [152].

These findings are consistent with the classical multi-step model of thyroid carcinogenesis. Risk factors, including exposure to radiation, induce genetic instability, resulting in early genetic alterations that involve the effectors of mitogen activated protein kinase (MAPK) signaling pathway such as *BRAF*. In this context, the possibly damaging *BRAF* mutations other than *BRAF*^{V600E} in exon 15 found in histologically benign thyroid tissue of cases with *BRAF*^{wt} and *BRAF*^{V600E} PTC by high sensitive semi-quantitative analysis seem to represent early weak neoplastic transformation events that result in “abortive” attempts at thyroid cancer development. Only in the case of *BRAF*^{V600E} mutation the drive to neoplastic transformation seems to be strong enough to result in a full blown PTC. Further functional characterization of possibly damaging *BRAF* mutations would be useful in order to understand whether the cells harboring these variant mutations show any significant growth advantage.

REFERENCES

1. Mohebati, A. and A.R. Shaha, *Anatomy of thyroid and parathyroid glands and neurovascular relations*. Clin Anat, 2012. **25**(1): p. 19-31.
2. Nussey, S. and S. Whitehead, *Endocrinology: An Integrated Approach*. 2001, BIOS Scientific Publishers: St. George's Hospital Medical School, London, UK Oxford.
3. Kondo, T., S. Ezzat, and S.L. Asa, *Pathogenetic mechanisms in thyroid follicular-cell neoplasia*. Nat Rev Cancer, 2006. **6**(4): p. 292-306.
4. DeLellis, R.A., et al., *World Health Organization Classification of Tumours. Pathology and Genetics of Tumours of Endocrine Organs* ed. I. Press. 2004, Lyon.
5. Fadare, O. and G. Tallini, *Thyroid: Oncocytic tumors*, in *Atlas of Genetics and Cytogenetics in Oncology and Haematology*. 2003.
6. Nikiforov, Y.E. and M.N. Nikiforova, *Molecular genetics and diagnosis of thyroid cancer*. Nat Rev Endocrinol, 2011. **7**(10): p. 569-80.
7. Nikiforova, M.N. and Y.E. Nikiforov, *Molecular diagnostics and predictors in thyroid cancer*. Thyroid, 2009. **19**(12): p. 1351-61.
8. Gharib, H., *Changing trends in thyroid practice: understanding nodular thyroid disease*. Endocr Pract, 2004. **10**(1): p. 31-9.
9. Guth, S., et al., *Very high prevalence of thyroid nodules detected by high frequency (13 MHz) ultrasound examination*. Eur J Clin Invest, 2009. **39**(8): p. 699-706.
10. Mazzaferri, E.L., *Thyroid cancer in thyroid nodules: finding a needle in the haystack*. Am J Med, 1992. **93**(4): p. 359-62.
11. Mazzaferri, E.L., *Management of a solitary thyroid nodule*. N Engl J Med, 1993. **328**(8): p. 553-9.
12. Rojascki, M.T. and H. Gharib, *Nodular thyroid disease. Evaluation and management*. N Engl J Med, 1985. **313**(7): p. 428-36.
13. Wiest, P.W., et al., *Thyroid palpation versus high-resolution thyroid ultrasonography in the detection of nodules*. J Ultrasound Med, 1998. **17**(8): p. 487-96.
14. Cooper, D.S., et al., *Management guidelines for patients with thyroid nodules and differentiated thyroid cancer*. Thyroid, 2006. **16**(2): p. 109-42.
15. Frates, M.C., et al., *Prevalence and distribution of carcinoma in patients with solitary and multiple thyroid nodules on sonography*. J Clin Endocrinol Metab, 2006. **91**(9): p. 3411-7.
16. Kim, D.L., K.H. Song, and S.K. Kim, *High prevalence of carcinoma in ultrasonography-guided fine needle aspiration cytology of thyroid nodules*. Endocr J, 2008. **55**(1): p. 135-42.
17. Nikiforov, Y.E., et al., *Molecular testing for mutations in improving the fine-needle aspiration diagnosis of thyroid nodules*. J Clin Endocrinol Metab, 2009. **94**(6): p. 2092-8.
18. Papini, E., et al., *Risk of malignancy in nonpalpable thyroid nodules: predictive value of ultrasound and color-Doppler features*. J Clin Endocrinol Metab, 2002. **87**(5): p. 1941-6.
19. DeLellis, R.A., *Pathology and genetics of thyroid carcinoma*. J Surg Oncol, 2006. **94**(8): p. 662-9.
20. Boyle, P. and J. Ferlay, *Cancer incidence and mortality in Europe, 2004*. Ann Oncol, 2005. **16**(3): p. 481-8.

21. *Italian cancer figures--report 2006: 1. Incidence, mortality and estimates.* Epidemiol Prev, 2006. **30**(1 Suppl 2): p. 8-10, 12-28, 30-101 passim.
22. McLeod, D.S., A.M. Sawka, and D.S. Cooper, *Controversies in primary treatment of low-risk papillary thyroid cancer.* Lancet, 2013. **381**(9871): p. 1046-57.
23. Davies, L., et al., *The increasing incidence of small thyroid cancers: where are the cases coming from?* Laryngoscope, 2010. **120**(12): p. 2446-51.
24. Davies, L. and H.G. Welch, *Increasing incidence of thyroid cancer in the United States, 1973-2002.* JAMA, 2006. **295**(18): p. 2164-7.
25. Leenhardt, L., et al., *Advances in diagnostic practices affect thyroid cancer incidence in France.* Eur J Endocrinol, 2004. **150**(2): p. 133-9.
26. Chen, A.Y., A. Jemal, and E.M. Ward, *Increasing incidence of differentiated thyroid cancer in the United States, 1988-2005.* Cancer, 2009. **115**(16): p. 3801-7.
27. Kazaure, H.S., S.A. Roman, and J.A. Sosa, *Aggressive variants of papillary thyroid cancer: incidence, characteristics and predictors of survival among 43,738 patients.* Ann Surg Oncol, 2012. **19**(6): p. 1874-80.
28. Morris, L.G. and D. Myssiorek, *Improved detection does not fully explain the rising incidence of well-differentiated thyroid cancer: a population-based analysis.* Am J Surg, 2010. **200**(4): p. 454-61.
29. Ceresini, G., et al., *Thyroid cancer incidence by histological type and related variants in a mildly iodine-deficient area of Northern Italy, 1998 to 2009.* Cancer, 2012. **118**(22): p. 5473-80.
30. Howe, H.L., et al., *Annual report to the nation on the status of cancer (1973 through 1998), featuring cancers with recent increasing trends.* J Natl Cancer Inst, 2001. **93**(11): p. 824-42.
31. Howlader, N., et al., *SEER Cancer Statistics Review, 1975-2010.* 2013, National Cancer Institute: Bethesda, MD.
32. Kazakov, V.S., E.P. Demidchik, and L.N. Astakhova, *Thyroid cancer after Chernobyl.* Nature, 1992. **359**(6390): p. 21.
33. Williams, D., *Cancer after nuclear fallout: lessons from the Chernobyl accident.* Nat Rev Cancer, 2002. **2**(7): p. 543-9.
34. McCurry, J., *Fukushima residents still struggling 2 years after disaster.* Lancet, 2013. **381**(9869): p. 791-2.
35. Ron, E., et al., *Thyroid cancer after exposure to external radiation: a pooled analysis of seven studies.* Radiat Res, 1995. **178**(2): p. AV43-60.
36. Ciampi, R., et al., *Oncogenic AKAP9-BRAF fusion is a novel mechanism of MAPK pathway activation in thyroid cancer.* J Clin Invest, 2005. **115**(1): p. 94-101.
37. Ahmed, R., S. Al-Shaikh, and M. Akhtar, *Hashimoto thyroiditis: a century later.* Adv Anat Pathol, 2012. **19**(3): p. 181-6.
38. Replinger, D., et al., *Is Hashimoto's thyroiditis a risk factor for papillary thyroid cancer?* J Surg Res, 2008. **150**(1): p. 49-52.
39. Kim, K.W., et al., *Elevated risk of papillary thyroid cancer in Korean patients with Hashimoto's thyroiditis.* Head Neck, 2011. **33**(5): p. 691-5.
40. Okayasu, I., et al., *Association of chronic lymphocytic thyroiditis and thyroid papillary carcinoma. A study of surgical cases among Japanese, and white and African Americans.* Cancer, 1995. **76**(11): p. 2312-8.
41. Ott, R.A., et al., *The incidence of thyroid carcinoma in Hashimoto's thyroiditis.* Am Surg, 1987. **53**(8): p. 442-5.
42. Burstein, D.E., et al., *Immunohistochemical detection of p53 homolog p63 in solid cell nests, papillary thyroid carcinoma, and hashimoto's thyroiditis: A stem*

- cell hypothesis of papillary carcinoma oncogenesis*. Hum Pathol, 2004. **35**(4): p. 465-73.
43. Cameselle-Teijeiro, J., C. Febles-Perez, and M. Sobrinho-Simoes, *Papillary and mucoepidermoid carcinoma of the thyroid with anaplastic transformation: a case report with histologic and immunohistochemical findings that support a provocative histogenetic hypothesis*. Pathol Res Pract, 1995. **191**(12): p. 1214-21.
 44. Cunha, L.L., et al., *Clinical and pathological implications of concurrent autoimmune thyroid disorders and papillary thyroid cancer*. J Thyroid Res, 2011. **2011**: p. 387062.
 45. Cameselle-Teijeiro, J., et al., *BRAF mutation in solid cell nest hyperplasia associated with papillary thyroid carcinoma. A precursor lesion?* Hum Pathol, 2009. **40**(7): p. 1029-35.
 46. Kawabata, W., et al., *Estrogen receptors (alpha and beta) and 17beta-hydroxysteroid dehydrogenase type 1 and 2 in thyroid disorders: possible in situ estrogen synthesis and actions*. Mod Pathol, 2003. **16**(5): p. 437-44.
 47. Lee, M.L., et al., *Induction of thyroid papillary carcinoma cell proliferation by estrogen is associated with an altered expression of Bcl-xL*. Cancer J, 2005. **11**(2): p. 113-21.
 48. Hemminki, K., C. Eng, and B. Chen, *Familial risks for nonmedullary thyroid cancer*. J Clin Endocrinol Metab, 2005. **90**(10): p. 5747-53.
 49. Bonora, E., G. Tallini, and G. Romeo, *Genetic Predisposition to Familial Nonmedullary Thyroid Cancer: An Update of Molecular Findings and State-of-the-Art Studies*. J Oncol, 2010. **2010**: p. 385206.
 50. Eng, C., *Familial papillary thyroid cancer--many syndromes, too many genes?* J Clin Endocrinol Metab, 2000. **85**(5): p. 1755-7.
 51. Harach, H.R. and G.A. Ceballos, *Thyroid cancer, thyroiditis and dietary iodine: a review based on the Salta, Argentina model*. Endocr Pathol, 2008. **19**(4): p. 209-20.
 52. Edge, S.B. and C.C. Compton, *The American Joint Committee on Cancer: the 7th edition of the AJCC cancer staging manual and the future of TNM*. Ann Surg Oncol, 2010. **17**(6): p. 1471-4.
 53. Edge, S., et al., *AJCC Cancer Staging Manual. Thyroid*. 7th edn. ed. 2010, New York: Springer.
 54. Lang, B.H., et al., *Staging systems for papillary thyroid carcinoma: a study of 2 tertiary referral centers*. Ann Surg, 2007. **246**(1): p. 114-21.
 55. Belge, G., et al., *Cytogenetic investigations of 340 thyroid hyperplasias and adenomas revealing correlations between cytogenetic findings and histology*. Cancer Genet Cytogenet, 1998. **101**(1): p. 42-8.
 56. Castro, P., et al., *Adenomas and follicular carcinomas of the thyroid display two major patterns of chromosomal changes*. J Pathol, 2005. **206**(3): p. 305-11.
 57. Sobrinho-Simoes, M., et al., *Molecular pathology of well-differentiated thyroid carcinomas*. Virchows Arch, 2005. **447**(5): p. 787-93.
 58. Knauf, J.A., et al., *Oncogenic RAS induces accelerated transition through G2/M and promotes defects in the G2 DNA damage and mitotic spindle checkpoints*. J Biol Chem, 2006. **281**(7): p. 3800-9.
 59. Mitsutake, N., et al., *Conditional BRAFV600E expression induces DNA synthesis, apoptosis, dedifferentiation, and chromosomal instability in thyroid PCCL3 cells*. Cancer Res, 2005. **65**(6): p. 2465-73.
 60. Saavedra, H.I., et al., *The RAS oncogene induces genomic instability in thyroid PCCL3 cells via the MAPK pathway*. Oncogene, 2000. **19**(34): p. 3948-54.

61. Kimura, T., et al., *Regulation of thyroid cell proliferation by TSH and other factors: a critical evaluation of in vitro models*. *Endocr Rev*, 2001. **22**(5): p. 631-56.
62. Krohn, K., et al., *Molecular pathogenesis of euthyroid and toxic multinodular goiter*. *Endocr Rev*, 2005. **26**(4): p. 504-24.
63. Frattini, M., et al., *Alternative mutations of BRAF, RET and NTRK1 are associated with similar but distinct gene expression patterns in papillary thyroid cancer*. *Oncogene*, 2004. **23**(44): p. 7436-40.
64. Soares, P., et al., *BRAF mutations and RET/PTC rearrangements are alternative events in the etiopathogenesis of PTC*. *Oncogene*, 2003. **22**(29): p. 4578-80.
65. Castellone, M.D. and M. Santoro, *Dysregulated RET signaling in thyroid cancer*. *Endocrinol Metab Clin North Am*, 2008. **37**(2): p. 363-74, viii.
66. Tallini, G. and S.L. Asa, *RET oncogene activation in papillary thyroid carcinoma*. *Adv Anat Pathol*, 2001. **8**(6): p. 345-54.
67. Rabes, H.M., et al., *Pattern of radiation-induced RET and NTRK1 rearrangements in 191 post-chernobyl papillary thyroid carcinomas: biological, phenotypic, and clinical implications*. *Clin Cancer Res*, 2000. **6**(3): p. 1093-103.
68. Fusco, A., et al., *Assessment of RET/PTC oncogene activation and clonality in thyroid nodules with incomplete morphological evidence of papillary carcinoma: a search for the early precursors of papillary cancer*. *Am J Pathol*, 2002. **160**(6): p. 2157-67.
69. Rhoden, K.J., et al., *Real-time quantitative RT-PCR identifies distinct c-RET, RET/PTC1 and RET/PTC3 expression patterns in papillary thyroid carcinoma*. *Lab Invest*, 2004. **84**(12): p. 1557-70.
70. Rhoden, K.J., et al., *RET/papillary thyroid cancer rearrangement in nonneoplastic thyrocytes: follicular cells of Hashimoto's thyroiditis share low-level recombination events with a subset of papillary carcinoma*. *J Clin Endocrinol Metab*, 2006. **91**(6): p. 2414-23.
71. Tallini, G. and G. Brandao, *Assessment of RET/PTC oncogene activation in thyroid nodules utilizing laser microdissection followed by nested RT-PCR*. *Methods Mol Biol*, 2005. **293**: p. 103-11.
72. Zhu, Z., et al., *Prevalence of RET/PTC rearrangements in thyroid papillary carcinomas: effects of the detection methods and genetic heterogeneity*. *J Clin Endocrinol Metab*, 2006. **91**(9): p. 3603-10.
73. de Biase, D., et al., *Molecular diagnosis of carcinomas of the thyroid gland*. *Front Biosci (Elite Ed)*, 2014. **6**: p. 1-14.
74. Vasko, V., et al., *Specific pattern of RAS oncogene mutations in follicular thyroid tumors*. *J Clin Endocrinol Metab*, 2003. **88**(6): p. 2745-52.
75. Nikiforova, M.N., et al., *RAS point mutations and PAX8-PPAR gamma rearrangement in thyroid tumors: evidence for distinct molecular pathways in thyroid follicular carcinoma*. *J Clin Endocrinol Metab*, 2003. **88**(5): p. 2318-26.
76. Garcia-Rostan, G., et al., *Mutation of the PIK3CA gene in anaplastic thyroid cancer*. *Cancer Res*, 2005. **65**(22): p. 10199-207.
77. Hou, P., et al., *Genetic alterations and their relationship in the phosphatidylinositol 3-kinase/Akt pathway in thyroid cancer*. *Clin Cancer Res*, 2007. **13**(4): p. 1161-70.
78. Ricarte-Filho, J.C., et al., *Mutational profile of advanced primary and metastatic radioactive iodine-refractory thyroid cancers reveals distinct pathogenetic roles for BRAF, PIK3CA, and AKT1*. *Cancer Res*, 2009. **69**(11): p. 4885-93.
79. Lloyd, R.V., B.R. Douglas, and W.F.J. Young, *Endocrine diseases. Atlas of nontumor pathology, Fascicle 1*. 2002, Washington, DC: Armed Forces Institute of Pathology.

80. LiVolsi, V.A., *Papillary thyroid carcinoma: an update*. Mod Pathol, 2011. **24 Suppl 2**: p. S1-9.
81. Cooper, D.S., E. Tiamson, and P.W. Ladenson, *Psammoma bodies in fine needle aspiration biopsies of benign thyroid nodules*. Thyroidology, 1988(1): p. 55-9.
82. Dugan, J.M., et al., *Psammoma bodies in fine needle aspirate of the thyroid in lymphocytic thyroiditis*. Acta Cytol, 1987. **31**(3): p. 330-4.
83. Fiorella, R.M., et al., *Multinodular goiter of the thyroid mimicking malignancy: diagnostic pitfalls in fine-needle aspiration biopsy*. Diagn Cytopathol, 1993. **9**(3): p. 351-5; discussion 355-7.
84. Riazmontazer, N. and G. Bedayat, *Psammoma bodies in fine needle aspirates from thyroids containing nontoxic hyperplastic nodular goiters*. Acta Cytol, 1991. **35**(5): p. 563-6.
85. Klinck, G.H. and T. Winship, *Psammoma bodies and thyroid cancer*. Cancer, 1959. **12**(4): p. 656-62.
86. Das, D.K., *Psammoma body: a product of dystrophic calcification or of a biologically active process that aims at limiting the growth and spread of tumor?* Diagn Cytopathol, 2009. **37**(7): p. 534-41.
87. Hunt, J.L. and E.L. Barnes, *Non-tumor-associated psammoma bodies in the thyroid*. Am J Clin Pathol, 2003. **119**(1): p. 90-4.
88. Johannessen, J.V. and M. Sobrinho-Simoes, *The origin and significance of thyroid psammoma bodies*. Lab Invest, 1980. **43**(3): p. 287-96.
89. Pyo, J.S., et al., *The prognostic relevance of psammoma bodies and ultrasonographic intratumoral calcifications in papillary thyroid carcinoma: reply*. World J Surg, 2014. **38**(3): p. 749.
90. Chan, J.K., *Papillary carcinoma of thyroid: classical and variants*. Histol Histopathol, 1990. **5**(2): p. 241-57.
91. Lloyd, R.V., et al., *Observer variation in the diagnosis of follicular variant of papillary thyroid carcinoma*. Am J Surg Pathol, 2004. **28**(10): p. 1336-40.
92. Ghossein, R. and V.A. Livolsi, *Papillary thyroid carcinoma tall cell variant*. Thyroid, 2008. **18**(11): p. 1179-81.
93. Adeniran, A.J., et al., *Correlation between genetic alterations and microscopic features, clinical manifestations, and prognostic characteristics of thyroid papillary carcinomas*. Am J Surg Pathol, 2006. **30**(2): p. 216-22.
94. Xing, M., *BRAF mutation in thyroid cancer*. Endocr Relat Cancer, 2005. **12**(2): p. 245-62.
95. Basolo, F., et al., *Correlation between the BRAF V600E mutation and tumor invasiveness in papillary thyroid carcinomas smaller than 20 millimeters: analysis of 1060 cases*. J Clin Endocrinol Metab, 2010. **95**(9): p. 4197-205.
96. Trovisco, V., et al., *BRAF mutations are associated with some histological types of papillary thyroid carcinoma*. J Pathol, 2004. **202**(2): p. 247-51.
97. Zhu, Z., et al., *Molecular profile and clinical-pathologic features of the follicular variant of papillary thyroid carcinoma. An unusually high prevalence of ras mutations*. Am J Clin Pathol, 2003. **120**(1): p. 71-7.
98. Fink, A., et al., *Occult micropapillary carcinoma associated with benign follicular thyroid disease and unrelated thyroid neoplasms*. Mod Pathol, 1996. **9**(8): p. 816-20.
99. Baloch, Z.W. and V.A. LiVolsi, *Microcarcinoma of the thyroid*. Adv Anat Pathol, 2006. **13**(2): p. 69-75.
100. Page, C., et al., *'Aggressive papillary' thyroid microcarcinoma*. Eur Arch Otorhinolaryngol, 2009. **266**(12): p. 1959-63.
101. Yu, X.M., et al., *Should all papillary thyroid microcarcinomas be aggressively treated? An analysis of 18,445 cases*. Ann Surg, 2011. **254**(4): p. 653-60.

102. Mazzaferri, E.L., *Management of low-risk differentiated thyroid cancer*. Endocr Pract, 2007. **13**(5): p. 498-512.
103. Neuhold, N., et al., *Incidental papillary microcarcinoma of the thyroid--further evidence of a very low malignant potential: a retrospective clinicopathological study with up to 30 years of follow-up*. Ann Surg Oncol, 2011. **18**(12): p. 3430-6.
104. Lupoli, G., et al., *Familial papillary thyroid microcarcinoma: a new clinical entity*. Lancet, 1999. **353**(9153): p. 637-9.
105. Corvi, R., et al., *Frequent RET rearrangements in thyroid papillary microcarcinoma detected by interphase fluorescence in situ hybridization*. Lab Invest, 2001. **81**(12): p. 1639-45.
106. Fugazzola, L., et al., *Correlation between B-RAFV600E mutation and clinicopathologic parameters in papillary thyroid carcinoma: data from a multicentric Italian study and review of the literature*. Endocr Relat Cancer, 2006. **13**(2): p. 455-64.
107. Kim, H.S., et al., *Factors influencing the detection of the BRAF T1799A mutation in papillary thyroid carcinoma*. Oncol Rep, 2011. **25**(6): p. 1639-44.
108. Sedliarou, I., et al., *The BRAFT1796A transversion is a prevalent mutational event in human thyroid microcarcinoma*. Int J Oncol, 2004. **25**(6): p. 1729-35.
109. Ugolini, C., et al., *Presence of BRAF V600E in very early stages of papillary thyroid carcinoma*. Thyroid, 2007. **17**(5): p. 381-8.
110. Viglietto, G., et al., *RET/PTC oncogene activation is an early event in thyroid carcinogenesis*. Oncogene, 1995. **11**(6): p. 1207-10.
111. Virk, R.K., et al., *BRAFV600E mutation in papillary thyroid microcarcinoma: a genotype-phenotype correlation*. Mod Pathol, 2013. **26**(1): p. 62-70.
112. Pacini, F., *Thyroid microcarcinoma*. Best Pract Res Clin Endocrinol Metab, 2012. **26**(4): p. 421-9.
113. <http://www.ensembl.org>.
114. <http://www.ncbi.nlm.nih.gov/gene/673>.
115. Sithanandam, G., et al., *B-raf and a B-raf pseudogene are located on 7q in man*. Oncogene, 1992. **7**(4): p. 795-9.
116. Marais, R. and C.J. Marshall, *Control of the ERK MAP kinase cascade by Ras and Raf*. Cancer Surv, 1996. **27**: p. 101-25.
117. Williams, N.G. and T.M. Roberts, *Signal transduction pathways involving the Raf proto-oncogene*. Cancer Metastasis Rev, 1994. **13**(1): p. 105-16.
118. Garnett, M.J. and R. Marais, *Guilty as charged: B-RAF is a human oncogene*. Cancer Cell, 2004. **6**(4): p. 313-9.
119. Nikiforov, Y.E., *Molecular diagnostics of thyroid tumors*. Arch Pathol Lab Med, 2011. **135**(5): p. 569-77.
120. Daum, G., et al., *The ins and outs of Raf kinases*. Trends Biochem Sci, 1994. **19**(11): p. 474-80.
121. Cutler, R.E., Jr., et al., *Autoregulation of the Raf-1 serine/threonine kinase*. Proc Natl Acad Sci U S A, 1998. **95**(16): p. 9214-9.
122. Tran, N.H., X. Wu, and J.A. Frost, *B-Raf and Raf-1 are regulated by distinct autoregulatory mechanisms*. J Biol Chem, 2005. **280**(16): p. 16244-53.
123. Dhillon, A.S., et al., *Regulation of Raf-1 activation and signalling by dephosphorylation*. EMBO J, 2002. **21**(1-2): p. 64-71.
124. Johnson, L.N., *Structural basis for substrate recognition and control in protein kinases*. Ernst Schering Res Found Workshop, 2001(34): p. 47-69.
125. Chong, H., J. Lee, and K.L. Guan, *Positive and negative regulation of Raf kinase activity and function by phosphorylation*. EMBO J, 2001. **20**(14): p. 3716-27.

126. Emuss, V., et al., *Mutations of C-RAF are rare in human cancer because C-RAF has a low basal kinase activity compared with B-RAF*. *Cancer Res*, 2005. **65**(21): p. 9719-26.
127. Mason, C.S., et al., *Serine and tyrosine phosphorylations cooperate in Raf-1, but not B-Raf activation*. *EMBO J*, 1999. **18**(8): p. 2137-48.
128. Matallanas, D., et al., *Raf family kinases: old dogs have learned new tricks*. *Genes Cancer*, 2011. **2**(3): p. 232-60.
129. Niault, T.S. and M. Baccarini, *Targets of Raf in tumorigenesis*. *Carcinogenesis*, 2010. **31**(7): p. 1165-74.
130. Wan, P.T., et al., *Mechanism of activation of the RAF-ERK signaling pathway by oncogenic mutations of B-RAF*. *Cell*, 2004. **116**(6): p. 855-67.
131. Wellbrock, C., M. Karasarides, and R. Marais, *The RAF proteins take centre stage*. *Nat Rev Mol Cell Biol*, 2004. **5**(11): p. 875-85.
132. Zhang, B.H. and K.L. Guan, *Activation of B-Raf kinase requires phosphorylation of the conserved residues Thr598 and Ser601*. *EMBO J*, 2000. **19**(20): p. 5429-39.
133. Mercer, K.E. and C.A. Pritchard, *Raf proteins and cancer: B-Raf is identified as a mutational target*. *Biochim Biophys Acta*, 2003. **1653**(1): p. 25-40.
134. Davies, H., et al., *Mutations of the BRAF gene in human cancer*. *Nature*, 2002. **417**(6892): p. 949-54.
135. Cohen, Y., et al., *BRAF mutation in papillary thyroid carcinoma*. *J Natl Cancer Inst*, 2003. **95**(8): p. 625-7.
136. Kimura, E.T., et al., *High prevalence of BRAF mutations in thyroid cancer: genetic evidence for constitutive activation of the RET/PTC-RAS-BRAF signaling pathway in papillary thyroid carcinoma*. *Cancer Res*, 2003. **63**(7): p. 1454-7.
137. Ciampi, R. and Y.E. Nikiforov, *Alterations of the BRAF gene in thyroid tumors*. *Endocr Pathol*, 2005. **16**(3): p. 163-72.
138. Akslen, L.A. and V.A. LiVolsi, *Prognostic significance of histologic grading compared with subclassification of papillary thyroid carcinoma*. *Cancer*, 2000. **88**(8): p. 1902-8.
139. Ciampi, R., Z. Zhu, and Y.E. Nikiforov, *BRAF copy number gains in thyroid tumors detected by fluorescence in situ hybridization*. *Endocr Pathol*, 2005. **16**(2): p. 99-105.
140. Nikiforova, M.N., et al., *BRAF mutations in thyroid tumors are restricted to papillary carcinomas and anaplastic or poorly differentiated carcinomas arising from papillary carcinomas*. *J Clin Endocrinol Metab*, 2003. **88**(11): p. 5399-404.
141. Lima, J., et al., *BRAF mutations are not a major event in post-Chernobyl childhood thyroid carcinomas*. *J Clin Endocrinol Metab*, 2004. **89**(9): p. 4267-71.
142. Lupi, C., et al., *Association of BRAF V600E mutation with poor clinicopathological outcomes in 500 consecutive cases of papillary thyroid carcinoma*. *J Clin Endocrinol Metab*, 2007. **92**(11): p. 4085-90.
143. Pennelli, G., et al., *BRAF(K601E) mutation in a patient with a follicular thyroid carcinoma*. *Thyroid*, 2011. **21**(12): p. 1393-6.
144. Trovisco, V., et al., *Type and prevalence of BRAF mutations are closely associated with papillary thyroid carcinoma histotype and patients' age but not with tumour aggressiveness*. *Virchows Arch*, 2005. **446**(6): p. 589-95.
145. Kumar, R., et al., *BRAF mutations in metastatic melanoma: a possible association with clinical outcome*. *Clin Cancer Res*, 2003. **9**(9): p. 3362-8.
146. Ikenoue, T., et al., *Functional analysis of mutations within the kinase activation segment of B-Raf in human colorectal tumors*. *Cancer Res*, 2003. **63**(23): p. 8132-7.

147. Hou, P. and M. Xing, *Absence of germline mutations in genes within the MAP kinase pathway in familial non-medullary thyroid cancer*. *Cell Cycle*, 2006. **5**(17): p. 2036-9.
148. Xing, M., *The T1799A BRAF mutation is not a germline mutation in familial nonmedullary thyroid cancer*. *Clin Endocrinol (Oxf)*, 2005. **63**(3): p. 263-6.
149. James, M.R., et al., *Rapid screening of 4000 individuals for germ-line variations in the BRAF gene*. *Clin Chem*, 2006. **52**(9): p. 1675-8.
150. Brzezianska, E., et al., *Investigation of V600E BRAF mutation in papillary thyroid carcinoma in the Polish population*. *Neuro Endocrinol Lett*, 2007. **28**(4): p. 351-9.
151. Hay, R., et al., *BRAF mutations in melanocytic lesions and papillary thyroid carcinoma samples identified using melting curve analysis of polymerase chain reaction products*. *Arch Pathol Lab Med*, 2007. **131**(9): p. 1361-7.
152. Lin, J., et al., *Polyclonality of BRAF mutations in primary melanoma and the selection of mutant alleles during progression*. *Br J Cancer*, 2011. **104**(3): p. 464-8.
153. Lin, J., et al., *Polyclonality of BRAF mutations in acquired melanocytic nevi*. *J Natl Cancer Inst*, 2009. **101**(20): p. 1423-7.
154. <http://cancer.sanger.ac.uk/cancergenome/projects/cosmic/>.
155. Tie, J., et al., *Optimizing targeted therapeutic development: analysis of a colorectal cancer patient population with the BRAF(V600E) mutation*. *Int J Cancer*, 2011. **128**(9): p. 2075-84.
156. Dahlman, K.B., et al., *BRAF(L597) mutations in melanoma are associated with sensitivity to MEK inhibitors*. *Cancer Discov*, 2012. **2**(9): p. 791-7.
157. Heidorn, S.J., et al., *Kinase-dead BRAF and oncogenic RAS cooperate to drive tumor progression through CRAF*. *Cell*, 2010. **140**(2): p. 209-21.
158. Santarpia, L., et al., *Detection and molecular characterization of a novel BRAF activated domain mutation in follicular variant of papillary thyroid carcinoma*. *Hum Pathol*, 2009. **40**(6): p. 827-33.
159. Gill, M., et al., *Lack of BRAF mutations in Spitz nevi*. *J Invest Dermatol*, 2004. **122**(5): p. 1325-6.
160. Brose, M.S., et al., *BRAF and RAS mutations in human lung cancer and melanoma*. *Cancer Res*, 2002. **62**(23): p. 6997-7000.
161. Rajagopalan, H., et al., *Tumorigenesis: RAF/RAS oncogenes and mismatch-repair status*. *Nature*, 2002. **418**(6901): p. 934.
162. Fratev, F., et al., *Molecular basis of inactive B-RAF(WT) and B-RAF(V600E) ligand inhibition, selectivity and conformational stability: an in silico study*. *Mol Pharm*, 2009. **6**(1): p. 144-57.
163. Garnett, M.J., et al., *Wild-type and mutant B-RAF activate C-RAF through distinct mechanisms involving heterodimerization*. *Mol Cell*, 2005. **20**(6): p. 963-9.
164. Rushworth, L.K., et al., *Regulation and role of Raf-1/B-Raf heterodimerization*. *Mol Cell Biol*, 2006. **26**(6): p. 2262-72.
165. Chiosea, S., et al., *A novel complex BRAF mutation detected in a solid variant of papillary thyroid carcinoma*. *Endocr Pathol*, 2009. **20**(2): p. 122-6.
166. De Falco, V., et al., *Functional characterization of the novel T599I-VKSRdel BRAF mutation in a follicular variant papillary thyroid carcinoma*. *J Clin Endocrinol Metab*, 2008. **93**(11): p. 4398-402.
167. Hou, P., D. Liu, and M. Xing, *Functional characterization of the T1799-1801del and A1799-1816ins BRAF mutations in papillary thyroid cancer*. *Cell Cycle*, 2007. **6**(3): p. 377-9.

168. Moretti, S., et al., *Biochemical and molecular characterization of the novel BRAF(V599Ins) mutation detected in a classic papillary thyroid carcinoma.* *Oncogene*, 2006. **25**(30): p. 4235-40.
169. Oler, G., et al., *Investigation of BRAF mutation in a series of papillary thyroid carcinoma and matched-lymph node metastasis reveals a new mutation in metastasis.* *Clin Endocrinol (Oxf)*, 2005. **62**(4): p. 509-11.
170. Trovisco, V., et al., *A new BRAF gene mutation detected in a case of a solid variant of papillary thyroid carcinoma.* *Hum Pathol*, 2005. **36**(6): p. 694-7.
171. Xing, M., et al., *BRAF mutation predicts a poorer clinical prognosis for papillary thyroid cancer.* *J Clin Endocrinol Metab*, 2005. **90**(12): p. 6373-9.
172. Nucera, C., et al., *B-Raf(V600E) and thrombospondin-1 promote thyroid cancer progression.* *Proc Natl Acad Sci U S A*, 2010. **107**(23): p. 10649-54.
173. Melillo, R.M., et al., *The RET/PTC-RAS-BRAF linear signaling cascade mediates the motile and mitogenic phenotype of thyroid cancer cells.* *J Clin Invest*, 2005. **115**(4): p. 1068-81.
174. Kim, C.S. and X. Zhu, *Lessons from mouse models of thyroid cancer.* *Thyroid*, 2009. **19**(12): p. 1317-31.
175. Knauf, J.A., et al., *Targeted expression of BRAFV600E in thyroid cells of transgenic mice results in papillary thyroid cancers that undergo dedifferentiation.* *Cancer Res*, 2005. **65**(10): p. 4238-45.
176. Vasko, V., et al., *High prevalence and possible de novo formation of BRAF mutation in metastasized papillary thyroid cancer in lymph nodes.* *J Clin Endocrinol Metab*, 2005. **90**(9): p. 5265-9.
177. Salvatore, G., et al., *BRAF is a therapeutic target in aggressive thyroid carcinoma.* *Clin Cancer Res*, 2006. **12**(5): p. 1623-9.
178. Begum, S., et al., *BRAF mutations in anaplastic thyroid carcinoma: implications for tumor origin, diagnosis and treatment.* *Mod Pathol*, 2004. **17**(11): p. 1359-63.
179. Kim, S.W., et al., *BRAFV600E mutation analysis in fine-needle aspiration cytology specimens for evaluation of thyroid nodule: a large series in a BRAFV600E-prevalent population.* *J Clin Endocrinol Metab*, 2010. **95**(8): p. 3693-700.
180. Baloch, Z.W., et al., *Diagnostic terminology and morphologic criteria for cytologic diagnosis of thyroid lesions: a synopsis of the National Cancer Institute Thyroid Fine-Needle Aspiration State of the Science Conference.* *Diagn Cytopathol*, 2008. **36**(6): p. 425-37.
181. Xing, M., B.R. Haugen, and M. Schlumberger, *Progress in molecular-based management of differentiated thyroid cancer.* *Lancet*, 2013. **381**(9871): p. 1058-69.
182. Wang, C.C., et al., *A large multicenter correlation study of thyroid nodule cytopathology and histopathology.* *Thyroid*, 2011. **21**(3): p. 243-51.
183. Chung, K.W., et al., *Detection of BRAFV600E mutation on fine needle aspiration specimens of thyroid nodule refines cyto-pathology diagnosis, especially in BRAF600E mutation-prevalent area.* *Clin Endocrinol (Oxf)*, 2006. **65**(5): p. 660-6.
184. Dilorenzo, M.M., et al., *False-Positive FNA Due to Highly Sensitive BRAF Assay.* *Endocr Pract*, 2014. **20**(1): p. e8-e10.
185. Kwak, J.Y., et al., *Dual priming oligonucleotide-based multiplex PCR analysis for detection of BRAFV600E mutation in FNAB samples of thyroid nodules in BRAFV600E mutation-prevalent area.* *Head Neck*, 2010. **32**(4): p. 490-8.
186. Cooper, D.S., et al., *Revised American Thyroid Association management guidelines for patients with thyroid nodules and differentiated thyroid cancer.* *Thyroid*, 2009. **19**(11): p. 1167-214.

187. Elisei, R., et al., *BRAF(V600E) mutation and outcome of patients with papillary thyroid carcinoma: a 15-year median follow-up study*. J Clin Endocrinol Metab, 2008. **93**(10): p. 3943-9.
188. O'Neill, C.J., et al., *BRAF(V600E) mutation is associated with an increased risk of nodal recurrence requiring reoperative surgery in patients with papillary thyroid cancer*. Surgery, 2010. **148**(6): p. 1139-45; discussion 1145-6.
189. Xing, M., et al., *BRAF mutation testing of thyroid fine-needle aspiration biopsy specimens for preoperative risk stratification in papillary thyroid cancer*. J Clin Oncol, 2009. **27**(18): p. 2977-82.
190. Romei, C., et al., *BRAFV600E mutation, but not RET/PTC rearrangements, is correlated with a lower expression of both thyroperoxidase and sodium iodide symporter genes in papillary thyroid cancer*. Endocr Relat Cancer, 2008. **15**(2): p. 511-20.
191. Liu, D., et al., *Suppression of BRAF/MEK/MAP kinase pathway restores expression of iodide-metabolizing genes in thyroid cells expressing the V600E BRAF mutant*. Clin Cancer Res, 2007. **13**(4): p. 1341-9.
192. Riesco-Eizaguirre, G., et al., *The BRAFV600E oncogene induces transforming growth factor beta secretion leading to sodium iodide symporter repression and increased malignancy in thyroid cancer*. Cancer Res, 2009. **69**(21): p. 8317-25.
193. Xing, M., *Prognostic utility of BRAF mutation in papillary thyroid cancer*. Mol Cell Endocrinol, 2010. **321**(1): p. 86-93.
194. Howell, G.M., et al., *Both BRAF V600E mutation and older age (>= 65 years) are associated with recurrent papillary thyroid cancer*. Ann Surg Oncol, 2011. **18**(13): p. 3566-71.
195. Fugazzola, L., et al., *BRAF mutations in an Italian cohort of thyroid cancers*. Clin Endocrinol (Oxf), 2004. **61**(2): p. 239-43.
196. Ito, Y., et al., *BRAF mutation in papillary thyroid carcinoma in a Japanese population: its lack of correlation with high-risk clinicopathological features and disease-free survival of patients*. Endocr J, 2009. **56**(1): p. 89-97.
197. Kim, T.Y., et al., *The BRAF mutation is not associated with poor prognostic factors in Korean patients with conventional papillary thyroid microcarcinoma*. Clin Endocrinol (Oxf), 2005. **63**(5): p. 588-93.
198. Jo, Y.S., et al., *Influence of the BRAF V600E mutation on expression of vascular endothelial growth factor in papillary thyroid cancer*. J Clin Endocrinol Metab, 2006. **91**(9): p. 3667-70.
199. Kwak, J.Y., et al., *Association of BRAFV600E mutation with poor clinical prognostic factors and US features in Korean patients with papillary thyroid microcarcinoma*. Radiology, 2009. **253**(3): p. 854-60.
200. Lee, X., et al., *Analysis of differential BRAF(V600E) mutational status in high aggressive papillary thyroid microcarcinoma*. Ann Surg Oncol, 2009. **16**(2): p. 240-5.
201. Lin, K.L., et al., *The BRAF mutation is predictive of aggressive clinicopathological characteristics in papillary thyroid microcarcinoma*. Ann Surg Oncol, 2010. **17**(12): p. 3294-300.
202. Niemeier, L.A., et al., *A combined molecular-pathologic score improves risk stratification of thyroid papillary microcarcinoma*. Cancer, 2011. **118**(8): p. 2069-77.
203. Brown, R.L., J.A. de Souza, and E.E. Cohen, *Thyroid cancer: burden of illness and management of disease*. J Cancer, 2011. **2**: p. 193-9.
204. Mazzaferri, E.L. and S.M. Jhiang, *Long-term impact of initial surgical and medical therapy on papillary and follicular thyroid cancer*. Am J Med, 1994. **97**(5): p. 418-28.

205. Busaidy, N.L. and M.E. Cabanillas, *Differentiated thyroid cancer: management of patients with radioiodine nonresponsive disease*. J Thyroid Res, 2012. **2012**: p. 618985.
206. Durante, C., et al., *Long-term outcome of 444 patients with distant metastases from papillary and follicular thyroid carcinoma: benefits and limits of radioiodine therapy*. J Clin Endocrinol Metab, 2006. **91**(8): p. 2892-9.
207. Sherman, S.I., *Targeted therapies for thyroid tumors*. Mod Pathol, 2011. **24 Suppl 2**: p. S44-52.
208. Carmeliet, P., *Mechanisms of angiogenesis and arteriogenesis*. Nat Med, 2000. **6**(4): p. 389-95.
209. Ferrara, N. and R.S. Kerbel, *Angiogenesis as a therapeutic target*. Nature, 2005. **438**(7070): p. 967-74.
210. Lennard, C.M., et al., *Intensity of vascular endothelial growth factor expression is associated with increased risk of recurrence and decreased disease-free survival in papillary thyroid cancer*. Surgery, 2001. **129**(5): p. 552-8.
211. Mitsiades, C.S., et al., *Targeting BRAFV600E in thyroid carcinoma: therapeutic implications*. Mol Cancer Ther, 2007. **6**(3): p. 1070-8.
212. Ouyang, B., et al., *Inhibitors of Raf kinase activity block growth of thyroid cancer cells with RET/PTC or BRAF mutations in vitro and in vivo*. Clin Cancer Res, 2006. **12**(6): p. 1785-93.
213. King, A.J., et al., *Demonstration of a genetic therapeutic index for tumors expressing oncogenic BRAF by the kinase inhibitor SB-590885*. Cancer Res, 2006. **66**(23): p. 11100-5.
214. Zambon, A., et al., *Small molecule inhibitors of BRAF in clinical trials*. Bioorg Med Chem Lett, 2012. **22**(2): p. 789-92.
215. Haugen, B.R. and S.I. Sherman, *Evolving approaches to patients with advanced differentiated thyroid cancer*. Endocr Rev, 2013. **34**(3): p. 439-55.
216. Ahmad, T. and T. Eisen, *Kinase inhibition with BAY 43-9006 in renal cell carcinoma*. Clin Cancer Res, 2004. **10**(18 Pt 2): p. 6388S-92S.
217. Sharma, A., et al., *Targeting mitogen-activated protein kinase/extracellular signal-regulated kinase kinase in the mutant (V600E) B-Raf signaling cascade effectively inhibits melanoma lung metastases*. Cancer Res, 2006. **66**(16): p. 8200-9.
218. Tuveson, D.A., B.L. Weber, and M. Herlyn, *BRAF as a potential therapeutic target in melanoma and other malignancies*. Cancer Cell, 2003. **4**(2): p. 95-8.
219. Whittaker, S., et al., *Gatekeeper mutations mediate resistance to BRAF-targeted therapies*. Sci Transl Med, 2010. **2**(35): p. 35ra41.
220. Eisen, T., et al., *Sorafenib in advanced melanoma: a Phase II randomised discontinuation trial analysis*. Br J Cancer, 2006. **95**(5): p. 581-6.
221. Bergers, G., et al., *Benefits of targeting both pericytes and endothelial cells in the tumor vasculature with kinase inhibitors*. J Clin Invest, 2003. **111**(9): p. 1287-95.
222. Ferrara, N., *VEGF and the quest for tumour angiogenesis factors*. Nat Rev Cancer, 2002. **2**(10): p. 795-803.
223. Shen, C.T., Z. Qiu, and Q.Y. Luo, *Sorafenib in radioiodine-refractory differentiated thyroid cancer: a meta-analysis*. Endocr Relat Cancer, 2013.
224. Tsai, J., et al., *Discovery of a selective inhibitor of oncogenic B-Raf kinase with potent antimelanoma activity*. Proc Natl Acad Sci U S A, 2008. **105**(8): p. 3041-6.
225. Yang, H., et al., *RG7204 (PLX4032), a selective BRAFV600E inhibitor, displays potent antitumor activity in preclinical melanoma models*. Cancer Res, 2010. **70**(13): p. 5518-27.

226. Poulikakos, P.I., et al., *RAF inhibitors transactivate RAF dimers and ERK signalling in cells with wild-type BRAF*. Nature, 2010. **464**(7287): p. 427-30.
227. Flaherty, K.T., et al., *Inhibition of mutated, activated BRAF in metastatic melanoma*. N Engl J Med, 2010. **363**(9): p. 809-19.
228. Chapman, P.B., et al., *Improved survival with vemurafenib in melanoma with BRAF V600E mutation*. N Engl J Med, 2011. **364**(26): p. 2507-16.
229. Dancey, J.E., et al., *The genetic basis for cancer treatment decisions*. Cell, 2012. **148**(3): p. 409-20.
230. Prahallad, A., et al., *Unresponsiveness of colon cancer to BRAF(V600E) inhibition through feedback activation of EGFR*. Nature, 2012. **483**(7387): p. 100-3.
231. Sieben, N.L., et al., *In ovarian neoplasms, BRAF, but not KRAS, mutations are restricted to low-grade serous tumours*. J Pathol, 2004. **202**(3): p. 336-40.
232. Salerno, P., et al., *Cytostatic activity of adenosine triphosphate-competitive kinase inhibitors in BRAF mutant thyroid carcinoma cells*. J Clin Endocrinol Metab, 2010. **95**(1): p. 450-5.
233. Nucera, C., et al., *Targeting BRAFV600E with PLX4720 displays potent antimigratory and anti-invasive activity in preclinical models of human thyroid cancer*. Oncologist, 2011. **16**(3): p. 296-309.
234. Kim, K.B., et al., *Clinical responses to vemurafenib in patients with metastatic papillary thyroid cancer harboring BRAF(V600E) mutation*. Thyroid, 2013. **23**(10): p. 1277-83.
235. Falchook, G.S., et al., *Dabrafenib in patients with melanoma, untreated brain metastases, and other solid tumours: a phase 1 dose-escalation trial*. Lancet, 2012. **379**(9829): p. 1893-901.
236. Poulikakos, P.I., et al., *RAF inhibitor resistance is mediated by dimerization of aberrantly spliced BRAF(V600E)*. Nature, 2011. **480**(7377): p. 387-90.
237. Su, F., et al., *Resistance to selective BRAF inhibition can be mediated by modest upstream pathway activation*. Cancer Res, 2012. **72**(4): p. 969-78.
238. Vergani, E., et al., *Identification of MET and SRC activation in melanoma cell lines showing primary resistance to PLX4032*. Neoplasia, 2012. **13**(12): p. 1132-42.
239. Liu, R., D. Liu, and M. Xing, *The Akt inhibitor MK2206 synergizes, but perifosine antagonizes, the BRAF(V600E) inhibitor PLX4032 and the MEK1/2 inhibitor AZD6244 in the inhibition of thyroid cancer cells*. J Clin Endocrinol Metab, 2012. **97**(2): p. E173-82.
240. Montero-Conde, C., et al., *Relief of feedback inhibition of HER3 transcription by RAF and MEK inhibitors attenuates their antitumor effects in BRAF-mutant thyroid carcinomas*. Cancer Discov, 2013. **3**(5): p. 520-33.
241. Tuononen, K., et al., *Comparison of targeted next-generation sequencing (NGS) and real-time PCR in the detection of EGFR, KRAS, and BRAF mutations on formalin-fixed, paraffin-embedded tumor material of non-small cell lung carcinoma-superiority of NGS*. Genes Chromosomes Cancer, 2013. **52**(5): p. 503-11.
242. Chin, E.L., C. da Silva, and M. Hegde, *Assessment of clinical analytical sensitivity and specificity of next-generation sequencing for detection of simple and complex mutations*. BMC Genet, 2013. **14**: p. 6.
243. Sanger, F., S. Nicklen, and A.R. Coulson, *DNA sequencing with chain-terminating inhibitors*. Proc Natl Acad Sci U S A, 1977. **74**(12): p. 5463-7.
244. Jin, L., et al., *BRAF mutation analysis in fine needle aspiration (FNA) cytology of the thyroid*. Diagn Mol Pathol, 2006. **15**(3): p. 136-43.

245. Morandi, L., et al., *Allele specific locked nucleic acid quantitative PCR (ASLNAqPCR): an accurate and cost-effective assay to diagnose and quantify KRAS and BRAF mutation*. PLoS One, 2012. **7**(4): p. e36084.
246. Hassell, L.A., E.M. Gillies, and S.T. Dunn, *Cytologic and molecular diagnosis of thyroid cancers: is it time for routine reflex testing?* Cancer Cytopathol, 2012. **120**(1): p. 7-17.
247. Kim, I.J., et al., *Development and applications of a BRAF oligonucleotide microarray*. J Mol Diagn, 2007. **9**(1): p. 55-63.
248. Guerra, A., et al., *The primary occurrence of BRAF(V600E) is a rare clonal event in papillary thyroid carcinoma*. J Clin Endocrinol Metab, 2012. **97**(2): p. 517-24.
249. de Biase, D., et al., *Next-Generation Sequencing of Lung Cancer EGFR Exons 18-21 Allows Effective Molecular Diagnosis of Small Routine Samples (Cytology and Biopsy)*. PLoS One, 2013. **8**(12): p. e83607.
250. <http://www.454.com/>.
251. Bedard, P.L., et al., *Tumour heterogeneity in the clinic*. Nature, 2013. **501**(7467): p. 355-64.
252. Meyerson, M., S. Gabriel, and G. Getz, *Advances in understanding cancer genomes through second-generation sequencing*. Nat Rev Genet, 2010. **11**(10): p. 685-96.
253. Burrell, R.A., et al., *The causes and consequences of genetic heterogeneity in cancer evolution*. Nature, 2013. **501**(7467): p. 338-45.
254. Greaves, M. and C.C. Maley, *Clonal evolution in cancer*. Nature, 2012. **481**(7381): p. 306-13.
255. Nowell, P.C., *The clonal evolution of tumor cell populations*. Science, 1976. **194**(4260): p. 23-8.
256. Gatenby, R.A. and R.J. Gillies, *A microenvironmental model of carcinogenesis*. Nat Rev Cancer, 2008. **8**(1): p. 56-61.
257. Bozic, I., et al., *Accumulation of driver and passenger mutations during tumor progression*. Proc Natl Acad Sci U S A, 2010. **107**(43): p. 18545-50.
258. Brunelli, M., et al., *Genotypic intratumoral heterogeneity in breast carcinoma with HER2/neu amplification: evaluation according to ASCO/CAP criteria*. Am J Clin Pathol, 2009. **131**(5): p. 678-82.
259. Buob, D., et al., *The complex intratumoral heterogeneity of colon cancer highlighted by laser microdissection*. Dig Dis Sci, 2012. **57**(5): p. 1271-80.
260. Katona, T.M., et al., *Genetically heterogeneous and clonally unrelated metastases may arise in patients with cutaneous melanoma*. Am J Surg Pathol, 2007. **31**(7): p. 1029-37.
261. Maley, C.C., et al., *Genetic clonal diversity predicts progression to esophageal adenocarcinoma*. Nat Genet, 2006. **38**(4): p. 468-73.
262. Mancuso, A., et al., *Patient with colorectal cancer with heterogeneous KRAS molecular status responding to cetuximab-based chemotherapy*. J Clin Oncol, 2010. **28**(36): p. e756-8.
263. Taniguchi, K., et al., *Intratumor heterogeneity of epidermal growth factor receptor mutations in lung cancer and its correlation to the response to gefitinib*. Cancer Sci, 2008. **99**(5): p. 929-35.
264. Turke, A.B., et al., *Preexistence and clonal selection of MET amplification in EGFR mutant NSCLC*. Cancer Cell, 2010. **17**(1): p. 77-88.
265. Yancovitz, M., et al., *Intra- and inter-tumor heterogeneity of BRAF(V600E) mutations in primary and metastatic melanoma*. PLoS One, 2012. **7**(1): p. e29336.

266. Gandolfi, G., et al., *Allele percentage of the BRAF V600E mutation in papillary thyroid carcinomas and corresponding lymph node metastases: no evidence for a role in tumor progression*. J Clin Endocrinol Metab, 2013. **98**(5): p. E934-42.
267. Turner, N.C. and J.S. Reis-Filho, *Genetic heterogeneity and cancer drug resistance*. Lancet Oncol, 2012. **13**(4): p. e178-85.
268. Meldrum, C., M.A. Doyle, and R.W. Tothill, *Next-generation sequencing for cancer diagnostics: a practical perspective*. Clin Biochem Rev, 2011. **32**(4): p. 177-95.
269. Metzker, M.L., *Sequencing technologies - the next generation*. Nat Rev Genet, 2010. **11**(1): p. 31-46.
270. Gargis, A.S., et al., *Assuring the quality of next-generation sequencing in clinical laboratory practice*. Nat Biotechnol, 2012. **30**(11): p. 1033-6.
271. Nikiforova, M.N., et al., *Targeted next-generation sequencing panel (ThyroSeq) for detection of mutations in thyroid cancer*. J Clin Endocrinol Metab, 2013. **98**(11): p. E1852-60.
272. <http://www.wma.net/en/30publications/10policies/b3/>.
273. Han, S.X., et al., *Molecular beacons: a novel optical diagnostic tool*. Arch Immunol Ther Exp (Warsz), 2013. **61**(2): p. 139-48.
274. <http://www.molecular-beacons.org/>.
275. Tyagi, S. and F.R. Kramer, *Molecular beacons: probes that fluoresce upon hybridization*. Nat Biotechnol, 1996. **14**(3): p. 303-8.
276. Latorra, D., et al., *Enhanced allele-specific PCR discrimination in SNP genotyping using 3' locked nucleic acid (LNA) primers*. Hum Mutat, 2003. **22**(1): p. 79-85.
277. Livak, K.J. and T.D. Schmittgen, *Analysis of relative gene expression data using real-time quantitative PCR and the 2⁻(-Delta Delta C(T)) Method*. Methods, 2001. **25**(4): p. 402-8.
278. Liu, L., et al., *Comparison of next-generation sequencing systems*. J Biomed Biotechnol, 2012. **2012**: p. 251364.
279. Hofreiter, M., et al., *DNA sequences from multiple amplifications reveal artifacts induced by cytosine deamination in ancient DNA*. Nucleic Acids Res, 2001. **29**(23): p. 4793-9.
280. Marchetti, A., L. Felicioni, and F. Buttitta, *Assessing EGFR mutations*. N Engl J Med, 2006. **354**(5): p. 526-8; author reply 526-8.
281. <http://genetics.bwh.harvard.edu/pph2/>.
282. Ghossein, R.A., N. Katabi, and J.A. Fagin, *Immunohistochemical detection of mutated BRAF V600E supports the clonal origin of BRAF-induced thyroid cancers along the spectrum of disease progression*. J Clin Endocrinol Metab, 2013. **98**(8): p. E1414-21.